LONG RANGE FORECASTING OF COLORADO STREAMFLOWS BASED ON HYDROLOGIC, ATMOSPHERIC, AND OCEANIC DATA

by

Jose D. Salas and Chongjin Fu
Department of Civil and Environmental Engineering
Colorado State University, Fort Collins, CO

and

Balaji Rajagopalan
Department of Civil and Architectural Engineering
University of Colorado, Boulder, CO

ABSTRACT

Climatic fluctuations have profound effects on water resources variability in the western United States. The effects are manifested in several ways and scales particularly in the occurrence, frequency, and magnitude of extreme events. The research reported herein centers on streamflow predictability at the medium and long range scales in the headwaters of six rivers that originate in the State of Colorado. Specifically, we want to improve the capability of forecasting seasonal and yearly flows. The analysis will focus on forecasting seasonal (April-July) and yearly (April-March) and (October-September) streamflows based on atmospheric-oceanic forcing factors, such as geopotential height, wind, and sea surface temperature (SST), as well as hydrologic factors such as snow water equivalent (SWE). The approach followed in the study includes: search for potential predictors, apply Principal Component Analysis (PCA) and multiple linear regression (MLR) for forecasting at individual sites, apply Canonical Correlation Analysis (CCA) for forecasting at multiple sites, and test the forecasting models. The forecast models have been tested in two modes: (a) fitting and (b) evaluation. In addition, some measures of forecast skill have been utilized. The study includes comparisons of forecasts using all possible predictors, i.e. hydrologic, atmospheric, and oceanic variables, using atmospheric and oceanic variables only, and using oceanic predictors only. In addition, we compared forecasts at the six sites by using aggregation and disaggregation procedures. The study brought into relevance the significant benefits of using atmospheric and oceanic predictors, in addition to hydrological predictors, for long range streamflow forecasting. It has been shown that forecasts based on PCA applied to individual sites give very good results based on various forecast performance measures for both seasonal as well as yearly time scales. Also it has been shown that even though the PCA has been applied on a site by site basis yet the forecasts approximate well the historical cross-correlation although some underestimation was noted for two sites. We also found that forecasts made using CCA are less efficient than those based on PCA even regarding the cross-correlations among sites. Furthermore, the forecast procedures based on aggregation and disaggregation (in the case of multiple sites) produced only modest results.

Keywords: Forecasting streamflows, atmospheric/oceanic predictors, flow prediction, stochastic analysis, PCA, CCA.

Long Range Forecasting of Colorado Streamflows Based on Hydrologic, Atmospheric, and Oceanic Data

1. Introduction

Although the State of Colorado is located in a semiarid climate it has important water resources because of its high elevation and significant amount of snowfall every year. Several major rivers originate in the State of Colorado, such as the Colorado River, Arkansas River, Rio Grande and others. Agriculture, municipal water supply, hydropower generation, and recreational activities from the headwater regions down heavily rely on the river waters. Such water demand has been increasing as the western U.S. continues developing and the population growing. Thus balancing a limited and variable water supply and competing increasing water demands must be tackled by water resources management so as to make sufficient amount of water available at the time is needed. It is a critical aspect of conservation, development, and management of water resources systems particularly in Colorado because of its semiarid climate. However, water availability may be severely impacted because of extreme hydroclimatic events such as droughts. Understanding the variability of such phenomena, particularly determining their predictability are the main focus of the research reported herein.

There is growing evidence of the effects of atmospheric-oceanic features on the hydrology of the western basins. Quantifying such effects in the headwaters of Colorado rivers is difficult because of the varied topography in the Rocky Mountains and because the headwater' rivers lie outside the regions most strongly influenced by large scale climatic forcing such as ENSO. The rivers that originate in the State of Colorado and flow downstream across semiarid and arid lands are prone to frequent and often long periods of low flows. Being important sources of water supply for many users, they have been developed and controlled with many river diversions and dams along the system. Operating such systems requires reliable streamflow forecasts. Every year management decisions for operating the systems are made early in the year in anticipation of the forthcoming spring and summer streamflows. Thus long range streamflow forecasting may be of particular interest for improving system operations.

Colorado is a mountainous region and a major source of the streamflows is melting snow. Therefore snowfall in the preceding months of the season of interest must be an important factor for streamflow forecasting. However, there are several other factors that affect the fluctuations of

the streamflows such as the water content in the atmosphere and its transportation to the area. For example, Geopotential Height (GH) is a direct indicator of the conditions leading to precipitation, which could eventually be turned into streamflow. Other variables that could be used as predictors for streamflow forecasting are air temperature, humidity, and wind. Temperature and humidity are very much related to the amount of moisture in the air and wind is an important predictor since it is a determinant factor for moisture transport in the atmosphere. Also as the oceans are the largest water resources of moisture on earth, ocean dynamics play a significant role of streamflow variability. Perhaps the most important variable representing oceanic conditions is sea surface temperature (SST) and many oceanic climatic indices have been developed such as the Southern Oscillation Index (SOI) and the Pacific Decadal Oscillation (PDO) index. Since streamflow is a part of the global hydrological circulation, and the changes of the atmospheric and oceanic conditions certainly affect the variations of streamflows, forecast models of Colorado rivers must include key atmospheric and oceanic variables as predictors in addition to snow water equivalent and other hydrological variables that may be of relevance for the system at hand.

The scope of the study herein centers on streamflow predictability at the medium range and long range scales in the headwaters of the rivers that originate in the State of Colorado. The specific objective of the study is to develop and assess models and methods for forecasting seasonal (April-July) and yearly (April-March and October-September) streamflows for the Yampa, Gunnison, San Juan, Poudre, Arkansas, and Rio Grande rivers. The models will include forecasting at single and multiple sites. The forecasts will be based on identifying hydrologic predictors such as snow water equivalent and predictors from various atmospheric-oceanic forcing factors such as, geopotential height, zonal and meridional wind, air temperature, precipitation, sea surface temperature (SST), and streamflows in the study area.

2. Brief Review of Related Studies

Existing medium and long range streamflow forecasting models for Colorado River basins commonly rely on previous records of snow water equivalent, precipitation, and streamflows as predictors. And the typical model has been the well known multiple linear regression. Haltiner and Salas (1988) and Wang and Salas (1991) in studies of the Rio Grande basin have shown that significant improvements in forecasting efficiency can be achieved using time series analysis techniques such as transfer function models. Also recent literature have

demonstrated the significant relationships between climatic signals such as SST, ENSO, PDO, and others on precipitation and streamflow variations (e.g. Cayan and Webb, 1992; Mantua et al, 1997; Clark et al, 2001) and that seasonal and longer-term streamflow forecasts can be improved by using such climatic factors (e.g. Hamlet and Lettenmaier, 1999; Clark et al, 2001; Eldaw et al, 2003; Grantz et al, 2005; Salas et al, 2005). Thus the literature suggests that it is worthwhile examining in closer detail forecasting schemes that incorporate not only the usual predictors (e.g. snow water equivalent, precipitation, and streamflows,) but also climatic factors that may improve the seasonal and long range forecasts of streamflows in the headwaters of Colorado. Also, previous studies suggested that despite the influence of major climatic factors such as ENSO on the hydrology of the Colorado basin, there are significant differences in their effects from basin to basin (McCabe and Dettinger, 2002). This is the reason why in our research we considered three major streams in the Colorado headwaters (Yampa, Gunnison, and San Juan) and three other rivers flowing in other directions such as the Poudre, Arkansas, and Rio Grande rivers.

Therefore, in addition to the typical indices such as ENSO as mentioned before, we considered predictors directly identified from sea surface temperature, and other atmospheric circulation features such as geopotential heights (e.g. 700 mb) and zonal meridional winds. Many studies have pointed out the strong connection between the extreme phases of the El Niño Southern Oscillation (ENSO) episodes and fluctuations of precipitation and streamflow all over the world (e.g. Ropelewski and Halpert, 1987; Cayan et al, 1998). For example significant relationship was found between El Niño and extreme drought years in the Pacific northwest and a strong relationship between dry conditions in the southern United States and La Niña events (e.g. Piechota and Dracup, 1996). Also during El Niño above normal precipitation was found in the desert Southwest (e.g. Cayan and Webb, 1992; Dettinger et al, 1998). Higgins et al (2000) in forecasting studies of precipitation and surface air temperature in the U.S. based on ENSO, SST, tropical precipitation, geopotential height, winds and AO found that the dominant factors are tropical precipitation and AO. Also ENSO influences have been observed on snow water equivalent (Clark et al, 2001) and streamflows (e.g. Piechota et al, 1997; Maurer et al, 2003). In studying the Mississippi River basin Maurer et al (2003) found that in the eastern part of the basin ENSO and AO indices are more important than the land surface stage indicators such as soil moisture and snow. They also claimed that for 3 months or greater lead times the effects of

ENSO and AO are more significant. And Maurer et al (2004) studied the predictability of seasonal runoff in the Continental U.S. between 25° and 53° N as a function of NAO, AO, NP, PNA, AMO, Niño3.4, and PDO. For example, they found that a positive phase of El Niño 3.4 is useful for forecasting the MAM runoff while a negative phase Niño 3.4 is useful for forecasting the DJF runoff. In addition, effects on decadal time scales primarily driven by the Pacific Decadal Oscillation (PDO) have been found (e.g. Mantua et al, 1997; McCabe and Dettinger, 1999; McCabe et al, 2004).

Furthermore, Moss et al (1994) used the Southern Oscillation Index (SOI) as a predictor of the probability of low flows in New Zealand. Eltahir (1996) showed that up to 25% of the natural variability of the Nile River annual flows is associated with ENSO events and Eldaw et al (2003) reported that SST in the Pacific and Atlantic oceans in conjunction with precipitation at the Gulf of Guinea may be used as predictors for forecasting the total streamflows in the Blue Nile River several months in advance. In addition, Salas et al (2005) in studying the predictability of droughts in the Poudre River utilized SSTs in the Pacific to forecast the next years' flows that may occur in the basin. Also Grantz et al (2005) developed a forecast model using SST, GH, and SWE as predictors for forecasting April-July streamflows at the Truckee and Carson rivers in Nevada. They found that forecast skills are significant for up to 5 months lead time based on SST and GH. Regonda et al (2006) reported successful results for forecasting streamflows in the Gunnison River using various climatic forcing factors. Maity and Kumar (2008) developed a forecasting model for monthly streamflows in India based on ENSO and climatic index of the tropical Indian Ocean. Also in a study of 639 U.S. rivers Tootle et al (2005) found significant relationships between the ENSO, PDO, AMO, and NAO indices and streamflows, and suggested that their findings may be useful for streamflow forecasts. In addition, in studying the Colorado River, Canon et al (2007) reported significant relationships between SPI (standardized precipitation index) and the climatic indices PDO and BEST.

Detailed descriptions of PCA and CCA methods for streamflow forecasting can be found in many books and papers. According to Jolliffe (1986) the original work on PCA has been done by Pearson in the early 1900's. In the 1930's Hotelling presented the PCA method in more complete scientific content (e.g. Manly, 1994). Lorenz has been one of the pioneers (Barnett, 1987) in applying PCA to the hydro-meteorology field. Haan (2002) and Wilks (2006) discuss various practical issues about PCA. CCA was first introduced by Hoteling in 1936 (Glahn,

1968). Detailed descriptions can be found in the books by Haan (2002), Giri (2004), and Wilks (2006). Also, Manly (1994) provides a very easy reading text on CCA.

The applications of PCA and CCA (not limited to streamflow forecasts) have been documented by many researchers. For example, Barnett and Preisendorfer (1987) employed CCA for forecasting air temperature over the U.S. Also CCA has been applied extensively for forecasting various climate variables such as surface temperature, precipitation, and geopotential heights for the northern hemisphere (Barnston, 1994). Also Barnston and He (1996) applied CCA for forecasting the 3-month climate in Hawaii and Alaska. Likewise, He and Barnston (1996) use CCA for forecasting seasonal precipitation in the Tropical Pacific Islands and Shabbar and Barnston (1996) also applied CCA for forecasting 3-month mean surface temperature and precipitation for Canada.

3. Study Area and Data

Six streamflow sites in rivers that originate in the State of Colorado are selected for the study and models for forecasting streamflow volumes for seasonal and yearly time scales are built and compared. The flow sites include the Arkansas River, Gunnison River, Poudre River, Rio Grande, San Juan River, and the Yampa River. Figure 1 shows the locations of the flow sites and additional information are given in Table 1. Note that the Rio Grande site considered for the study is not far from the State line (Colorado and New Mexico) and the site for San Juan has portion of the basin contributing from tributaries located in New Mexico.

The data used in this study are naturalized monthly streamflows. The data for the Gunnison, San Juan, and Yampa rivers were obtained from the Colorado Hydrological Study Group of the U.S. Bureau of Reclamation (add website here) . The data for the Poudre River have been obtained from the Northern Colorado Water Conservation District and the data for the Arkansas and Rio Grande rivers were obtained from the Hydrology and Climate Data Network (HCDN) of the U.S. Geological Survey. Other data such as snow water equivalent (SWE) and Palmer drought severity index (PDSI) were obtained from the National Resources Conservation Services and the National Climate Data Center of NOAA (National Oceanic and Atmospheric Administration). In addition, the atmospheric and oceanic data were obtained from the Physical Science Division of the Earth System Research Laboratory, NOAA. Pertinent data were obtained from NOAA's Climate Diagnostic Center website (http://www.cdc.noaa.gov) and Kalnay et al (1996). They include climatic data such as sea surface temperature (SST), Southern

Oscillation Index (SOI), Pacific Decadal Oscillation (PDO), North Atlantic Oscillation (NAO), the SST observations for the El Niño regions, geopotential heights (GH), temperature, relative humidity, outgoing longwave radiation, and wind. And the time period of the data used for the study is 1949 - 2001.

4. Methodology

The methods assume that a suitable number of hydrologic, atmospheric, and oceanic predictors can be found to forecast streamflows for different time frames and river sites considered in the study. The potential hydrologic predictors include: snow water equivalent (SWE), precipitation, streamflows, and Palmer drought severity index (PDSI). Likewise, the potential atmospheric and oceanic predictors include geopotential height at 700 mb (GH), meridional wind at 700 mb (MW), zonal wind at 700 mb (ZW), air temperature (AT), outgoing long-wave radiation (OLWR), relative humidity (RH), Artic Oscillation (AO) index, Pacific Decadal Oscillation (PDO) index, Southern Oscillation Index (SOI), North Atlantic Oscillation (NAO) index, sea surface temperature (SST), and SSTs related to El Niño-2, El Niño-3, and El Niño-4. The potential atmospheric and oceanic predictors listed above may arise from data that are available at every pixel worldwide.

4.1 Correlation analysis for selecting potential predictors

Correlation analysis between the predictand (the streamflow data at each flow site) and the potential predictors are performed. For any variable that may be utilized as a potential predictor, e.g. SST at a given location (pixel), various possible predictors may be selected. They are defined at time periods that are lagged behind or before the time period specified for the predictand. For example, if the intent is to forecast the total flows for the period April to July (i.e. for months AMJJ), then a possible predictor may be average SST for the preceding months, i.e. SST(JFM), SST(OND), SST(ONDJFM), and so on (where OND is the period for October to December of the previous year, etc.). Since there are many potential predictors, the ones that are selected for further analysis are those with statistical significant correlations. Note that for those variables that are available worldwide for every pixel (e.g. geopotential height) or across all oceans (e.g. SST), correlation maps are created that show with color codes the values of the correlations. From these maps areas not less than 5°×5° with significant correlations are identified and selected as the potential predictors. Also for other variables such as SWE, PDO, etc. where correlation maps are not applicable, the same statistical criteria for selecting potential

predictors is utilized. The significance of the correlation between the streamflow data and the variable (predictor) considered is determined using $r_c = t_{.975}^2 / \sqrt{N+1}$ where r_c is the critical correlation coefficient, $t_{.975}$ is the 97.5% quantile of the t-distribution with N-1 degrees of freedom, and N is the sample size. Thus a potential predictor is selected for further analysis if the calculated correlation coefficient r (in absolute value) is bigger than r_c. Since in all cases the sample size of the data used in this study is 53 (recall the data used is for the period 1949 ~ 2001), the critical correlation coefficient is ± 0.28.

4.2 Principal Component Analysis (PCA)

In this method a linear transformation is made on the potential predictors to obtain uncorrelated Principal Component (or PCs). The mathematics and formulations of PCA are summarized here. Consider p standardized variables $\boldsymbol{x_1}, \boldsymbol{x_2}, \ldots, \boldsymbol{x_p}$. The following linear transformation can be made

$$\boldsymbol{z} = \boldsymbol{x}\boldsymbol{W} \tag{1a}$$

i.e.

$$\boldsymbol{z}_j = w_{1j}\,\boldsymbol{x}_1 + w_{2j}\,\boldsymbol{x}_2 + \cdots + w_{pj}\,\boldsymbol{x}_p \quad , \quad j=1,\ldots,p \tag{1b}$$

where $\boldsymbol{z}$ and $\boldsymbol{x}$ are $1\times p$ vectors, $\boldsymbol{W}$ is a $p\times p$ matrix that consists of column vectors $\boldsymbol{w_1}, \boldsymbol{w_2}, \ldots \boldsymbol{w_p}$. Thus the $\boldsymbol{x}$ variables are transformed to the $\boldsymbol{z}$ variables that are called the Principal Components of $\boldsymbol{x}$. The idea of PCA is to find the $\boldsymbol{z}$ variables such that a few of them contain the majority of the variance of the $\boldsymbol{x}$ variables, and the $\boldsymbol{z}$ variables are uncorrelated to each other. Thus the PC coefficient matrix $\boldsymbol{W}$ is defined as

$$\boldsymbol{W} = \begin{bmatrix} \boldsymbol{w}_1 & \boldsymbol{w}_2 & \ldots & \boldsymbol{w}_p \end{bmatrix} = \begin{bmatrix} w_{11} & w_{12} & \ldots & w_{1p} \\ w_{21} & w_{22} & \ldots & w_{2p} \\ \vdots & \vdots & \ddots & \vdots \\ w_{p1} & w_{p2} & \ldots & w_{pp} \end{bmatrix} \tag{2a}$$

Suppose there are N observations of each variable $\boldsymbol{x}_1,\ldots,\boldsymbol{x}_p$ and let $\boldsymbol{X}$ be an $N\times p$ matrix representing the data of the $\boldsymbol{x}$ variables (note that we have assumed that each variable has been standardized), then the values of the $\boldsymbol{z}$ variables, called the PC scores, are obtained by

$$\boldsymbol{Z} = \boldsymbol{X}\boldsymbol{W} \tag{3}$$

where $\boldsymbol{Z}$ is an $N\times p$ matrix. The key for PCA is to figure out the matrix $\boldsymbol{W}$ which will make the $\boldsymbol{z}$ variables to have the desired properties. It turns out that the columns of the $\boldsymbol{W}$ matrix are the

eigenvectors corresponding to each eigenvalue of the variance-covariance matrix of the $\boldsymbol{x}$ variables, i.e.

$$\boldsymbol{S} = \frac{1}{N-1}\,\boldsymbol{X}^{\boldsymbol{T}}\boldsymbol{X} \tag{4}$$

where $\boldsymbol{S}$ is a $p \times p$ symmetric matrix. Also there exists p scalars $\lambda_1, \ldots, \lambda_p$ that are called eigenvalues of matrix $\boldsymbol{S}$. It may be shown that the λ's can be found by solving the determinant equation

$$\left|S - \lambda I\right| = 0 \tag{5}$$

where I is the $p \times p$ identity matrix. The solution of (5) leads to p roots $\lambda_1, \lambda_2, \ldots, \lambda_p$. Once the eigenvalues are obtained, the eigenvectors $\boldsymbol{w}_i$ corresponding to each λ_i are determined by

$$(\boldsymbol{S} - \lambda_i \boldsymbol{I})\,\boldsymbol{w}_i = 0 \quad , \qquad i=1,2, \ldots, p \tag{6}$$

in which the $\boldsymbol{w}_i$ are given by (2). Note that for Eq.(6) to have nontrivial solutions, the following constraint $\boldsymbol{w}_i^{\,T}\boldsymbol{w}_i = 1$ must hold because we assumed the original data standardized.

In summary, the PCA procedure is solving for the eigenvalues of matrix $\boldsymbol{S}$ by using Eq. (5), and then solving for the eigenvectors corresponding to each eigenvalue by using Eq.(6). Finally, the PC scores are obtained from Eq.(3). After obtaining the PCs, one must decide on how many of them are to be used for further analysis. One criterion is selecting the PCs that explain a given amount of the variance. Further selection may be made using stepwise regression. Detailed procedures using PCs as the predictors in a multiple linear regression framework are given in a subsequent section.

4.3 Canonical Correlation Analysis (CCA)

CCA is a method used to determine the relationship between two groups of variables. Assume a system that consists of two groups of variables: p independent variables $\boldsymbol{x} = [\boldsymbol{x_1}\ \boldsymbol{x_2}\ \ldots\ \boldsymbol{x_p}]$ and q dependent variables $\boldsymbol{y} = [\boldsymbol{y_1}\ \boldsymbol{y_2}\ \ldots\ \boldsymbol{y_q}]$, where $\boldsymbol{x}$ is a $1 \times p$ vector, $\boldsymbol{y}$ is a $1 \times q$ vector and each $\boldsymbol{x}_i$ and $\boldsymbol{y}_i$ are column vectors where the elements are observations, i.e. vectors of size $1 \times N$. CCA creates two new variables $\boldsymbol{u} = [\boldsymbol{u_1}\ \boldsymbol{u_2}\ \ldots\ \boldsymbol{u_n}]$ and $\boldsymbol{v} = [\boldsymbol{v_1}\ \boldsymbol{v_2}\ \ldots\ \boldsymbol{v_n}]$, where $n = min(p,q)$, i.e. $\boldsymbol{u}$ and $\boldsymbol{v}$ are $1 \times n$ vectors and each $\boldsymbol{u}_i$ and $\boldsymbol{v}_j$ are also column vectors of size $1 \times N$. The $\boldsymbol{u}$ variables are formed by a linear combination of the $\boldsymbol{x}$ variables, i.e. $\boldsymbol{u} = \boldsymbol{xa}$ where $\boldsymbol{a}$ is a $p \times n$ matrix. Similarly, the $\boldsymbol{v}$ variables are formed by a linear combination of the $\boldsymbol{y}$ variables, i.e. $\boldsymbol{v} = \mathbf{y}\boldsymbol{b}$ where $\boldsymbol{b}$ is a $q \times n$ matrix. It follows

$$\begin{aligned} \boldsymbol{u}_1 &= a_{11}\boldsymbol{x}_1 + a_{21}\boldsymbol{x}_2 + \cdots + a_{\mathrm{p1}}\boldsymbol{x}_p \\ \boldsymbol{u}_2 &= a_{12}\,\boldsymbol{x}_1 + a_{22}\,\boldsymbol{x}_2 + \ldots + a_{p2}\,\boldsymbol{x}_p \\ &\vdots \\ \boldsymbol{u}_n &= a_{1n}\,\boldsymbol{x}_1 + a_{2n}\,\boldsymbol{x}_2 + \ldots + a_{pn}\,\boldsymbol{x}_p \end{aligned} \tag{7}$$

where the transformation matrix $\boldsymbol{a}$ is given by

$$a = \begin{pmatrix} \mathrm{a}_{11} & \mathrm{a}_{12} & \cdots & \mathrm{a}_{1\mathrm{n}} \\ \mathrm{a}_{21} & \mathrm{a}_{22} & \cdots & \mathrm{a}_{2\mathrm{n}} \\ \vdots & \vdots & \vdots & \vdots \\ \mathrm{a}_{\mathrm{p1}} & \mathrm{a}_{\mathrm{p2}} & \cdots & \mathrm{a}_{\mathrm{pn}} \end{pmatrix} \tag{8}$$

Similarly,

$$\begin{aligned} \boldsymbol{v}_1 &= b_{11}\;\boldsymbol{y}_1 + b_{21}\;\boldsymbol{y}_2 + \ldots + b_{q1}\;\boldsymbol{y}_q \\ \boldsymbol{v}_2 &= b_{12}\;\boldsymbol{y}_1 + b_{22}\;\boldsymbol{y}_2 + \ldots + b_{q2}\;\boldsymbol{y}_q \\ &\vdots \\ v_n &= b_{1\mathrm{n}}\,\boldsymbol{y}_1 + b_{2\mathrm{n}}\,\boldsymbol{y}_2 + \cdots + b_{\mathrm{qn}}\,\boldsymbol{y}_q \end{aligned} \tag{9}$$

where the transformation matrix $\boldsymbol{b}$ is

$$b = \begin{bmatrix} b_{11} & b_{12} & \ldots & b_{1n} \\ b_{21} & b_{22} & \ldots & b_{2n} \\ \vdots & \vdots & \vdots & \vdots \\ b_{q1} & b_{q2} & \cdots & b_{qn} \end{bmatrix} \tag{10}$$

The variables $\boldsymbol{u}$ and $\boldsymbol{v}$ are called canonical variables and are paired so that $\boldsymbol{u_1}$ and $\boldsymbol{v_1}$ are correlated with the so-called *canonical correlation coefficient* ρ_1, $\boldsymbol{u_2}$ and $\boldsymbol{v_2}$ are correlated with ρ_2, etc. The following is a schematic explanation of CCA

$$\left.\begin{matrix} \boldsymbol{y}_1 \\ \boldsymbol{y}_2 \\ \vdots \\ \boldsymbol{y}_q \end{matrix}\right\} = \boldsymbol{y} \rightarrow \boldsymbol{y}\boldsymbol{b} = \boldsymbol{v} = \left\{\begin{matrix} \boldsymbol{v}_1 & \leftarrow \rho_1 \rightarrow & \boldsymbol{u}_1 \\ \boldsymbol{v}_2 & \leftarrow \rho_2 \rightarrow & \boldsymbol{u}_2 \\ \vdots & \cdots & \vdots \\ \boldsymbol{v}_n & \leftarrow \rho_n \rightarrow & \boldsymbol{u}_n \end{matrix}\right\} = \boldsymbol{u} = \boldsymbol{x}\boldsymbol{a} \leftarrow \boldsymbol{x} = \left\{\begin{matrix} \boldsymbol{x}_1 \\ \boldsymbol{x}_2 \\ \vdots \\ \boldsymbol{x}_p \end{matrix}\right.$$

where $\rho_1 > \rho_2 > \cdots > \rho_n$ (note that this assumes that the canonical correlations have been arranged to comply with ρ_1 being the largest and so on.) The values of the canonical variates are often called the scores of the canonical variates and the matrices $\boldsymbol{a}$ and $\boldsymbol{b}$ are called *canonical loadings*.

The canonical correlation coefficients $\boldsymbol{\rho}$ and the matrices $\boldsymbol{a}$ and $\boldsymbol{b}$ may be estimated using the CCA procedure as follows (Manley, 1994). Firstly matrix $\boldsymbol{S}_a$ is obtained as

$$\boldsymbol{S}_a = \boldsymbol{S}_{xx}^{-1}\,\boldsymbol{S}_{xy}\,\boldsymbol{S}_{yy}^{-1}\,\boldsymbol{S}_{xy}^{T} \tag{11}$$

in which $\boldsymbol{S}_{wz}$ is the covariance matrix of the variables w and z. Then matrix **a** is estimated using the eigenvalues and eigenvectors of matrix $\boldsymbol{S}_a$. Likewise, matrix $\boldsymbol{S}_b$ is determined as

$$\boldsymbol{S}_b = \boldsymbol{S}_{yy}^{-1}\,\boldsymbol{S}_{xy}^{T}\,\boldsymbol{S}_{xx}^{-1}\,\boldsymbol{S}_{xy} \tag{12}$$

and matrix $\boldsymbol{b}$ is obtained by calculating the eigenvalues and eigenvectors of matrix $\boldsymbol{S}_b$. It may be shown that the eigenvalues of matrix $\boldsymbol{S}_b$, i.e. $\lambda_1,...,\lambda_n$ are related to the canonical correlation coefficients $\rho's$ as $\lambda_1 = \rho_1^2$, $\lambda_2 = \rho_2^2$, ⋯ , $\lambda_n = \rho_n^2$. Thus these relations can be used to obtain the $\rho's$ from the $\lambda's$. Alternatively, the $\rho's$ can be obtained by correlating the vectors $\boldsymbol{u}_i$ and $\boldsymbol{v}_i$ of Eqs.(7) and (9), respectively.

To test the significance of the canonical correlation coefficients we tested the null against the alternative hypothesis as

$\boldsymbol{H_0}$: $\rho_1 = \rho_2 = ... = \rho_r = 0$

$\boldsymbol{H_a}$: at least $\rho_i \neq 0$, i=1,2, …, r

where r is taken successively as r=1, …,n. The test statistic is

$$C = -\left[n - \frac{1}{2}(p+q+6)\right] \times \sum_{i=1}^{r} \ln(1-\rho_i^2)$$

which is χ^2 distributed with number of degrees of freedom equal to pq. A large value of the test statistic suggests that the null hypotheses must be rejected. After testing for the significance of the $\rho's$ the relationships between the $\boldsymbol{v}$'s and $\boldsymbol{u}$'s are established by using simple linear regressions as

$$\boldsymbol{v}_i = \beta_i\,\boldsymbol{u}_i \quad , \quad i = 1,...,n \tag{13}$$

where the $\beta_i, i = 1,...,r$ are the parameters of the regression equations. Then the forecast for $\boldsymbol{y}$ is obtained by inverting Eq.(9) as

$$\boldsymbol{y} = \boldsymbol{v}\,\boldsymbol{b}^{-1} \tag{14}$$

Detailed procedures for the models using CCA are given in subsequent sections of this paper.

4.4 Forecast models for single sites

Stepwise regression analysis is conducted for specifying the forecast model at single sites. This technique is applied either using the original variables or the PCs as the predictors. The purpose of the stepwise regression is selecting the most suitable combination of predictors to ensure that the model provides an optimal forecast. The criteria for deciding whether a given predictor is selected or not is based on the F-test which tests the significance of the coefficient associated with the predictor. The greater the value of the F-statistic, the more significant is the predictor.

The forecast model based on MLR may be written as

$$\hat{y} = \sum_{j=1}^{m} \beta_j x_j \tag{15}$$

where $\hat{y}$ is the streamflow forecast (standardized) , β_i , i= 1, …,m are the parameters, x_i , i = 1, …,m are the predictors (standardized), m is the number of the predictors, and the variables x_i represent the predictors such as SST, SWE, etc, in their original domain and the $\beta's$ are estimated using least squares method and stepwise regression analysis.

Alternatively, the forecast model using MLR can be set up based on PCs as the predictors

$$\hat{y} = \sum_{i=1}^{p} \beta_i PC_i \tag{16}$$

where $\hat{y}$ is the streamflow forecast (standardized), $\beta_i, i = 1,..., p$ are the parameters, $PC_i, i = 1,..., p$ are the predictors (in terms of principal components), and p is the number of predictors (note that we have assumed that the underlying variables have been standardized). The PCs of Eq.(16) are those obtained using stepwise regression analysis. Also some PCs with very small amount of variances are not included into the forecast model even though they may have been selected in the stepwise regression analysis. The parameters $\beta_1, \beta_2, ...$ are estimated using the least squares method.

4.5 Forecast models for multiple sites

Before building the CCA model, a pre-orthogonal analysis is made where PCA is performed on both the streamflows and the potential predictors. The reason for performing PCA on the streamflows is to find out whether the streamflow variations over the study region are homogeneous. If so, it may be useful conducting the forecast by using an aggregation of the streamflow, or by using a few PCs of the streamflow. Also the analysis is needed for reducing

the number of variables in the CCA. In this study, the predictants (either in their original form or as PCs) and the number of the PCs used in the CCA model are determined based on the results of the pre-orthogonal analysis. Similar to the single site PCA model, the performances of the CCA model relies on which PCs are used. Although the first several PCs may account for the majority of the variances, not all of them may be good predictors for the CCA model. To select the PCs into the CCA model, the model residuals are analyzed. The total model residual is computed using the following equation

$$\sum_{i=1}^{q}\sum_{j=1}^{N}(\hat{y}_i^j - y_i^j)^2$$

where $\hat{y}_i^j$ are forecasted flows, y_i^j are the observed flows, i is a particular time in the sequence of observations (or forecasts), j denotes the site, and N and n are the total number of time steps and sites, respectively. The PCs that cause the increase of the sum of square residuals are eliminated from the forecast model. After the PCs of the predictors are decided, then CCA is carried out for the streamflows and the selected PCs. Significance tests are then conducted for the canonical correlation coefficients between the canonical variate pairs. Based on the results of the significance tests, the canonical variates that will be further used in the CCA forecast models are decided.

Next, the relationships between the pairs of the canonical variates $\boldsymbol{v}$ and $\boldsymbol{u}$ are established as

$$\boldsymbol{v}_i = \beta_{0,i} + \beta_{1,i}\boldsymbol{u}_i \quad , \quad \text{i} = 1,2, \ldots, q \tag{17}$$

where $\boldsymbol{v}$ and $\boldsymbol{u}$ are the canonical variates used in the CCA model (obtained from Eqs.7 and 9, respectively) and β are the parameters. Then to do the forecasts Eq.(7) is applied to obtain the values of $u_1,...,u_n$ given the values of the predictors $x_1,...,x_p$, and the v_i values are obtained from Eq.(17) which are inverted back to the real space by Eq.(14) as $\hat{\boldsymbol{y}} = \hat{\boldsymbol{v}}\, b^{-1}$. If PCs for the streamflows were used for the CCA model, then another invertion is needed to obtain the streamflows back from the forecasted PCs. However, in this study the original streamflows were used in the CCA forecasts. Therefore no further inversion was needed.

4.6 Model performance: fitting and validation analysis

The coefficient of determination R^2 and the adjusted coefficient of determination R_a^2 are often used for measuring the performances of forecast models. They are calculated as

$$R^2 = 1 - \frac{\sum_{i=1}^{N} (\hat{Y}_i - Y_i)^2}{\sum_{i=1}^{N} (Y_i - \overline{Y})^2} \tag{18}$$

$$R_a^2 = 1 - [(1 - R^2)(N-1)/(N-p)] \tag{19}$$

where $\hat{Y}_i$ is the forecasted streamflow, Y_i is the observed streamflow, $\overline{Y}$ is the mean of the observations, N is the number of observations, and p is the number of parameters of the model.

Also forecast skill scores are used for the same purpose. Two commonly used forecast skill scores are the *Accuracy* (*AC*) and the *Heidke Skill Scores (HSS)*. The *Accuracy* is an overall forecast skill score, which indicates the fraction of the forecasts that are in the same category as the observations. The categories of streamflows are determined based on percentiles. In this study the four categories defined by the 25th, 50th, and 75th percentiles are utilized. It is given by

$$AC = \frac{1}{N} \sum_{i=1}^{k} n(F_i O_i) \tag{20}$$

where $n(F_i O_i)$ is the number of the forecasts that are in the same category as the corresponding observations, N is the total number of observations, and k is the number of categories. AC ranges between 0 and 1 where 1 indicates a perfect forecast. *HSS* measures the fraction of correct forecasts after eliminating those that would be correct due to purely random chance. It is given by

$$HSS = \frac{\frac{1}{N} \sum_{i=1}^{k} n(F_i O_i) - \frac{1}{N^2} \sum_{i=1}^{k} n(F_i) n(O_i)}{1 - \frac{1}{N^2} \sum_{i=1}^{k} n(F_i) n(O_i)} \tag{21}$$

where $n(F_i)$ is the number of forecasts in category i, and $n(O_i)$ is the number of the observations in category i. *HSS* ranges from - ∞ to 1; a value of 0 indicates no forecast skill while 1 indicates a perfect forecast.

In evaluating the performance of the forecast models (applying the various metrics and comparisons as suggested above), two procedures are used to calculate the forecasts (using the models). The first one, which is referred to as the "fitting" method, a forecast model is fitted based on all of the data, which is then applied to forecast the streamflows successively. In the second procedure to evaluate the model performance part of the streamflow data are removed

from the available historical sample, a model is fitted based on the remaining data, which is then applied for forecasting the streamflows that were removed. Thus, the forecast errors can be evaluated. Subsequently the data that were removed are put back into the original data set and a second part of the data are removed, a model is fitted based on the remaining data, and the 2nd model is now used to forecast the 2nd set of values removed and to estimate the ensuing forecast errors. And this procedure is continued until the data set permits. For example, in the so-called "drop one" approach one removes a single data at a time, and the model fitting and forecast and error evaluation are determined one at a time. In this procedure the number of fitted forecast models is the same as the data sample size. In this study we also use a drop 10% approach whereby 10 % of the data set are dropped each time and the model fitting, forecast, and error estimation are made successively as explained above

5. Results and Discusion

5.1 Preliminary Data Analysis

Table 2 shows the basic statistics of the April-July streamflows for the 6 study sites. The means of the streamflows for these sites are basically in two groups, the first around 200~400 thousand acre-feet (TAF) and the second around 700~1000 TAF. The coefficient of variation (CV) for all sites are less than 1 and the lag-1 correlation coefficients are generally small (less than 0.25). The skewness coefficients vary in the range 0.25-1.30 and data transformations (to normal) are needed for some sites. The logarithmic transformation has been applied for some sites to decrease the skewness (not shown). Also similar results for the annual streamflows (April-March and October-September) were determined and the results for the two periods (not shown) are similar except for the skewness and ensuing transformation for Gunnison. In addition, Table 3 gives the cross-correlation coefficients of the April–July streamflows of the six sites. The cross-correlations vary in the range 0.40-0.95. Also the cross-correlation coefficients between the annual streamflows vary in the same range (not shown). As expected the magnitude of the correlations becomes smaller as the distance between the stations increases.

5.2 Correlation analysis and selection of potential predictors for April-July streamflows

Correlation analysis made between the April-July streamflows and the potential predictors such as snow water equivalent and sea surface temperature shows that for the 6 study sites the correlation coefficients between the streamflows and hydrological variables are high, and generally have the highest values compared to those for other types of variables. For

example, the correlation coefficients between the streamflows and SWE vary in the range 0.46-0.85. Also the correlation coefficients between the streamflows and PDSI vary in the range 0.28-0.70. On the other hand, the correlations with the April-July streamflows of the previous year (i.e. lag-1 correlation) are generally small and not significant. For illustration the correlations obtained for the Gunnison River for the predictors with absolute correlations greater or equal to 0.40 are shown in Table 7. Similar correlations were estimated for all six streamflow sites (all results are not shown for space limitations). Some atmospheric variables such as geopotential height and wind also have significant correlations with the streamflows. The values of the correlation coefficients for these variables vary in the range -0.67 to + 0.61. For example, Fig. 8 shows the correlation map for the April–July streamflows of the San Juan River versus the previous year Oct-Dec. global geopotential height (700 mb). It may be observed that the correlations vary in the range – 0.50 and +0.50 and there are several areas where the correlation coefficient may be about -0.4 or + 0.40. Note that part of the southwest U.S. has a correlation coefficient of about - 0.46. Figure 9 is another example showing the correlation map for the April–July streamflows of the Yampa River versus the global zonal wind for Oct-Dec of the previous year. The map shows that the zonal winds over the southwest U.S. have about 0.56 correlation with the Apr-Jul streamflows while the correlation is about – 0.52 for the zonal wind over western Canada. Similar correlation maps for other atmospheric variables and river sites are shown in Figures of the Appendix A1-A6.

Furthermore, sea surface temperature (SST) and some oceanic-atmospheric indices such as PDO may be also significantly correlated with the April-July streamflows for some of the sites in the study area. For example, Figure 10 is a correlation map of the April-July streamflows of Gunnison River versus the Oct-Dec (previous year) global SST. One may observe two large regions in the northern Pacific Ocean with significant correlation coefficients. One region shows positive correlation of about 0.45 and the other shows negative correlation of about – 0.45. The correlation maps for other time periods and sites show similar patterns. Thus from the correlation analysis several variables that have significant correlations with the streamflows are identified for each site. These variables are used as the potential predictors for further modeling and forecast. The number of the potential predictors for the April–July streamflow forecasts for the six sites ranges from 21 to 48. For illustration Table 17 shows the 20 variables (potential predictors) having the highest correlations for Gunnison River.

Likewise, correlation analysis was conducted for yearly streamflows for the Poudre and Gunnison rivers. For example, Figure 11 shows the correlation map for the yearly April–March streamflows of the Gunnison River and the global Jan-Mar SST. The map shows correlations varying in the range – 0.5 to + 0.5. Table xx shows 19 variables having the highest correlations for the April–March annual streamflows of Gunnison River. The correlation coefficients vary in the range – 0.49 to + 0.82. The table includes the variables identified as potential predictors but for comparison it also includes the correlation with the lag-1 streamflows, i.e. streamflows of the previous period April-March. Clearly SWE is the variable having the highest correlation. The results for the Poudre River are shown in Table A8.1 of Appendix A8. Also Fig. 12 shows the correlation map for the yearly October-September streamflows of the Gunnison River and the global July-Sept. SST. Table 19 shows that the potential predictors used for the October–September annual streamflows of the Gunnison River vary in the range – 0.45 to + 0.52. Note that in this case the correlations with SWE drops to 0.33. In fact, the results for the Poudre (not shown) suggest that SWE becomes insignificant. Clearly the time period where the year is defined is important. In the case of the year during the period April-March SWE plays a significant role because much of the runoff in the following months arises from the snowmelt that has been on the ground by April 1st. On the other hand, for the year defined in the period October-September either the role of SWE is small or not significant at all because much of the snow that has been on the ground by April 1st has been melted and does not contribute to the streamflow in the period that begins in October.

5.3 Forecast results for April–July streamflows at single sites

Table 20 shows the predictors included for forecasting the April–July streamflows based on the stepwise regression method for all six sites. Generally, there are 3 to 8 predictors and, as expected, SWE is the most important predictor for every site except for the Yampa River where it is 2nd best. Also the Palmer Index is an important predictor for Gunnisson and Yampa rivers but it is not an important predictor for the other sites. SST is an important predictor for 4 sites (Poudre, Arkansas, Gunnisson, and R. Grande) but it is not included as predictor for the San Juan and Yampa rivers. Wind (zonal or Meridional wind) is an important predictor for 5 of the 6 sites. Geopotential height (700 mb) and relative humidity are also good predictors for 4 of the 6 sites. And outgoing long wave radiation is a good predictor for two of the sites. Using the predictors shown in Table 20 (in standardized form) forecast models are built for the

standardized April–July streamfllows. The MLR forecast model has been fitted using all variables (predictand and predictors) in their original form. For easy of reference we refer to these models simply as MLR. The forecast equations for all sites are shown in Table 21. As expected the equations suggest that there is a time delay for the streamflows to respond to the variations of the atmospheric and oceanic variables.

The R-squares, forecast skill scores, and cross-correlation coefficients for the forecasted streamflow based on the MLR are shown in Tables 22a to 23b. In general the results obtained are quite good. For example, the Adj. R^2 for the drop-1 results of Table 22a show values in the range 0.48–0.80. The smaller values 0.48 and 0.49 correspond to the Arkansas and Poudre Rivers, respectively, while values in the range 0.68 to 0.80 correspond to the other four sites. Also the forecast skill results are quite reasonable with accuracy (AC) values for drop-1 in the range 0.49-0.68 and HSS for drop-1 in the range 0.32-0.57. Considering the various metrics it is clear that the better values are obtained for Gunnison, R. Grande, S. Juan, and Yampa rivers than for Arkansas and Poudre rivers. In addition, one may also judge how good the forecasts results are by observing the time series plots of the observed and forecasted values as well as the x-y plots of the observed versus the forecasts. The plots shown in Figures 13 and 14 for the Gunnison River illustrate that the forecasts obtained are quite good. The cross-correlation coefficients for the forecasted April–July streamflows are generally somewhat lower than those obtained from the historical data. This is especially noticeable for the Arkansas and Poudre rivers. The lower values obtained for the cross correlations are expected since the forecasts in this section were made on a site by site basis. Nevertheless the results are quite good for the Gunnison, R. Grande, S. Juan, and Yampa rivers.

In addition, we also applied PCA is carried out on all the potential predictors for each site. Then the PCs that explain most of the variance are used to fit a forecast model based on MLR. This type of model is referred simply as PCA model for short. For illustration Table 24 shows the variances of all the PCs for the Poudre River. From these results it is clear that the first 15 PCs generally accounts for at least 90% of the variance. Thus we considered the first 15 PCs for further analysis and the other PCs were ignored. Then MLR using the stepwise method was applied for predicting the April-July streamflows based on PCs. Table 25 shows the PCs that were obtained for each site and the estimated model parameters. Note that for most of the sites the first 3 PCs are included and the total number of PCs included in the model is either 5 or 6.

The forecasts results including the model performance, forecast skills, and cross-correlation coefficients for the streamflows using the PCA forecast models are shown in Tables 26 and 27. In general the forecasts using the PCA models are pretty good for most of the sites. The values of the drop-1 adj. R^2 are in the range 0.49–0.77. Again the smallest values are 0.49 and 0.54 for the Poudre and Arkansas rivers, respectively, and the values for the other sites are about 0.74 (average). Also the drop-1 forecast skill scores *AC* are in the range 0.49–0.68 and *HSS* vary around 0.32–0.57. It is noted that the drop-1 AC values for the Poudre and Arkansas rivers are 0.49 and 0.53, respectively, while the average AC for the other 4 rivers are about 0.61. Likewise, the drop-1 HSS scores for the Poudre and Arkansass rivers are 0.32 and 0.37, respectively, while the average HSS for the other sites are about 0.49. These performance measures confirm that there is some noted difference in the forecast performances of the six rivers where the better performance is obtained for the Gunnison, R. Grande, S. Juan, and Yampa rivers than for Poudre and Arkansas. As expected the cross-correlation coefficients of the forecasted streamflows are somewhat smaller than those of the observed streamflows because the forecasts have been made for each site independently. In this case still the cross-correlation for the Arkansas River are noticeable smaller than the historical ones, however overall it must be noted that the cross-correlations obtained using PCA are better than those obtained using the MLR model described above. Furthermore, Figs. 15 and 16 shows …..

5.4 Comparing Forecasts for Various Types of Predictors

In the previous section we assessed the forecast performances using the group of hydrologic, atmospheric, and oceanic predictors. Here we analyze the performance obtained by different groups of predictors. For example, because snow water equivalent (SWE) is considered to be the most (obvious) important predictor of streamflows during the period April-July and also the Palmer drought severity index (PDSI) has been in most cases the second best predictor, we examined the results we would obtain if we eliminated SWE and PDSI from the pool of predictors. This case is relevant especially for ungaged basins where no rainfall and snowfall data over the basin information may be available. Thus we considered two cases where, only the atmospheric and oceanic variables are included as possible predictors or only oceanic variables are included (as predictors) for forecasting the April-July streamflows. For this purpose we used the data of the Gunnison River only. Table 28 gives the forecast models obtained and Tables 29 and yy give the results of the model performance and the forecast skill scores, respectively. The

scatter plots and time series of the forecast results for this model as compared to the historical can be found in Figure D6.1 and D6.2 of Appendix D6. The adj. R^2 values for drop-1 validation is about 0.50 and the values for AC and HSS forecast skill scores are 0.47 and 0.30, respectively. The results show that the forecast model based on atmospheric/oceanic predictors only can still capture a good portion of the streamflows variations of the observed data.

Figure 18 (top) compares the R^2s (fitting and drop-1) obtained for the forecast models based on PCA considering the three cases: all predictors, i.e. hydrologic + atmospheric + oceanic, atmospheric + oceanic predictors, and oceanic predictors only. Also Fig. 18 (middle and lower) compares the *AC* and *HSS* forecasts skill scores for the three cases. As expected the model using all of the variables has better performance than those using only the atmospheric/oceanic (climatic) variables or using only oceanic variables. But the comparison, rather than highlighting the fact that the model that includes all variables has better performance than the other, is actually to point out how beneficial may be for long range forecasting based solely on atmospheric/oceanic variables. In addition, one may observe from Figure D6.1 that the model based on atmospheric/oceanic variables only tends to underestimate the high flows and overestimate the low flows. The range of the forecasted flows is narrower than that arising from the model where all variables are included. Figure D6.2 compares the time series of observed and forecasted flows. It shows that using a forecast model based solely on atmospheric/oceanic variables can capture reasonably well the streamflow variations of the Gunnison River.

5.5 Forecast results for April-July streamflows based on multisite models

Forecast models are fitted for all six sites simultaneously using the CCA method and the results are compared with those obtained using the single site PCA models. Before building the CCA model, PCA was performed on all the potential predictors for all sites, and some of the resulting PCs are selected and used in the CCA model. To select the proper PCs, the variance loadings of each PC are examined. Table 30 shows the variances of the PCs obtained (a total of 207 PCs because there are 207 potential predictors for all six sites as listed in Tables A7.1-A7.6 of Appendix A7). It may be seen that the percentage variance drops steadily as the number of PCs increases and the first 20 PCs account for a major part of the variance and that each of the PCs beyond the 20th only counts for less than 1% of the variances. Thus based on the loadings of each PC and how the loading of the PCs are flattening out, the first 20 PCs are considered for further modeling, and the PCs that eventually are selected in the CCA model will be determined

according to the residual analysis described in the following section. The PCs that gave bigger residuals were eliminated. The first 20 PCs are added into the CCA model one at a time until all the 20 PCs are added. For illustration Figure 20 shows for the Poudre River the sum of squared residuals obtained from CCA models fitted by adding the PCs sequentially (up to 20 PCs are shown). One may observe that adding the PC5 increases sharply the sum of squared residuals. For other sites this was also observed for PC8. Consequently these two PCs were removed from the CCA model. Meanwhile the PCs beyond the 11^{th} either cause more errors or have little effects. Therefore the final CCA model uses the PCs 1-4, 6, 7, and 9-11 as the predictors.

After the determination of the PCs, CCA model parameters are estimated. The estimated eigen values are: $\lambda_1 = 0.929$, $\lambda_2 = 0.781$, $\lambda_3 = 0.755$, $\lambda_4 = 0.587$, $\lambda_5 = 0.396$, and $\lambda_6 = 0.207$ (note that the square roots of λ's are the canonical correlation coefficients ρ's). The matrices $\boldsymbol{a}$ and $\boldsymbol{b}$ are shown in Tables B3.1 and B3.2 of Appendix B3. The significant test is then performed on the ρ's. The value for the test statistic is 81.6 which is greater than the critical value of 41.2. Therefore, the correlation between the PCs selected into the CCA model and the streamflows of the 6 sites is significant, and all the canonical variates should be used in the CCA model.

Tables 31 and 32 show the results of the forecasts using the CCA model and Figures 21 and 22 show the comparison of the forecasted streamflows using the CCA model versus the observed flows of the Gunnison River. Similar plots for all other sites can be found in the Appendix D2. For all the sites except Poudre the adj-R^2 (for validation drop-1) are higher than 0.5, and the forecast skill scores (for validation drop-1) are higher than 0.3. The drop-1 adj. R^2 for the Poudre is 0.33 but for the other 5 sites it is about 0.59 (average), which is pretty good. Likewise, the drop-1 *AC* score for Poudre is 0.43 while for the other sites it is about 0.55. And the drop-1 *HSS* score for the Poudre is 0.24 while for the other sites is about 0.40. Thus as in the previous results there is a clear difference of the results obtained for the Gunnison, R. Grande, S. Juan, Yampa, and Arkansas respect to that obtained for the Poudre river. Note that in previous results the forecasts for Poudre and Arkansas were inferior to the other four, but in this case only Poudre is inferior to the other five. As before, some of the cross-correlation coefficients are somewhat underestimated relative to those of the observations. The main difference occurs with cross-correlations that involve Arkansas although the largest underestimation occurs for the cross-correlation between Gunnison and R. Grande. On the average the percent difference is about – 8% but the error could be as high as – 43.5 % (for Gunnison and R. Grande). The scatter

plot and time series, however, reveal some underestimation of the forecasted streamflows particularly for low magnitude or high magnitude flows (Figures 21 and 22).

Figure 23 compares the R^2s obtained for the forecasts based on the PCA and CCA models for all sites. As expected the R^2s for the PCA models are somewhat better (higher) than those obtained from the CCA models (except for Arkansas). But generally the differences are not large. The biggest difference is for S. Juan River for drop-1 R^2 that gives 0.77 for PCA versus 0.62 for CCA. Also comparing the forecast skill scores obtained from PCA (Table 26b) versus those obtained from CCA (Table 31b) suggest that the PCA forecast performances are generally better than those for the CCA. Comparing the results of the cross-correlations it appears that the cross-correlations obtained from CCA are not better than those from PCA and in fact in two cases they are much worse. This contradicts what one would have expected. Also Figures D2.1-D2.6 in Appendix D2, compares the time series of the forecasts and the historical time series obtained from PCA and CCA models. And Figures D4.1-D4.6 compares the corresponding scatter plots. It is clear that in many cases the CCA underestimates the peaks while the PCA does a better job in this regard.

In addition to CCA a forecast procedure was evaluated whereby all April-July streamflows for all 6 sites were aggregated to form a single time series at an index station. Then PCA was applied to forecast the aggregated flows at the single station, which were spatially disaggregated into the April-July flows at the six individual sites. The spatial disaggregation was carried out using the Valencia-Schaake model. The R^2s varied across the study region with drop-1 adj. R^2s equal to 0.19 and 0.35 for Poudre and Yampa and about 0.54 (average) for the other 4 rivers. Also the drop-1 *AC* scores varied in the range 0.32-0.57 with about 0.38 (average) for Poudre, S. Juan, and Yampa while about 0.52 (average) for Arkansas, Gunnison, and R. Grande. Likewise, the drop-1 *HSS* scores vary in the range 0.10-0.42 with about 0.17 (average) for Poudre, S. Juan, and Yampa and about 0.36 (average) for Arkansas, Gunnison, and R. Grande rivers. Thus it is apparent that the R^2s and forecast skill scores give modest values for one group of rivers and better (although still modest) values for another group. Also scatter plots and time series comparisons of the forecasted and historical values were made. The forecast results for the aggregation–disaggregation method are not very good for some sites such as the Poudre, S. Juan, and Yampa rivers. For the other sites the results are better and perhaps reasonable. The cross-correlations are not well reproduced, in fact half of the cross-correlations are significantly

underestimated. Figure 27 compares the R^2s obtained for forecast based on PCA, CCA, and aggregation-disaggregation methods. It is clear that in most cases the latter method has lower R^2s values than the other two methods. Likewise, comparing the forecast skill scores for half of the rivers the scores obtained by the aggregation-disaggregation method are significantly smaller than those obtained by the other two methods. Therefore, it is concluded that the aggregation-disaggregation method does not offer any advantage respect to PCA and CCA methods.

5.6 Forecast results for yearly streamflows

Forecasts for yearly April-March and October-September streamflows have been done for the Gunnison and Poudre rivers. We wanted to examine how the PCA forecast models performed for a long time period, i.e. a year, and for two different definitions of years because the antecedent conditions for both may be quite different.

Figure 11 shows the correlation map for January-March SST versus the yearly April-March streamflows of the Gunnison River. The predictors have been selected by using similar correlation maps and the results for both Poudre and Gunnison rivers are shown in Tables A8.1 and A8.3, respectively in Appendix A8. Also Table 35 gives the parameters of the PCA model for Gunnison River and Tables 36 and C1.1 (in Appendix C1) give the forecast performance results for eh Gunnison and Poudre rivers, respectively. It is clear that the performance results for the Gunnison are quite good with drop-1 adj. R^2s of 0.64 and forecast skill scores *AC* and *HSS* of 0.57 and 0.42, respectively. Compared to the corresponding results for the April-July forecasts the values are 0.73, 0.57, and 0.42, respectively. The performance results for the Poudre are lower than for Gunnison but still are acceptable.

In comparison with the results of the April-July streamflow forecast by the PCA model for the Gunnison River, the potential predictors are very similar for both models. However, the number of the potential predictors for the annual streamflow forecast model is fewer than for April-July, mostly because the SST regions with significant correlations are fewer for the annual streamflow forecast. As expected SWE is still the best predictor (Table A8.3) for predicting the April-March streamflows as was for predicting the April-July flows, however, PDSI is not included in the pool of significant predictors as was the case for the April-July forecast. For Poudre SWE is also the most important predictor as shown in Table A8.1 but in this case PDSI is included in the pool of predictors. The PCA results are quite similar for the two models with the variance loadings for the first PC around 30% for both models. The patterns of declining of the

PC loadings are also similar for both models. As far as the forecast results, the forecast for the April-July streamflows are better than for the annual streamflow forecast, but the analysis proved that good forecasts can be obtained at the annual time scale April-March.

The forecasts for the annual period October-September is more challenging than forecasting for April-March and the reason is that in the latter there is the benefit of knowing how much snow fell and accumulated on the basin during the previous months (i.e. using SWE). On the other hand, for the year that begins in October the snowpack say as of April 1st gives very little information because most if not all of the snowpack as of April 1st likely melts during the Summer months and does not contribute to the runoff in the following year (October-September). Therefore, how efficient the streamflow forecast is for the year that begins in October largely depends on the state of the atmospheric/oceanic information prior to October. Table 19 shows the list of potential predictors obtained from the correlation maps for the yearly October-September streamflows for the Gunnison River. Likewise, Table A8.2 gives the predictors for Poudre River. Note that for Gunnison SWE for May still appears as a potential predictor but this is not so for the Poudre.

The PCA model parameters for Gunnison River are shown in Table 37 and the performance measures are given in Table 38. And the performance measures for the Poudre River are shown in Table C1.2 of Appendix C1. Table 38 shows quite reasonable values for R^2, *AC*, and *HSS*. For example, the drop-1 adj. R^2 is 0.50 and the corresponding values of AC and HSS are 0.47 and 0.30, respectively. As expected these forecast performance measures are somewhat smaller than those obtained for the year April-March. For example, the drop-1 adj. R^2 drops from 0.64 (April-March) to 0.50 (October-September). Nevertheless as stated above the performance measures obtained are quite reasonable.

In comparison to the results of the April–March annual streamflow forecast for the Gunnison River the PCA results are a little bit different for the two models because the patterns of the PC loadings declining is a little different, and the variance loading for the 1st PC is lower for the October–September yearly model. As far as the forecast results, the forecast for the October–September annual streamflows are worse than those for the April–March annual streamflow. The biggest reason for this is obviously the absence of SWE as a predictor for the October-September period. Nevertheless the forecast performance even at the yearly time frame are still quite reasonable.

6. Conclusions and Recommendations

Water resources management has been an important subject in the State of Colorado for many decades. The increasing water demands due to population growth in the state and the additional water requirements for various other uses have made the management problem more complex. In addition, the concerns of the effects of climate variability and change on water resources have made the management problem even more challenging and water systems managers and administrators have been looking for ways to make improved and efficient management decisions. The research reported herein concerns on streamflow forecasting on a seasonal and yearly basis.

Forecast models were developed for two time scales, namely for total streamflows during April–July, and for yearly streamflows for the periods April–March and October–September (i.e. the water year streamflows). Also different modeling schemes were adopted and the role of hydrologic and atmospheric/oceanic factors in forecast performance examined. They are summarized as: (1) Single site models for forecasting April-July streamflows. MLR models were fitted where the predictors (independent variables) and the predictand (dependent variable) are in the original domain. Alternatively PCA models were fitted where the predictors are PCs but the dependent variable (streamflow) is in the original domain, i.e. a MLR is built where the predictand is streamflow and the predictors are PCs. (2) Also PCA models were built to analyze the forecast performance of using models based on atmospheric and oceanic predictors only, i.e. hydrologic variables such as SWE and PDSI were not included. This analysis was made for the Gunnison River only. (3) Multisite models for forecasting the April-July total streamflows. A CCA model was applied to forecast the April-July streamflows and results were compared with those obtained from the PCA models. Also an alternative method was developed to forecast streamflows at all six sites. Firstly, the April-July streamflows at the 6 sites were aggregated into a single series, then a forecast model was built for the single site aggregated flows. The forecast made for the total streamflow are then dissagregated spatially to obtain the flows at the individual sites. (4) Single site models for forecasting yearly streamflows. PCA models were used to forecast yearly streamflows for the periods April-March and October-September. In this case the analysis was made for the Gunnison and Poudre rivers only.

The various forecast models, applications and comparisons thereof as summarized above led to the following conclusions:

(1) Correlation analysis conducted for forecasting seasonal and annual streamflows for six rivers in the State of Colorado indicates that hydrological variables such as snow water equivalent (SWE) and Palmer drought severity index (PDSI) have the highest significant correlations especially with seasonal April-July streamflows. It has been shown that SWE is still the predictor with the highest correlation for forecasting yearly April-March streamflows. However, a number of atmospheric/oceanic variables such as global geopotential heights, wind, relative humidity, and sea surface temperature also have significant correlations and can be useful predictors for forecasting seasonal and yearly streamflows.

(2) The forecast performances of multiple linear regression (MLR) and principal component analysis (PCA) models for forecasting the seasonal April-July total streamflows in the State of Colorado (represented by six major rivers) by using hydrologic, atmospheric, and oceanic predictors are very good. The performances measures obtained from MLR and PCA models are quite comparable. The advantage of using MLR models over PCA models is perhaps in the direct specification and identification of the various predictors that enter in the models. In contrast PCA models involve predictors in terms of principal components (PCs). On the other hand, the advantage of using PCA models has been in a better reproduction of historical cross-correlations among sites (compared to MLR models).

(3) It has shown that the role atmospheric and oceanic factors play in forecasting seasonal and yearly streamflows in Colorado rivers is very significant. For example, for forecasting the April-July streamflows for Gunnison River the drop-1 adj. R^2 is about 0.5, which is pretty good. Likewise, forecasting the yearly October-September streamflows is essentially based on atmospheric/oceanic predictors yet the results are quite reasonable. It is concluded that atmospheric/oceanic predictors alone can predict reasonable well the streamflow variations of the Gunnison River on a seasonal and yearly time scales.

(4) PCA models were applied for forecasting yearly April-March and October-September streamflows. It has been shown that good forecasting performances can be achieved for such yearly time scales. Better results are obtained for forecasting the yearly April-March than for the yearly October-September streamflows, because the former has the advantage of including hydrologic predictors such as snow water equivalent, i.e. the state

of wetness and snowpack in the basin prior to the year of concern are known or estimated, whereas for the latter such information is less significant or not useful because for the year that begins in October most if not all potential snowpack in the basin may have been melted already. Thus the forecasts for the yearly October-September rely almost solely on atmospheric and oceanic data. Nevertheless the forecast results obtained are quite reasonable.

(5) Two methods were developed to forecasts April-July streamflows at the six study sites jointly. The first method involves applying canonical correlation analysis (CCA) and the second one is based on PCA and aggregation-disaggregation. The forecast results obtained based on CCA are quite good. However, the results are inferior to those obtained from PCA. This is also true when comparing the cross-correlations. Therefore, it is concluded that in forecasting the April-July streamflows for Colorado rivers using CCA we did not find any advantage over the forecasts obtained from using PCA at single sites. We also tested the applicability of forecasting the aggregated streamflows (April-July) for all six sites using PCA and then disaggregating that quantity into the streamflows for the individual sites. Our experiments suggest that for some sites the results are modest and for other sites the results are poor. It is concluded that the aggregation-disaggregation procedure does not offer any advantage respect to the PCA and CCA methods.

(6) Finally in applying the various forecasting methods as described above for six rivers in the State of Colorado, namely Poudre, Arkansas, Rio Grande, San Juan, Gunnison, and Yampa, it has been clear that much better forecast performance is achieved for the last four rivers than for Poudre and Arkansas. It is not clear the reason why of the difference except to note that these two streams are much smaller than the other four, i.e. the means and standard deviations for these two rivers are smaller than for the other four. Likewise the skewness for Poudre are significantly bigger than for the others.

The study reported herein suggests the following recommendations:

1. The study undertaken as describe above centered on forecasting seasonal April-July and yearly April-March and October-September. It may be useful exploring streamflow forecasting for other time scales and time periods, shorter and longer than those experimented here.

2. The study reported here made a limited examination of estimating monthly streamflows based on the forecasted total streamflows for a given time period, e.g. April-July. The estimation of monthly streamflows was carried using a parametric disaggregation scheme. And the results have been quite limited. A logical extension of the study would be exploring other estimation procedures such as nonparametric techniques. Likewise, a procedure for forecasting at all sites jointly was developed by aggregating the flows at all sites, conducting a forecast for the aggregated flows, and then disaggregating such total to obtain the streamflows (forecasts) at every other site in the region. The results were modest at best, but could be improved by further examination of alternative procedures based on nonparametric techniques.
3. The study reported herein concentrated on forecasting at the seasonal and yearly time frames with a brief limited exploration on monthly. It may be worth expanding the initial efforts to forecasting at finer time scales such as weekly and daily.

References

Barnett, T.P., and R.W. Preisendorfer. 1987. *Origins and levels of monthly and seasonal forecast skill for United States surface air temperatures determined by canonical correlation analysis.* Mon. Wea. Rev., 115, 1825-1850.

Barnston, A.G. 1994. *Linear statistical short-term climate predictive skill in the northern hemisphere.* J. of Climate, Vol. 7, Issue 10, pp1513–1564.

Barnston, A.G., and Y. He, 1996. *Skill of CCA forecasts of 3-month mean surface climate in Hawaii and Alaska.* J. Climate, Vol. 9.

Cane, M.A., S.E. Zebiak, and S.C. Dolan. 1986. *Experimental forecasts of El Nino*. Nature, 321, 827-832.

Canon, J., J. Gonzalez, and J. Valdes. 2007. *Precipitation in the Colorado River Basin and its low frequency associations with PDO and ENSO signals*. Journal of Hydrology, 333, 252– 264.

Cayan D.R., and R.H. Webb. 1992. *El Niño/Southern Oscillation and streamflow in the western United States.* In: Historical and Paleoclimate Aspects of the Southern Oscillation, Ed. H.F. Diaz and V. Markgraf, Cambridge University Press, pp. 29–68.

Cayan D.R., M.D. Dettinger, H.F. Diaz, and N. Graham. 1998. *Decadal variability of precipitation over western North America.* J. Climate, 11**,** 3148–3166.

Clark, M.P., M.C. Serreze, and G.J. McCabe. 2001. *Historical effects of El Niño and La Niña events on seasonal evolution of the montane snowpack in the Columbia and Colorado River Basins.* Water Resources Research, 37(3), 741-757.

Chen, L., and A. Bradley. 2006. *Adequacy of using surface humidity to estimate atmospheric moisture availability for probable maximum precipitation*. Water Resour. Research, Vol. 42.

Derksen, C., K. Misurak, E. LeDrew, J. Piwowar, and B. Goodison. 1997. *Relationship between snow cover and atmospheric circulation, central North America winter 1988*. Annals of Glaciology 25.

Dettinger, M.D., D.R. Cayan, H.F. Diaz, and D. Meko. 1998. *North-south precipitation patterns in western North America on interannual-to-decadal time scales*. J. Climate, 11, 3095-3111.

Eldaw, A.K., J.D. Salas, and L.A. Garcia. 2003. *Long range forecasting of the Nile River flow using large scale oceanic atmospheric forcing.* J. Appl. Meteor., Vol. 42.

Eltahir, E.A.B. 1996. *El Niño and the natural variability in the flow of the Nile River*. Water Resources Research, 32 (1),131-137.

Garson, G.D. 2003. *Canonical correlation*. Available at: http://www2.chass.ncsu.edu/garson/pa765/canonic.htm.

Fujikoshi, Y. 1977. *Asymptotic expansions for the distributions of some multivariate tests*. In: P.R. Krishnaiah (Ed.), Multivariate Analysis-IV, North-Holland, Amsterdam, 1977, pp. 55-71.

Giri, N.C. 2004. *Multivariate Statistical Analysis*. Second Edition, Revised and Expanded, Marcel Dekker, Inc.

Glahn, H.R. 1968. *Canonical correlation and its relationship to discriminant analysis and multiple regression.* Journal of the Atmospheric Sciences, Vol. 25, 23-31.

Grantz, K., B. Rajagopalan, M. Clark, and E. Zagona. 2005. *A Technique for incorporating large-scale climate information in basin-scale ensemble streamflow forecasts*. Water Resources Research, 41.

Haan, C.T. 2002. *Statistical Methods in Hydrology*. Second Edition, The Iowa State Press, 312-313.

Haltiner J.P., and J.D. Salas. 1988. *Short-Term forecasting of snowmelt runoff using ARMAX model*. Water Resources Bulletin, 24(5), 1083-1089.

Hamlet, A.F., and D.P. Lettenmaier. 1999. *Effects of climate change on hydrology and water resources in the Columbia River Basin*. Am. Water Res. Assoc., 35(6), 1597-1623.

He, Y., and A.G. Barnston. 1996. *Long-lead forecasts of seasonal precipitation in the tropical Pacific islands using CCA.* J. of Climate, Vol. 9, 2020–2035.

Hidalgo, H.G., and J.A. Dracup. 2003. *ENSO and PDO effects on hydroclimate variations of the Upper Colorado River Basin.* J. Hydrometeorol., 4.

Higgins, R.W., A. Leetmaa, Y. Xue, and A. Barnston. 2000. *Dominant factors influencing the seasonal predictability of U.S. precipitation and surface temperature*. J. Climate 13, 3994-4017.

Johnson, R.A., and D.W. Wichern. 1988. *Applied Multivariate Statistical Analysis*. 2nd edition, Prentice-Hall, Inc.

Jolliffe, I.T. 1986. *Principal Component Analysis.* Sringer-Verlag, New York.

Kalnay E., M. Kanamitsu, R. Kistler, W. Collins, D. Deaven, L. Gandin, M. Iredell, S. Saha, G. White, J. Woollen, Y. Zhu, M. Chelliah, W. Ebisuzaki, W.Higgins, J. Janowiak, K. C. Mo, C. Ropelewski, J. Wang, A. Leetmaa, R. Reynolds, R. Jenne, and D. Joseph. 1996. *The NCEP/NCAR 40-Year Reanalysis Project.* Bulletin of the American Meteorological Society 77 (3): 437–471.

Kendall, M. 1980. *Multivariate Analysis*. Second Edition, MacMillan Publishing Co., Inc., New York.

Manly, B.F.J. 1994. *Multivariate Statistical Methods-A Primer*. Second Edition, Chapman & Hall.

Maity, R., and D.N. Kumar. 2008. *Basin-scale stream-flow forecasting using the information of large-scale atmospheric circulation phenomena*. Hydrological Processes, 22 (5), pp. 643-650.

Mantua, N.J., S.R. Hare, Y. Zhang, J.M. Wallace, and R.C. Francis. 1997. *A Pacific decadal climate oscillation with impacts on salmon.* Bulletin of the American Meteorological Society, Vol. 78, pp 1069-1079.

Maurer, E.P., and D.P. Lettenmaier. 2003. *Predictability of seasonal runoff in the Mississippi River basin.* J. Geophys. Res., 108.

Maurer, E.P., D.P. Lettenmaier, and N.J. Mantua. 2004. *Variability and potential sources of predictability of North American runoff*. Water Resour. Research, Vol. 40.

McCabe, G.J. and M.D. Dettinger. 1999. *Decadal variations in the strength of ENSO teleconnections with precipitation in the western United States.* International Journal of Climatology. 19: 1399-1410.

McCabe, G.J., and M.D. Dettinger. 2002. *Primary modes and predictability of year-to-year snowpack variations in the western United States from teleconnections with Pacific Ocean climate*. Journal of Hydrometeorology, v. 3, p. 13-25.

McCabe, G.J., M.A. Palecki, and J.L. Betancourt. 2004. *Pacific and Atlantic Ocean influences on multidecadal drought frequency in the United States*. Proc. Nat. Acad. Sciences U.S.A.,101, 4136–4141.

Moss, M.E., C.P. Pearson, and A.I. McKerchar. 1994. *The Southern Oscillation index as a predictor of the probability of low streamflows in New Zealand*. Water Resour. Res*.,* 30, 2717–2713.

Piechota, T.C. and J.A. Dracup. 1996. *Drought and regional hydrologic variation in the United States: Associations with the El Niño-Southern Oscillation*. Water Resources Research 32 (5), pp. 1359–1373.

Piechota, T.C., J.A. Dracup, and R.G. Fovell. 1997. *Western U.S. streamflow and atmospheric circulation patterns during El Niño-Southern Oscillation (ENSO).* Journal of Hydrology, 201(1-4), 249-271.

Redmond, K.T., and R W. Koch. 1991. *Surface climate and streamflow variability in the western United States and their relationship to large scale circulation indices*. Water Resour. Res**,** 27*,* 2381–2399.

Regonda, S.K., B. Rajagopalan, M. Clark, and E. Zagona. 2006. *A multimodel ensemble forecast framework: Application to spring seasonal flows in the Gunnison River Basin*. Water Resources Research, Vol. 42.

Ribeiro-correa, J., G.S. Cavadias, B. Clement, and J. Rousselle. 1995. *Identification of hydrological neighborhoods using canonical correlation-analysis.* Journal of Hydrology, 173(1-4), pp71-89.

Ropelewski, C.F. and M.S. Halpert. 1987. *Global and regional scale precipitation patterns associated with El Niño/Southern Oscillation*. Mon. Wea. Rev. 115:1606-1626.

Salas J.D., C. Fu, A. Cancelliere, D. Dustin, D. Bode, A. Pineda A, and E. Vincent. 2005. *Characterizing the severity and risk of drought in the Poudre River, Colorado.* Journal of Water Resources Planning and Management 131(5): 383-393.

Shabbar, A., and A.G. Barnston. 1996. *Skill of seasonal climate forecasts in Canada using Canonical Correlation Analysis.* Mon. Wea. Rev., Vol. 124, 2370-2385.

Shahin, M. 1985. *Hydrology of the Nile Basin*. Elsevier Science Publishers B.V., Amsterdam, The Netherlands.

Srivastava, M.S. 2002. *Methods of Multivariate Statistics*. John Willey & Sons, Inc.

Statsoft, Inc. 2003. *Canonical Analysis*. Available at: http://www.statsoft.com/textbook/stcanan.html.

Thompson, B. 1984. *Canonical Correlation Analysis: Uses and Interpretation*. SAGE Publications, Inc.

Tootle, G.A., and T.C. Piechota. 2006. *Relationships between Pacific and Atlantic ocean sea surface temperatures and U.S. streamflow variability.* Water Resources Research, Vol. 42.

Tootle, G.A., T.C. Piechota, and A.K. Singh. 2005. *Coupled oceanic-atmospheric variability and U.S. streamflow*. Water Resour. Res., 41.

Wang D.C., and D. J. Salas. 1991. *Forecasting Streamflow for Colorado River Systems*. Colorado Water Resources Research Institute, Completion Report No. 164.

Wallace, J., and D. Gutzler. 1980. *Teleconnections in geopotential height field during the Northern Hemisphere winter*. Monthly Weather Review, Vol. 109.

Wilks, D.S. 2006. *Statistical Methods in the Atmospheric Sciences.* 2nd Edition, Elsevier Inc, pp519-522.

Table 1. Brief description of the river basins and stream gaging stations utilized in the study

River and site names	Basin	USGS ID	Coordinates		Elevation (ft)	Drainage Area (mi^2)
			Latitude	Longitude		
Cache la Poudre River at Mouth of Canyon, CO	South Platte	06752000	40°39'52"	105°13'26"	5,220	1,056
Arkansas River at Canon City, CO	Arkansas	07096000	38°26'02"	105°15'24"	5,342	3,117
Gunnison River above Blue Mesa Dam, CO	Colorado	09124700	38°27'08"	107°20'51"	7,149	3,453
Rio Grande below Taos Junction Bridge near Taos, NM	Rio Grande	08276500	36°19'12"	105°45'14"	6,050	9,730
San Juan River near Archuleta, NM	Colorado	09355500	36°48'05"	107°41'51"	5,653	3,260
Yampa River near Maybell, CO	Yampa-White	09251000	40°30'10"	108°01'58"	5,900	3,410

Table 2 Basic statistics for the April–July streamflows for the six stations used in the study

Sites	Mean	Std	CV	Skewness coef.	Min	Max	Lag-1 corr. coef.
Poudre	231,000	89,370	0.387	1.273	90,120	600,100	0.144
Arkansas	320,600	125,800	0.393	0.590	79,540	637,000	0.194
Gunnison	747,500	289,100	0.387	0.516	181,800	1456,000	0.111
Rio Grande	392,000	318,700	0.813	0.431	7,521	1068,000	0.151
San Juan	743,600	384,500	0.517	0.588	102,400	1747,000	-0.104
Yampa	995,200	352,100	0.354	0.268	298,800	1975,000	0.221

Table 3 Cross-correlation coefficients for April–July historical streamflows in the study area

Sites	Poudre	Arkansas	Gunnison	Rio Grande	San Juan	Yampa
Poudre	1	0.68	0.65	0.41	0.47	0.72
Arkansas	0.68	1	0.95	0.73	0.70	0.82
Gunnison	0.65	0.95	1	0.69	0.72	0.87
Rio Grande	0.41	0.73	0.69	1	0.88	0.46
San Juan	0.47	0.70	0.72	0.88	1	0.49
Yampa	0.72	0.82	0.87	0.46	0.49	1

Table 11 Variances of PCs for the April–July streamflows of the six study sites

PCs	Variance	% of total	Accumulated %
PC1	4.437	73.9	73.9
PC2	0.900	15.0	88.9
PC3	0.380	6.3	95.3
PC4	0.144	2.3	97.6
PC5	0.111	1.8	99.4
PC6	0.029	0.5	100.0

Table 12 PCA weights of the April–July streamflows of the six study sites

PCs	Flows (site name)					
	Poudre	Arkansas	Gunnison	Rio Grande	San Juan	Yampa
PC1	-0.358	-0.452	-0.452	-0.384	-0.391	-0.404
PC2	0.458	0.072	0.096	-0.563	-0.515	0.441
PC3	0.796	-0.254	-0.382	0.105	0.222	-0.308
PC4	-0.117	-0.582	-0.027	-0.277	0.553	0.515
PC5	0.032	0.234	0.366	-0.638	0.407	-0.488
PC6	0.118	-0.577	0.711	0.205	-0.248	-0.211

Table 13 Variances of PCs for the April–March streamflows of the six study sites

PCs	Variance	% of total	Accumulated %
PC1	4.60	76.7	76.7
PC2	0.78	13.0	89.7
PC3	0.35	5.9	95.6
PC4	0.15	2.4	98.1
PC5	0.08	1.4	99.5
PC6	0.03	0.5	100.0

Table 14 PCA weights of the April–March streamflows of six study sites

PCs	Flows (site name)					
	Poudre	Arkansas	Gunnison	Rio Grande	San Juan	Yampa
PC1	-0.356	-0.445	-0.443	-0.393	-0.402	-0.405
PC2	0.530	0.062	0.075	-0.551	-0.491	0.406
PC3	0.745	-0.262	-0.411	0.134	0.285	-0.330
PC4	-0.112	-0.550	-0.304	0.270	0.055	0.718
PC5	0.078	0.293	-0.258	0.627	-0.667	-0.056
PC6	0.138	-0.584	0.686	0.242	-0.261	-0.206

Table 15 Variances of PCs for the October – September streamflows of six sites

PCs	Variance	% of total	Accumulated %
PC1	4.44	74.0	74.0
PC2	0.87	14.6	88.6
PC3	0.37	6.1	94.7
PC4	0.17	2.8	97.5
PC5	0.12	2.0	99.5
PC6	0.03	0.5	100.0

Table 16 PCA weights of the October – September streamflows of six sites

PCs	Flows (site name)					
	Poudre	**Arkansas**	**Gunnison**	**Rio Grande**	**San Juan**	**Yampa**
PC1	-0.356	-0.451	-0.449	-0.387	-0.392	-0.405
PC2	0.500	0.078	0.091	-0.548	-0.523	0.403
PC3	0.772	-0.209	-0.412	0.126	0.240	-0.341
PC4	-0.057	-0.540	-0.314	0.358	-0.034	0.690
PC5	0.044	0.358	-0.190	0.598	-0.675	-0.145
PC6	-0.148	0.571	-0.697	-0.221	0.241	0.244

Table 17 Potential predictors for forecasting the April-July streamflows of the Arkansas River

No	Name	Variable	Time	Location	General description	Corr. Coef
1	AF1	Accumulated flow of previous months	Prev. Apr-Mar		Accumulated flow volumes for previous 12 months	0.23
2	SST1	Sea Surface Temperature	Jan-Mar	25°N-30°N 160°E-165°E	Northwest Pacific	-0.46
3	SST2	Sea Surface Temperature	Prev. Oct-Dec	25°N-30°N 160°E-165°E	Northwest Pacific	-0.39
4	SST3	Sea Surface Temperature	Prev. Jul-Sep	25°N-35°N 20°W-30°W	Northwest Atlantic	-0.45
5	SST4	Sea Surface Temperature	Prev. Apr-Jun	35°N-45°N 20°W-25°W	Northwest Atlantic	-0.35
6	GH1	Geopotential Height (700 mb)	Prev. Oct-Dec	38°N-47°N 116°W-122°W	Western U.S.	-0.39
7	GH2	Geopotential Height (700 mb)	Prev. Oct-Dec	42°N-50°N 70°W-80°W	Eastern Canada and U.S.	0.47
8	GH3	Geopotential Height (700 mb)	Prev. Oct-Dec	28°N-33°N 172°E-180°E	North central Pacific	-0.31
9	MW1	Meridional Wind (700 mb)	Prev. Oct-Dec	45°N-55°N 130°W-135°W	Northeast U.S.	0.50
10	MW2	Meridional Wind (700 mb)	Prev. Oct-Dec	35°N-45°N 55°W-60°W	Eastern Canada and eastern U.S.	0.53
11	ZW1	Zonal Wind (700 mb)	Prev. Oct-Dec	48°N-57°N 105°W-118°W	Southern Canada	-0.42
12	ZW2	Zonal Wind (700 mb)	Prev. Oct-Dec	27°N-32°N 100°W-118°W	Southern U.S.	0.50
13	AT1	Air Temperature	Prev. Oct-Dec	35°N-48°N 115°W-130°W	Northwest U.S.	-0.41
14	OLR1	Outgoing Long-Wave Radiation	Prev. Oct-Dec	40°N-45°N 115°W-120°W	Western mountain states of U.S.	-0.29
15	RH1	Relative Humidity	Prev. Oct-Dec	40°N-45°N 117°W-122°W	Western mountain states	0.37
16	RH2	Relative Humidity	Prev. Oct-Dec	28°N-35°N 75°W-80°W	Southeast coast of U.S.	0.49
17	PDSI1	Palmer Index	Jan-Mar		Climate Division	0.35
18	PDSI2	Palmer Index	Prev. Nov-Dec		Climate Division	0.28
19	SWE1	Snow Water Equivalent	Feb 1st		Basin average	0.56
20	SWE2	Snow Water Equivalent	Mar 1st		Basin average	0.56
21	SWE3	Snow Water Equivalent	Apr 1st		Basin average	0.60

Table 18 Potential predictors for forecasting the April-March streamflows of the Gunnison river

No	Name	Variable	Time	Location	General description	Corr. Coef
1	AF1	Lag-1 flow	Prev. Apr-Mar			0.15
2	SST1	Sea Surface Temperature	Jan-Mar	46°N-51°N 160°W-170°W	Northeast Pacific	0.48
3	SST2	Sea Surface Temperature	Jan-Mar	25°N-30°N 165°E-175°E	Northwestl Pacific	-0.39
4	SST3	Sea Surface Temperature	Prev. Oct-Dec	43°N-48°N 170°W-175°W	Northeast Pacific	0.41
5	SST4	Sea Surface Temperature	Prev. Oct-Dec	26°N-31°N 165°E-170°E	Northwest Pacific	-0.41
6	SST5	Sea Surface Temperature	Prev. Jul-Sep	27°N-32°N 25°W-30°W	Northeast Atlantic	-0.42
7	SSST1	Seesaw SST	Jan-Mar		SST1-SST2	0.49
8	SSST2	Seesaw SST	Prev. Oct-Dec		SST3-SST4	0.52
9	GH1	Geopotential Height (700 mb)	Jan-Mar	30°N-40°N 130°E-140°E	Northwest Pacific	-0.32
10	GH2	Geopotential Height (700 mb)	Prev. Oct-Dec	32°N-50°N 110°W-120°W	Over U.S.	-0.40
11	GH3	Geopotential Height (700 mb)	Prev. Oct-Dec	45°N-52°N 66°W-75°W	Southeast Canada	0.44
12	GH4	Geopotential Height (700 mb)	Prev. Oct-Dec	27°N-32°N 175°E-180°E	North central Pacific	-0.35
13	GH5	Geopotential Height (700 mb)	Prev. Jul-Sep	30°N-35°N 160°E-165°E	North central Pacific	-0.36
14	GH6	Geopotential Height (700 mb)	Prev. Apr-Jun	50°N-60°N 80°W-85°W	Northwest PAcific	-0.29
15	MW1	Meridional Wind (700 mb)	Prev. Oct-Dec	42°N-47°N 85°W-95°W	Northeast U.S.	0.49
16	MW2	Meridional Wind (700 mb)	Prev. Oct-Dec	45°N-50°N 125°W-130°W	West coast of Canada	-0.33
17	MW3	Meridional Wind (700 mb)	Prev. Oct-Dec	38°N-47°N 55°W-60°W	Northwest Atlantic	-0.38
18	ZW1	Zonal Wind (700 mb)	Jan-Mar	23°N-28°N 130°E-140°E	Northwest Pacific	0.38
19	ZW2	Zonal Wind (700 mb)	Prev. Oct-Dec	28°N-33°N 105°W-115°W	South U.S.	0.44
20	ZW3	Zonal Wind (700 mb)	Prev. Oct-Dec	50°N-55°N 110°W-115°W	South Canada	-0.39
21	AT1	Air Temperature	Prev. Oct-Dec	47°N-52°N 110°W-120°W	Northwest U.S.	-0.49
22	AT2	Air Temperature	Prev. Jul-Sep	26°N-31°N 115°W-120°W	West coast of Mexico	0.32
23	AT3	Air Temperature	Prev. Apr-Jun	47°N-52°N 70°W-85°W	Southeast Canada	-0.32
24	OLR1	Outgoing Long-Wave Radiation	Prev. Oct-Dec	35°N-44°N 110°W-120°W	Southwest U.S.	-0.44
25	OLR2	Outgoing Long-Wave Radiation	Prev. Apr-Jun	41°N-46°N 85°W-95°W	Northeast U.S.	-0.32
26	RH1	Relative Humidity	Prev. Oct-Dec	40°N-45°N 11°W-120°W	West U.S.	0.39
27	RH2	Relative Humidity	Prev. Oct-Dec	30°N-35°N 75°W-80°W	Southeast U.S.	0.51
28	RH3	Relative Humidity	Prev. Oct-Dec	27°N-32°N 160°W-165°W	Northeast Pacific	0.35
29	SWMR1	Southwest Monsoon Rainfall	Jan-Mar		Arizona and New Mexico rainfall	0.33
30	SWE1	Snow Water Equivalent	Feb 1st		Basin average	0.71
31	SWE2	Snow Water Equivalent	Mar 1st		Basin average	0.73
32	SWE3	Snow Water Equivalent	Apr 1st		Basin average	0.82

Table 19 Potential predictors for forecasting the October-September streamflows of the Gunnison River

No	Name	Variable	Time	Location	General description	Corr. Coef
1	AF1	Lag-1 flow	Prev. Oct-Sep			0.20
2	SST1	Sea Surface Temperature	Jul-Sep	35°N-40°N 155°E-175°E	North-west Pacific, east of Japan	-0.34
3	SST2	Sea Surface Temperature	Jul-Sep	11°S-16°S 85°W-115°W	South-east Pacific, west of Peru	0.28
4	SST3	Sea Surface Temperature	Apr-Jun	35°N-40°N 155°E-160°E	North-west Pacific, east of Japan	-0.35
5	SST4	Sea Surface Temperature	Apr-Jun	31°N-36°N 45°W-55°W	Central northern Atlantic, east of U.S.	-0.38
6	SST5	Sea Surface Temperature	Jan-Mar	47°N-52°N 165°W-170°W	North-east Pacific, south of Alaska	0.51
7	SST6	Sea Surface Temperature	Jan-Mar	21°N-26°N 155°E-165°E	North-west Pacific, east of Japan	-0.41
8	SSST1	Seesaw SST	Jul-Sep		SST1-SST2	0.36
9	SSST2	Seesaw SST	Jan-Mar		SST5-SST6	0.52
10	GH1	Geopotential Height (700 mb)	Jul-Sep	35°N-45°N 160°E-175°E	North-west Pacific, east of Japan	-0.35
11	GH2	Geopotential Height (700 mb)	Jul-Sep	28°N-35°N 50°W-60°W	Northern central Atlantic	-0.29
12	GH3	Geopotential Height (700 mb)	Apr-Jun	27°N-32°N 95°W-105°W	Southern states	-0.40
13	GH4	Geopotential Height (700 mb)	Apr-Jun	30°N-40°N 40°W-60°W	Northern central Atlantic	-0.35
14	GH5	Geopotential Height (1000 mb)	Jul-Sep	55°N-65°N 57°W-105°W	Eastern Canada	-0.31
15	GH6	Geopotential Height (1000 mb)	Jul-Sep	25°N-30°N 120°E-130°E	Western Pacific near China	0.32
16	GH7	Geopotential Height (1000 mb)	Apr-Jun	25°N-35°N 50°W-60°W	Northern central Atlantic	-0.40
17	MW1	Meridional Wind (700 mb)	Jul-Sep	28°N-35°N 150°E-155°E	Western Pacific, south-east of Japan	-0.45
18	MW2	Meridional Wind (700 mb)	Apr-Jun	25°N-28°N 110°W-118°W	East Pacific, near CA and Mexico	-0.37
19	MW3	Meridional Wind (surface)	Jul-Sep	25°N-31°N 150°E-155°E	Western Pacific, east of Japan	-0.34
20	ZW1	Zonal Wind (700 mb)	Jul-Sep	48°N-53°N 170°E-175°E	North-west Pacific, north-east of Japan	-0.28
21	ZW2	Zonal Wind (700 mb)	Jul-Sep	27°N-32°N 160°E-165°E	Western Pacific, east of Japan	0.43
22	ZW3	Zonal Wind (700 mb)	Jul-Sep	49°N-54°N 28°W-35°W	Central northern Atlantic, east of Canada	-0.29
23	AT1	Air Temperature	Jul-Sep	41°N-46°N 105°W-110°W	Western mountain states	-0.28
24	AT2	Air Temperature	Apr-Jun	35°N-40°N 100°W-105°W	Western mountain states	-0.42
25	OLR1	Outgoing Long-Wave Radiation	Apr-Jun	35°N-45°N 90°W-110°W	Central states and western mountain states	-0.43
26	AO1	Arctic Oscillation	Mar-May			-0.38
27	PDO1	Pacific Decadal Oscillation	Mar			0.29
28	PDO2	Pacific Decadal Oscillation	Sep			0.28
29	PNA1	Pacific/ North American Teleconnection Pattern	Mar-Apr			0.38
30	SWM1	South-West Monsoon Rainfall	Jan-Mar		Arizona and New Mexico rainfall	0.33
31	SWE4	Snow Water Equivalent	May 1st		Basin average	0.33

Table 20 Selected predictors for forecasting the April–July streamflows for the six study sites

No.	River	Name	Variable	Time	Corr. Coef.
1	Poudre	SST8	Sea Surface Temperature	Prev. Apr-Jun	-0.29
2		ZW3	Zonal Wind (700 mb)	Jan-Mar	0.41
3		SWE3	Snow Water Equivalent	Apr 1st	0.65
4	Arkansas	SST4	Sea Surface Temperature	Prev. Jul-Sep	-0.45
5		MW2	Meridional Wind (700 mb)	Prev. Oct-Dec	-0.53
6		RH2	Relative Humidity	Prev. Oct-Dec	0.49
7		SWE3	Snow Water Equivalent	Apr 1st	0.60
8	Gunnison	SST2	Sea Surface Temperature	Jan-Mar	-0.45
9		SST7	Sea Surface Temperature	Prev. Apr-Jun	0.40
10		SST9	Sea Surface Temperature	Prev. Apr-Jun	-0.31
11		GH5	Geopotential Height (700 mb)	Prev. Oct-Dec	-0.35
12		RH4	Relative Humidity	Prev. Oct-Dec	0.36
13		ZW2	Zonal Wind (700 mb)	Jan-Mar	0.34
14		PDSI1	Palmer Index	Jan-Mar	0.70
15		SWE3	Snow Water Equivalent	Apr 1st	0.85
16	Rio Grande	SSST1	Seesaw SST	Jan-Mar	0.54
17		GH6	Geopotential Height (700 mb)	Prev. Oct-Dec	-0.51
18		ZW4	Zonal Wind (700 mb)	Prev. Oct-Dec	-0.47
19		RH2	Relative Humidity	Prev. Oct-Dec	0.60
20		SWE3	Snow Water Equivalent	Apr 1st	0.65
21	San Juan	GH3	Geopotential Height (700 mb)	Prev. Oct-Dec	0.40
22		GH5	Geopotential Height (700 mb)	Prev. Jul-Sep	-0.42
23		OLR1	Outgoing Long-Wave Radiation	Jan-Mar	-0.58
24		OLR2	Outgoing Long-Wave Radiation	Prev. Oct-Dec	-0.48
25		SWE3	Snow Water Equivalent	Mar 1st	0.85
26	Yampa	GH1	Geopotential Height (700 mb)	Jan-Mar	-0.43
27		MW3	Meridional Wind (700 mb)	Prev. Oct-Dec	-0.41
28		OLR3	Outgoing Long-Wave Radiation	Prev. Oct-Dec	-0.49
29		PDSI1	Palmer Index	Jan-Mar	0.66
30		PDSI2	Palmer Index	Prev. Oct-Dec	0.40
31		SWE2	Snow Water Equivalent	Mar 1st	0.57

Table 21 Forecast equations based on MLR for forecasting the April-July streamflows for the six study sites

Site	Equations
Poudre River	$z = -0.24 \times SST8(A\text{-}J) + 0.412 \times ZW3(J\text{-}M) + 0.616 \times SWE3(Apr\ 1^{st})$
Arkansas River	$z = -0.294 \times SST4(J\text{-}S) - 0.140 \times MW2(O\text{-}D) + 0.423 \times \mathrm{RH}(O\text{-}D) + 0.392 \times SWE3(Apr\ 1^{st})$
Gunnison River	$z = 0.192 \times SST2(J\text{-}M) + 0.124 \times SST7(A\text{-}J) - 0.194 \times SST9(A\text{-}J) - 0.231 \times GH5(O\text{-}D) + 0.209 \times \mathrm{ZW2}(J\text{-}M) + 0.203 \times RH4(O\text{-}D) + 0.288 \times PDSI1(J\text{-}M) + 0.518 \times SWE3(Apr\ 1^{st})$
Rio Grande	$z = 0.249 \times SSST1(J\text{-}M) - 0.213 \times GH6(O\text{-}D) - 0.176 \times ZW4(O\text{-}D) + 0.360 \times RH2(O\text{-}D) + 0.425 \times SWE3(Apr\ 1^{st})$
San Juan River	$z = 0.187 \times GH3(O\text{-}D) - 0.172 \times GH5(J\text{-}S) - 0.170 \times OLR1(J\text{-}M) - 0.130 \times OLR2(O\text{-}D) + 0.623 \times SWE3(Apr\ 1^{st})$
Yampa River	$z = -0.307 \times GH1(J\text{-}M) - 0.174 \times \mathrm{MW3}(O\text{-}D) - 0.235 \times \mathrm{OLR2}(J\text{-}M) + 0.829 \times PDSI1(J\text{-}M) - 0.583 \times \mathrm{PDSI2}(O\text{-}D) + 0.273 \times SWE2(Mar\ 1^{st})$

Note: The parenthesis in the equations indicate the time period. For example, SST8(A-J) indicates the SST for the time period April-June of the previous year (refer to Table 13).

Table 22a Forecast model performance for single site based on MLR

Method	Item	Poudre	Arkansas	Gunnison	Rio Grande	San Juan	Yampa
Fitting	R^2	0.64	0.64	0.89	0.83	0.85	0.81
	adj. R^2	0.62	0.60	0.87	0.81	0.83	0.79
Drop one	R^2	0.52	0.52	0.83	0.77	0.79	0.72
	adj. R^2	0.49	0.48	0.80	0.75	0.77	0.68

Table 22b Forecast skill scores for single site MLR models

Method	Item	Poudre	Arkansas	Gunnison	Rio Grande	San Juan	Yampa
Fitting	*Accuracy*	0.53	0.53	0.72	0.68	0.64	0.72
	HSS	0.37	0.37	0.62	0.57	0.52	0.62
Drop one	*Accuracy*	0.49	0.53	0.68	0.68	0.60	0.66
	HSS	0.32	0.37	0.57	0.57	0.47	0.55

Table 23a Cross-correlation coefficient for single site MLR models (fitting)

Sites	Poudre	Arkansas	Gunnison	Rio Grande	San Juan	Yampa
Poudre	1	0.58	0.58	0.42	0.35	0.63
Arkansas	0.58	1	0.80	0.67	0.61	0.73
Gunnison	0.58	0.80	1	0.65	0.72	0.88
Rio Grande	0.42	0.67	0.65	1	0.84	0.53
San Juan	0.35	0.61	0.72	0.84	1	0.60
Yampa	0.63	0.73	0.88	0.53	0.60	1

Table 23b Cross-correlation coefficient for single site MLR models (drop one)

Sites	Poudre	Arkansas	Gunnison	Rio Grande	San Juan	Yampa
Poudre	1	0.54	0.58	0.41	0.32	0.61
Arkansas	0.54	1	0.74	0.64	0.57	0.67
Gunnison	0.58	0.74	1	0.63	0.69	0.85
Rio Grande	0.41	0.64	0.63	1	0.82	0.53
San Juan	0.32	0.57	0.69	0.82	1	0.59
Yampa	0.61	0.67	0.85	0.53	0.59	1

Table 24 Variances of PCs for April–July streamflows of Poudre River

PCs	Variance	%	Accum %	PCs	Variance	%	Accum %
1	10.05	27.9	27.9	19	0.31	0.9	95.1
2	4.95	13.7	41.7	20	0.29	0.8	95.9
3	2.66	7.4	49.1	21	0.27	0.7	96.6
4	2.35	6.5	55.6	22	0.24	0.7	97.3
5	2.08	5.8	61.4	23	0.18	0.5	97.8
6	1.70	4.7	66.1	24	0.14	0.4	98.2
7	1.57	4.4	70.4	25	0.13	0.4	98.6
8	1.28	3.6	74.0	26	0.11	0.3	98.9
9	1.17	3.3	77.3	27	0.10	0.3	99.1
10	1.12	3.1	80.4	28	0.08	0.2	99.4
11	0.97	2.7	83.0	29	0.07	0.2	99.5
12	0.76	2.1	85.2	30	0.05	0.1	99.7
13	0.73	2.0	87.2	31	0.04	0.1	99.8
14	0.66	1.8	89.0	32	0.03	0.1	99.9
15	0.55	1.5	90.5	33	0.02	0.1	99.9
16	0.51	1.4	92.0	34	0.01	0.0	100.0
17	0.44	1.2	93.2	35	0.01	0.0	100.0
18	0.38	1.1	94.2	36	0.00	0.0	100.0

Table 25 Model parameters of PCA model for each site

Poudre		Arkansas		Gunnison		Rio Grande		San Juan		Yampa	
PCs	beta	PCs	beta	PCs	beta	PCs	beta	PCs	beta	PCs	beta
PC1	-0.645	PC1	-0.731	PC1	-0.788	PC1	-0.809	PC1	-0.837	PC1	0.815
PC2	-0.315	PC3	0.189	PC2	-0.230	PC2	0.263	PC2	0.136	PC2	0.160
PC4	-0.173	PC4	-0.371	PC3	0.174	PC3	0.254	PC3	-0.143	PC3	0.190
PC10	0.228	PC10	-0.169	PC4	0.245	PC6	-0.160	PC7	-0.115	PC12	-0.163
PC12	-0.197	PC12	0.177	PC6	0.146	PC9	-0.152	PC8	-0.223	PC17	0.256
				PC12	0.162	PC11	0.115				

Table 26a Model performance for single site PCA models

Method	Item	Poudre	Arkansas	Gunnison	Rio Grande	San Juan	Yampa
Fitting	R^2	0.67	0.70	0.87	0.86	0.85	0.88
	adj. R^2	0.63	0.66	0.85	0.84	0.83	0.87
Drop one	R^2	0.54	0.58	0.76	0.73	0.77	0.79
	adj. R^2	0.49	0.54	0.73	0.70	0.74	0.77

Table 26b Forecast skill scores for single site PCA models

Method	**Item**	**Poudre**	**Arkansas**	**Gunnison**	**Rio Grande**	**San Juan**	**Yampa**
Fitting	*Accuracy*	0.55	0.57	0.60	0.66	0.74	0.70
	HSS	0.39	0.42	0.47	0.56	0.65	0.60
Drop one	*Accuracy*	0.49	0.53	0.57	0.58	0.68	0.62
	HSS	0.32	0.37	0.42	0.46	0.57	0.50

Table 27a Cross-correlation coefficient for single site PCA models (fitting)

Sites	Poudre	Arkansas	Gunnison	Rio Grande	San Juan	Yampa
Poudre	1	0.66	0.65	0.45	0.48	0.72
Arkansas	0.66	1	0.83	0.65	0.65	0.76
Gunnison	0.65	0.83	1	0.63	0.70	0.88
Rio Grande	0.45	0.65	0.63	1	0.86	0.56
San Juan	0.48	0.65	0.70	0.86	1	0.61
Yampa	0.72	0.76	0.88	0.56	0.61	1

Table 27b Cross-correlation coefficient for single site PCA models (drop one)

Sites	Poudre	Arkansas	Gunnison	Rio Grande	San Juan	Yampa
Poudre	1	0.67	0.66	0.45	0.48	0.72
Arkansas	0.67	1	0.78	0.61	0.64	0.72
Gunnison	0.66	0.78	1	0.60	0.67	0.86
Rio Grande	0.45	0.61	0.60	1	0.82	0.56
San Juan	0.48	0.64	0.67	0.82	1	0.61
Yampa	0.72	0.72	0.86	0.56	0.61	1

Table 28 Parameters of the forecast model that only use climatic variables for the April–July streamflows of Gunnison River

PCs	**beta**
PC1	0.717
PC2	0.177
PC5	-0.299

Table 29 Model performance for the model that only use climatic variables for the April–July streamflows of Gunnison River

Method	Values of R^2		Values of skill scores	
	Item	Values	Item	Values
Fitting	R^2	0.63	*Accuracy*	0.47
	adj. R^2	0.61	*HSS*	0.30
Drop one	R^2	0.53	*Accuracy*	0.47
	adj. R^2	0.50	*HSS*	0.30

Table 30 Variances of PCs obtained from all potential predictors for 6 sites

PCs	Variance	%	Accumulated %	PCs	Variance	%	Accumulated %	PCs	Variance	%	Accumulated %
1	51.7	25.1	25.1	26	1.4	0.7	92.5	52	0.2	0.1	100.0
2	23.4	11.4	36.5	27	1.2	0.6	93.1	53 ~ 207	0.0	0.0	100.0
3	15.0	7.3	43.7	28	1.2	0.6	93.7				
4	12.1	5.9	49.6	29	1.1	0.5	94.2				
5	11.4	5.6	55.2	30	1.0	0.5	94.7				
6	9.9	4.8	60.0	31	1.0	0.5	95.2				
7	7.8	3.8	63.8	32	1.0	0.5	95.6				
8	6.5	3.1	66.9	33	0.9	0.4	96.1				
9	5.9	2.9	69.8	34	0.8	0.4	96.5				
10	5.1	2.5	72.3	35	0.7	0.4	96.8				
11	4.7	2.3	74.5	36	0.7	0.3	97.1				
12	4.0	1.9	76.5	37	0.7	0.3	97.5				
13	3.8	1.8	78.3	38	0.6	0.3	97.7				
14	3.4	1.7	80.0	39	0.6	0.3	98.0				
15	3.2	1.6	81.5	40	0.5	0.2	98.3				
16	2.9	1.4	83.0	41	0.5	0.2	98.5				
17	2.6	1.3	84.2	42	0.4	0.2	98.7				
18	2.4	1.2	85.4	43	0.4	0.2	98.9				
19	2.3	1.1	86.5	44	0.4	0.2	99.1				
20	2.1	1.0	87.5	45	0.3	0.2	99.2				
21	2.0	1.0	88.5	46	0.3	0.1	99.4				
22	1.9	0.9	89.4	47	0.3	0.1	99.5				
23	1.8	0.9	90.3	48	0.3	0.1	99.7				
24	1.6	0.8	91.0	49	0.2	0.1	99.8				
25	1.6	0.8	91.8	50	0.2	0.1	99.8				

Table 31a Model performance for multisite CCA models

Method	Item	Poudre	Arkansas	Gunnison	Rio Grande	San Juan	Yampa
Fitting	R^2	0.58	0.78	0.78	0.76	0.75	0.82
	adj. R^2	0.52	0.74	0.74	0.71	0.68	0.80
Drop one	R^2	0.41	0.63	0.64	0.69	0.62	0.71
	adj. R^2	0.33	0.57	0.56	0.63	0.52	0.67

Table 31b Forecast skill scores for multisite CCA models

Method	Item	Poudre	Arkansas	Gunnison	Rio Grande	San Juan	Yampa
Fitting	*Accuracy*	0.47	0.57	0.53	0.60	0.60	0.66
	HSS	0.29	0.42	0.37	0.47	0.47	0.55
Drop one	*Accuracy*	0.43	0.57	0.49	0.57	0.55	0.57
	HSS	0.24	0.42	0.32	0.42	0.40	0.42

Table 32a Cross-correlation coefficient for multisite CCA models (fitting)

Sites	Poudre	Arkansas	Gunnison	Rio Grande	San Juan	Yampa
Poudre	1	0.78	0.78	0.48	0.53	0.85
Arkansas	0.78	1	0.96	0.68	0.73	0.91

Gunnison	0.78	0.96	1	0.64	0.76	0.93
Rio Grande	0.48	0.68	0.64	1	0.92	0.47
San Juan	0.53	0.73	0.76	0.92	1	0.55
Yampa	0.85	0.91	0.93	0.47	0.55	1

Table 32b Cross-correlation coefficient for multisite CCA models (drop one)

Sites	Poudre	Arkansas	Gunnison	Rio Grande	San Juan	Yampa
Poudre	1	0.67	0.66	0.39	0.50	0.77
Arkansas	0.67	1	0.78	0.50	0.67	0.73
Gunnison	0.66	0.78	1	0.39	0.65	0.81
Rio Grande	0.39	0.50	0.39	1	0.85	0.40
San Juan	0.50	0.67	0.65	0.85	1	0.58
Yampa	0.77	0.73	0.81	0.40	0.58	1

Table 33a Model performance for the aggregation – disaggregation models

Method	**Item**	**Poudre**	**Arkansas**	**Gunnison**	**Rio Grande**	**San Juan**	**Yampa**
Fitting	R^2	0.38	0.71	0.70	0.62	0.66	0.50
	adj. R^2	0.30	0.66	0.64	0.55	0.57	0.43
Drop one	R^2	0.30	0.63	0.63	0.58	0.62	0.44
	adj. R^2	0.19	0.57	0.57	0.51	0.51	0.35

Table 33b Forecast skill scores for the aggregation – disaggregation models

Method	**Item**	**Poudre**	**Arkansas**	**Gunnison**	**Rio Grande**	**San Juan**	**Yampa**
Fitting	*Accuracy*	0.34	0.64	0.51	0.55	0.34	0.47
	HSS	0.12	0.52	0.35	0.40	0.13	0.30
Drop one	*Accuracy*	0.32	0.57	0.47	0.51	0.38	0.43
	HSS	0.10	0.42	0.30	0.35	0.18	0.24

Table 34a Cross-correlation coefficient for the aggregation – disaggregation models (fitting)

Sites	Poudre	Arkansas	Gunnison	Rio Grande	San Juan	Yampa
Poudre	1	0.70	0.65	0.46	0.54	0.51
Arkansas	0.70	1	0.92	0.71	0.72	0.70
Gunnison	0.65	0.92	1	0.62	0.67	0.74
Rio Grande	0.46	0.71	0.62	1	0.83	0.26
San Juan	0.54	0.72	0.67	0.83	1	0.33
Yampa	0.51	0.70	0.74	1.26	0.33	1

Table 34b Cross-correlation coefficient for the aggregation – disaggregation models (drop one)

Sites	Poudre	Arkansas	Gunnison	Rio Grande	San Juan	Yampa
Poudre	1	0.68	0.67	0.11	0.30	0.66
Arkansas	0.68	1	0.92	0.30	0.37	0.77
Gunnison	0.67	0.92	1	0.34	0.44	0.82
Rio Grande	0.11	0.30	0.34	1	0.82	0.18
San Juan	0.30	0.37	0.44	0.82	1	0.26
Yampa	0.66	0.77	0.82	0.18	0.26	1

Table 35 Model parameters for the April – March streamflow forecast of Gunnison River

PCs	**beta**
PC1	-0.785
PC6	0.275
PC7	-0.175
PC11	0.165

Table 36 Model performance for the April – March streamflow forecast of Gunnison River

Method	Values of R^2		Values of skill scores	
	Item	Values	Item	Values
Fitting	R^2	0.75	*Accuracy*	0.62
	adj. R^2	0.73	*HSS*	0.50
Drop one	R^2	0.67	*Accuracy*	0.57
	adj. R^2	0.64	*HSS*	0.42

Table 37 Model parameters for October – September streamflow forecast of Gunnison River

PCs	**beta**
PC1	-0.670
PC5	-0.271
PC10	-0.298
PC11	0.188

Table 38 Model performance for October – September streamflow forecast of Gunnison River

Method	Values of R^2		Values of skill scores	
	Item	Values	Item	Values
Fitting	R^2	0.65	*Accuracy*	0.55
	adj. R^2	0.62	*HSS*	0.40
Drop one	R^2	0.54	*Accuracy*	0.47
	adj. R^2	0.50	*HSS*	0.30

Table 41 RMSE of the CCA model using random drop-10% method

Method	RMSE (AF)					
	Poudre	Arkansas	Gunnison	Rio Grande	San Juan	Yampa
For fitting part	55587	61714	137037	98003	196874	150513
For drop10% part	71566	74480	173282	114357	229386	196312

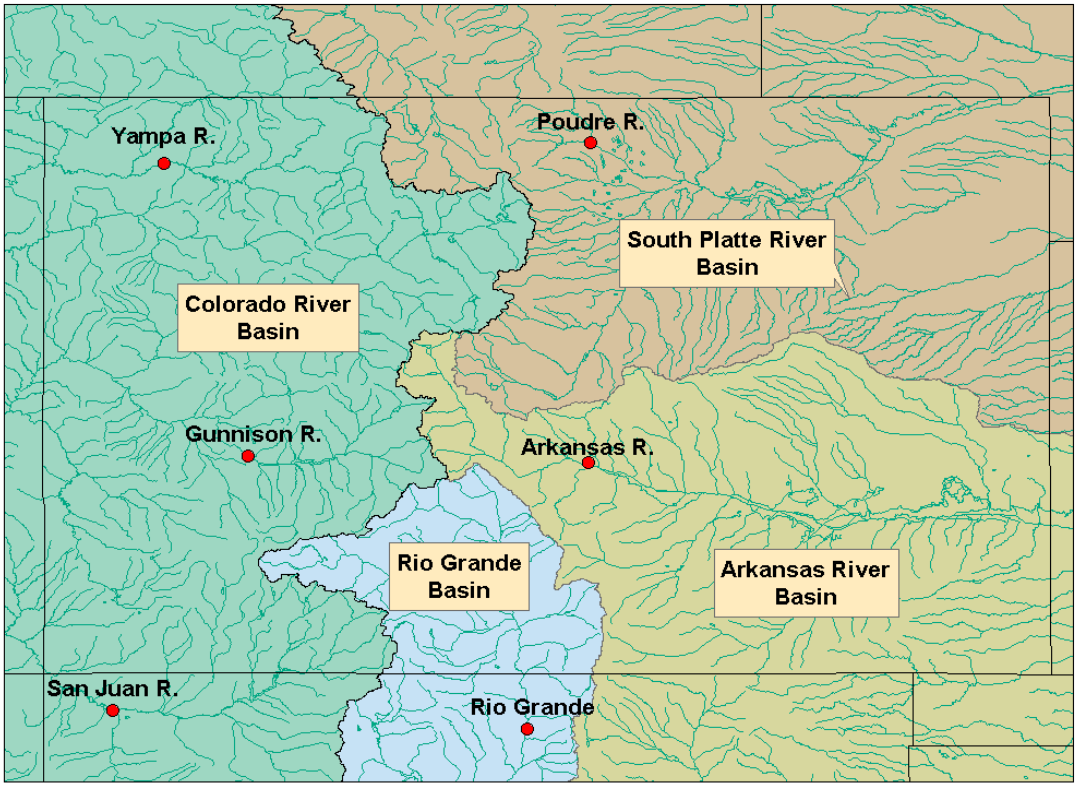

Figure 1. Map of flow sites

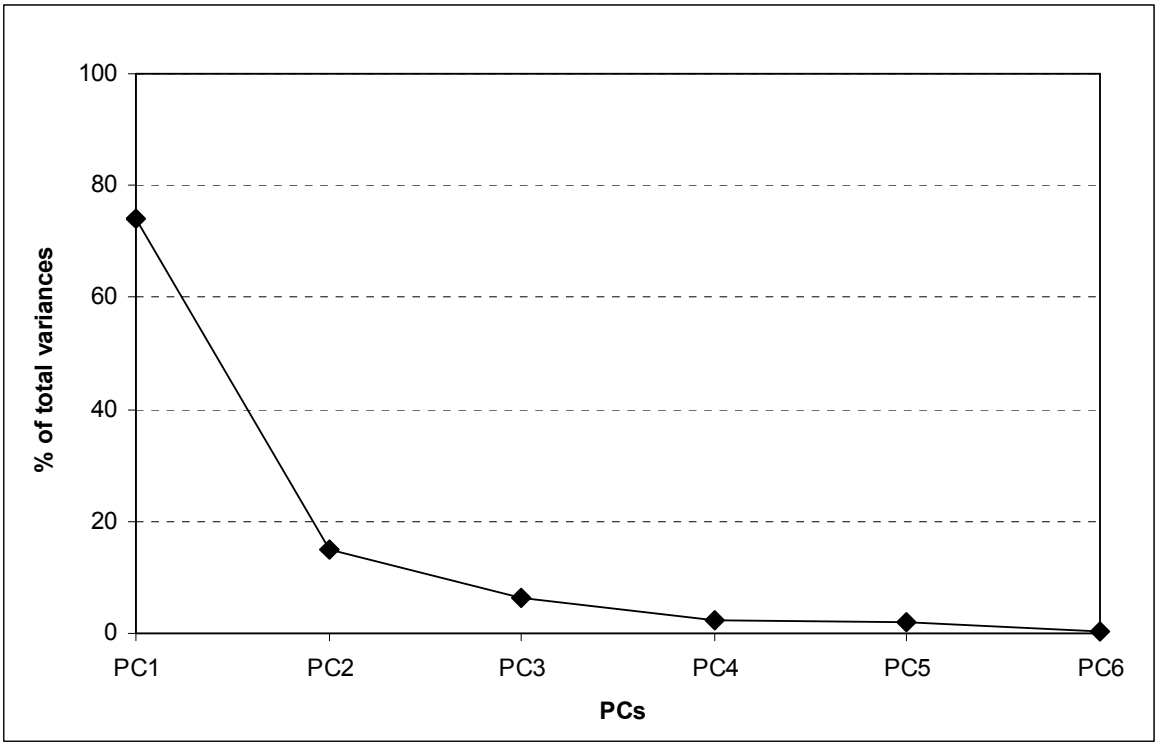

Figure 2 Plot of the variances of PCs for the April–July streamflows of the 6 sites

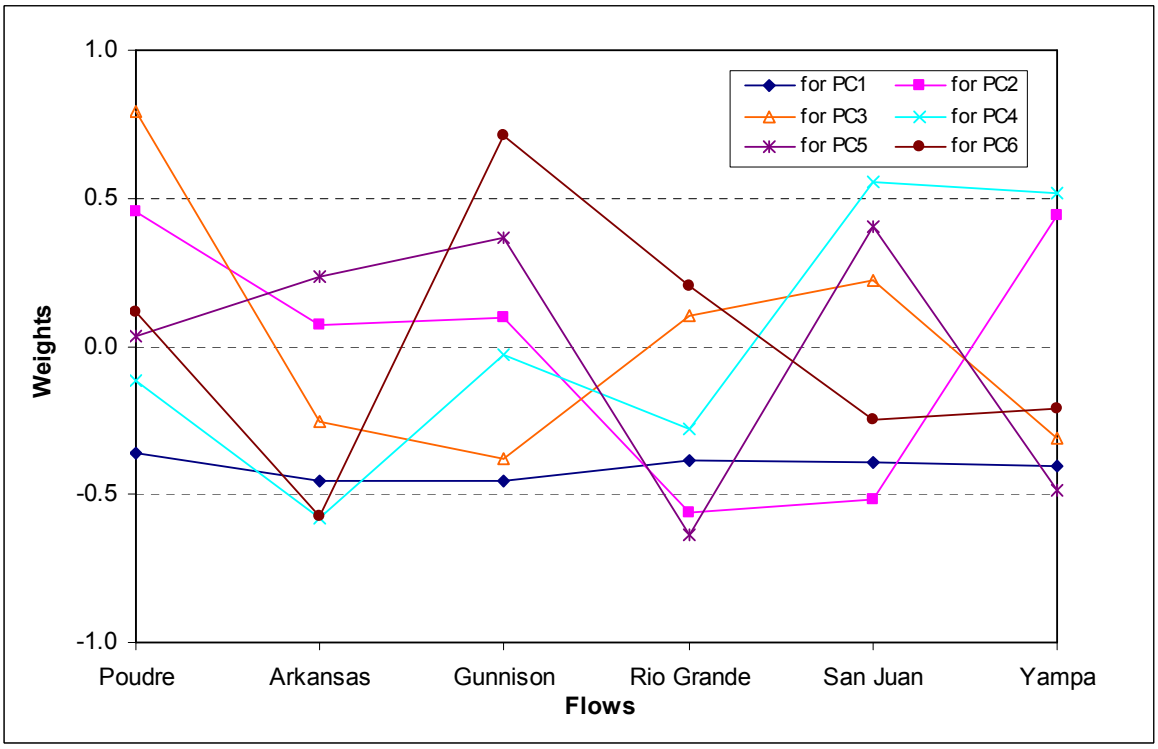

Figure 3 Plot of the weights for the April-July streamflows of the 6 sites

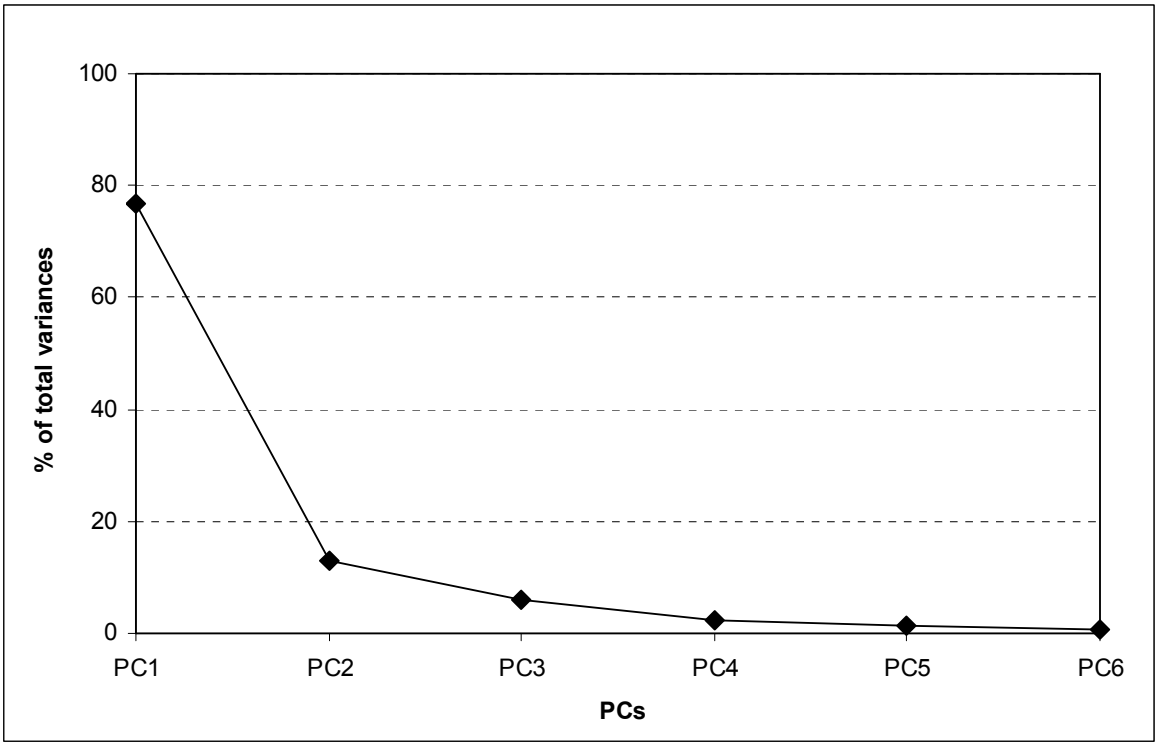

Figure 4 Plot of the variances of PCs for the April–March streamflows of the 6 sites

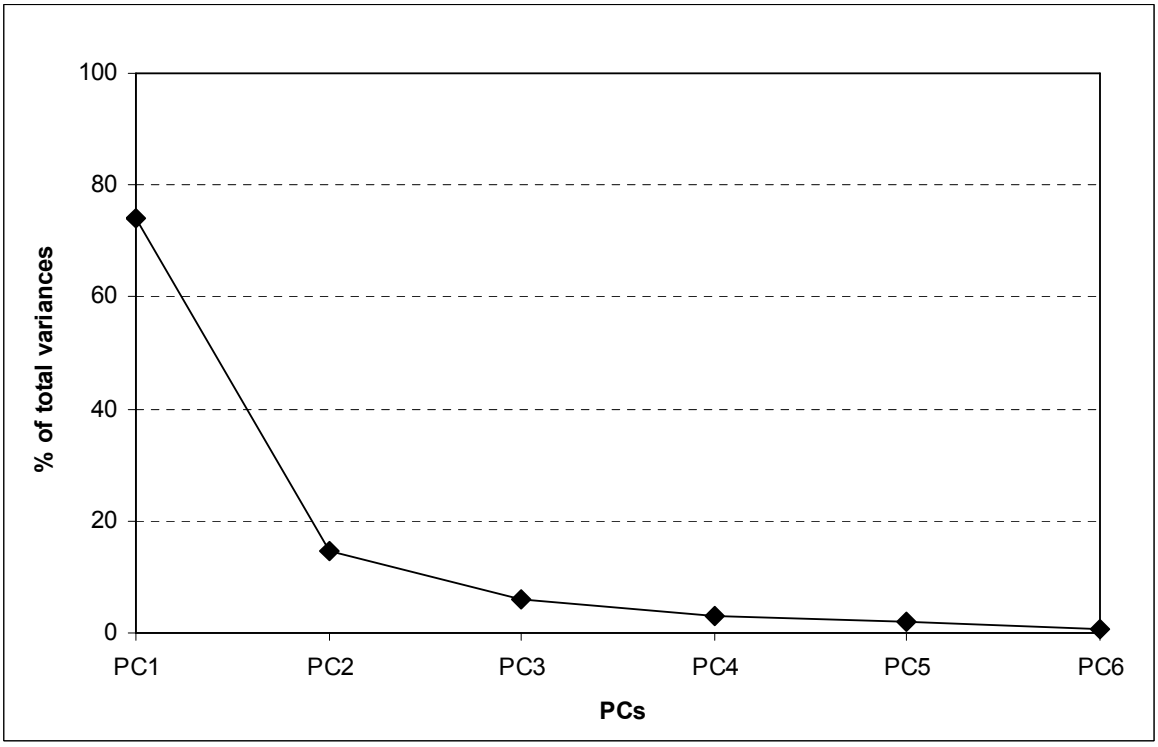

Figure 6 Plot of the variances of PCs for the October–September streamflows of the 6 sites

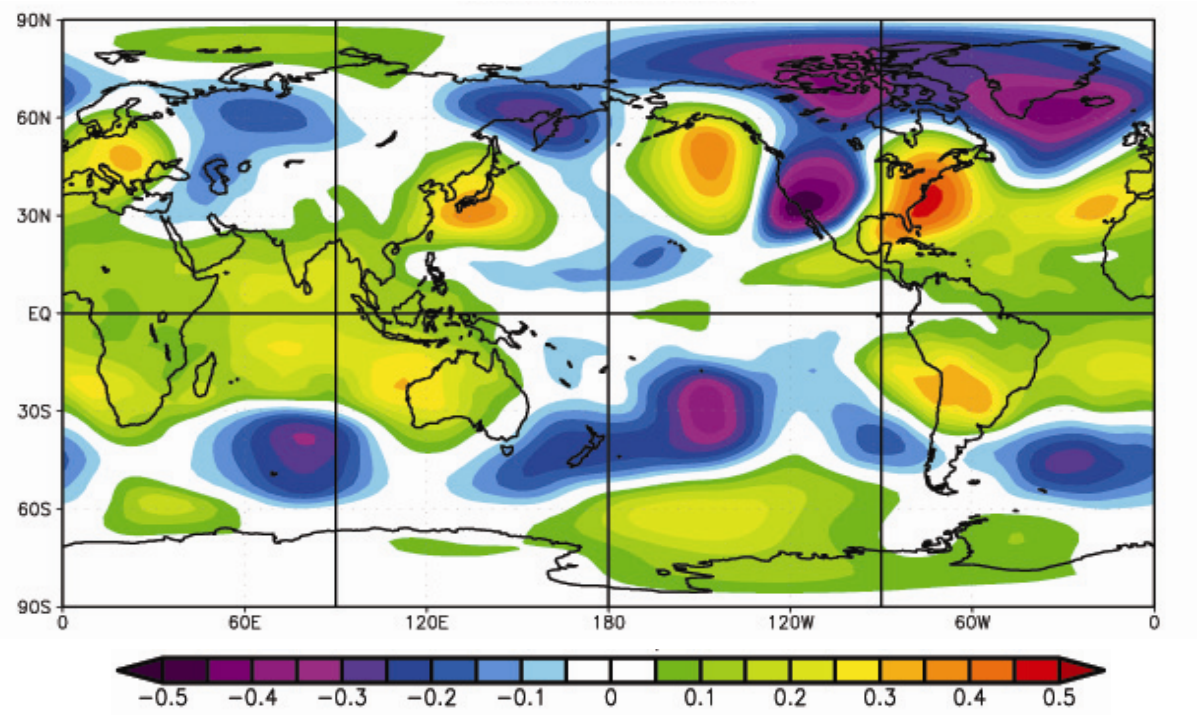

Figure 8. Correlation map for the April-July streamflows of the San Juan River versus previous year's October-December global mean 700 mb Geopotential Heights

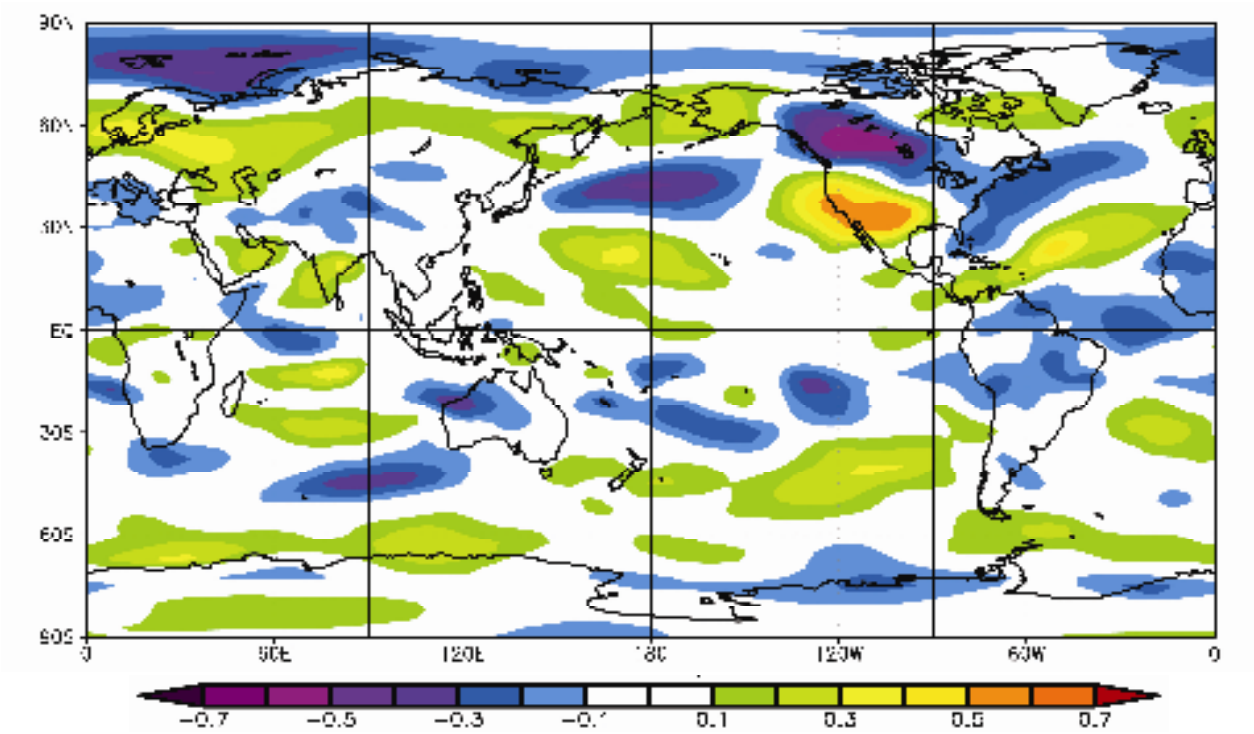

Figure 9. Correlation map for the April-July streamflows of the Yampa River versus previous year's October-December global zonal wind

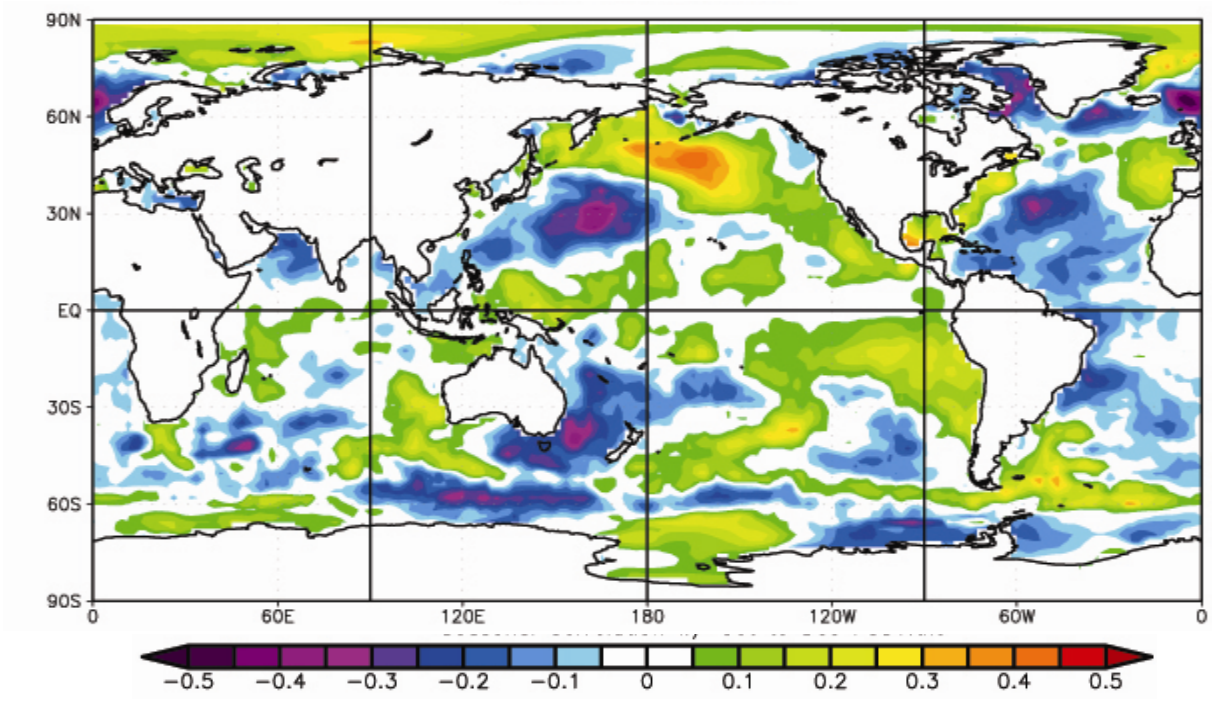

Figure 10. Correlation map for the April-July streamflows of the Gunnison versus previous year's October-December global SST

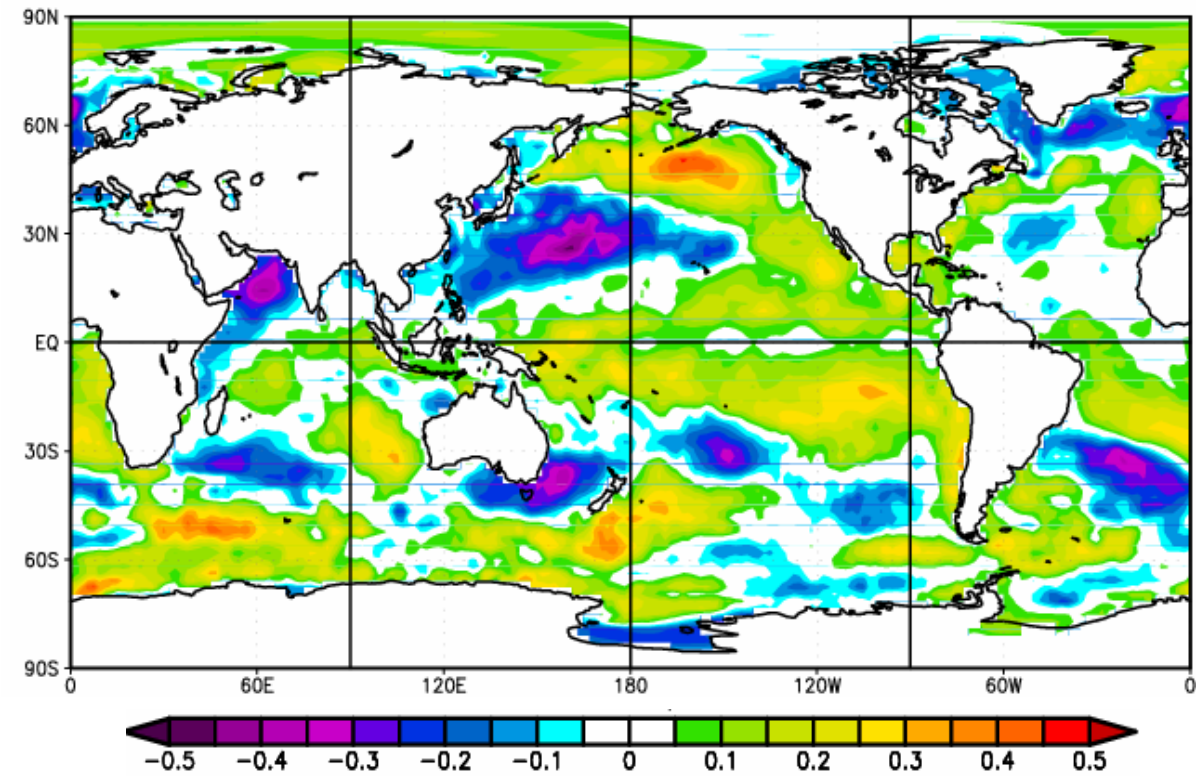

Figure 11. January-March SST vs. Gunnison River annual (April-March) streamflow

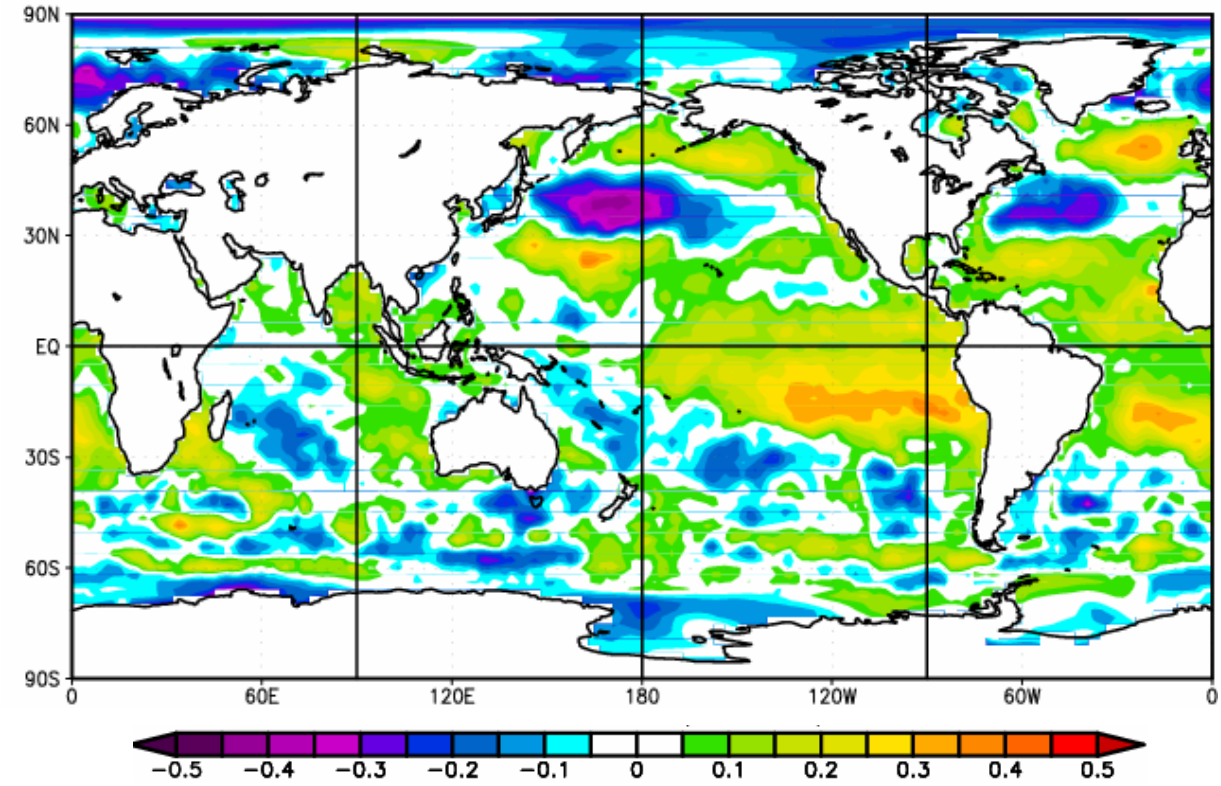

Figure 12. July-September SST vs. Gunnison River annual (October-September) streamflow

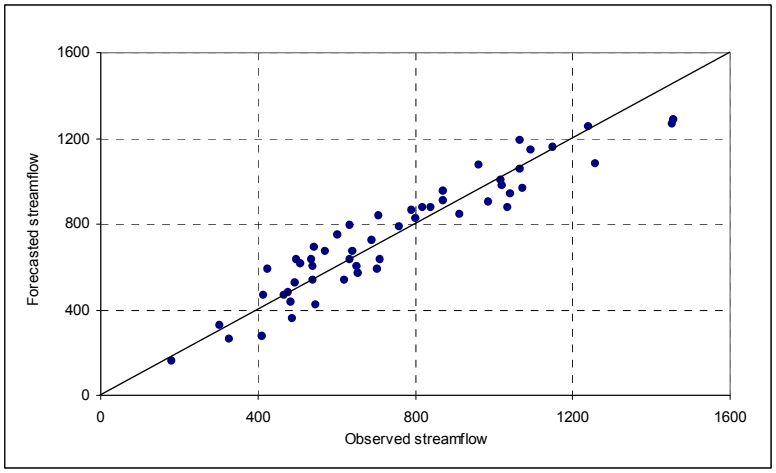

Fitting

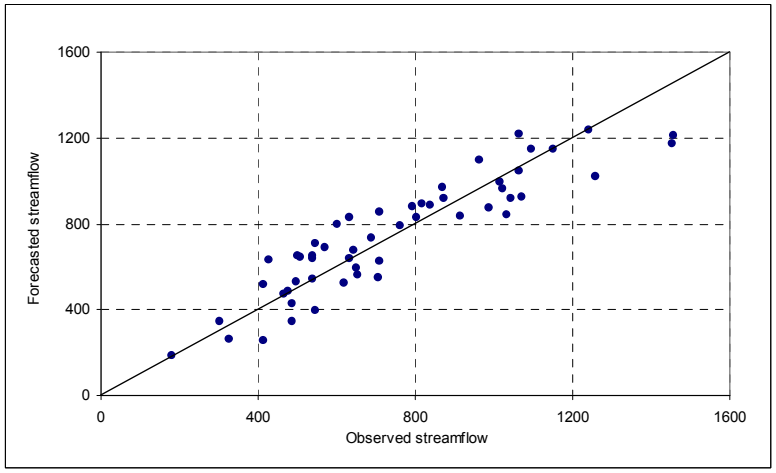

Drop one

Figure 13. Scatter plot of forecast results of the MLR model for Gunnison River

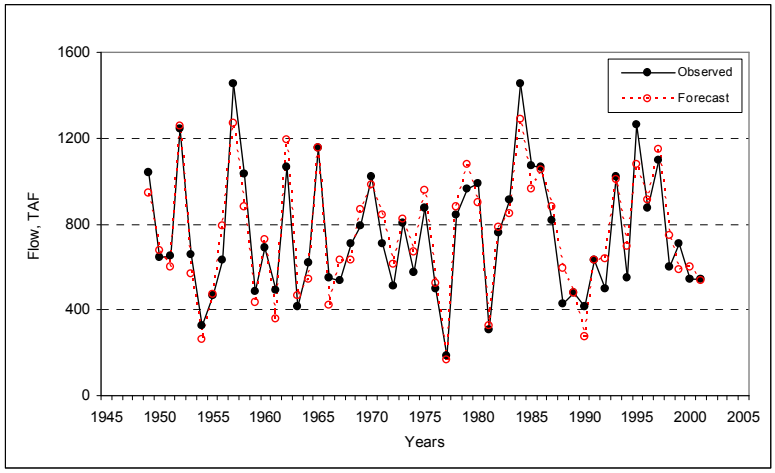

Fitting

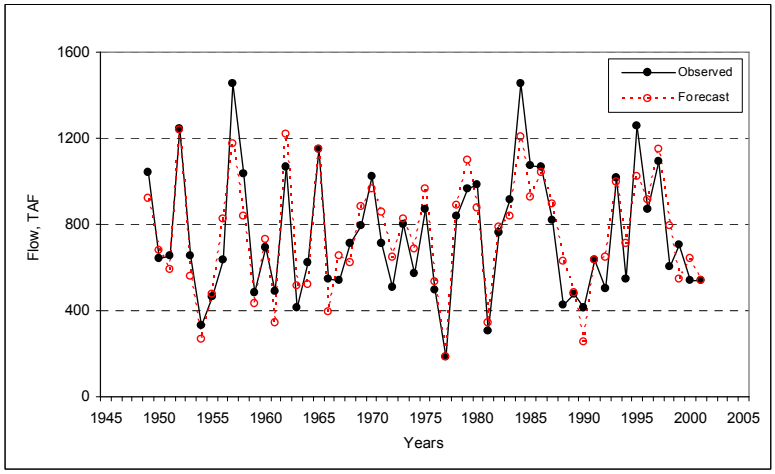

Drop one

Figure 14. Time series plots of the forecast results of MLR model for Gunnison River

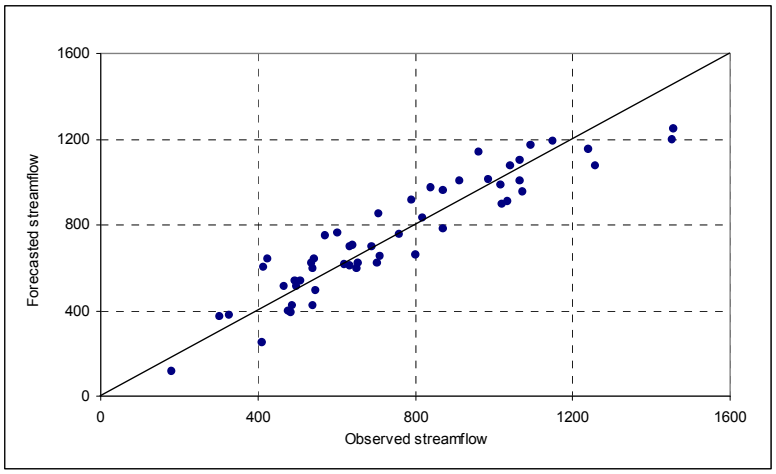

Fitting

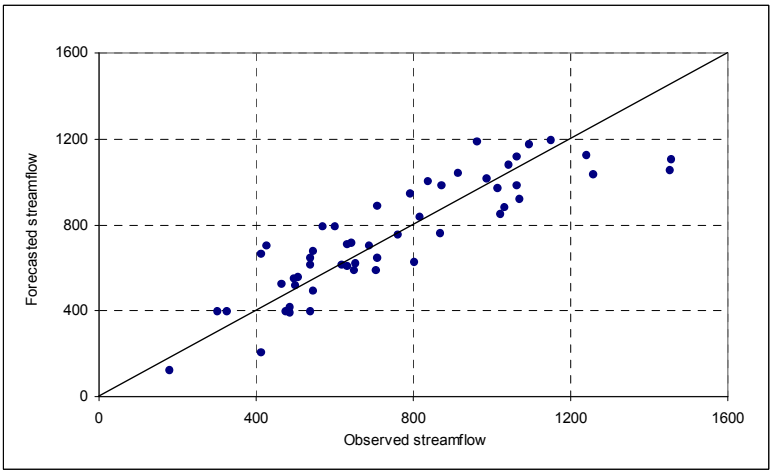

Drop one

Figure 15 Scatter plots of forecasted streamflows by PCA model for the Gunnison River

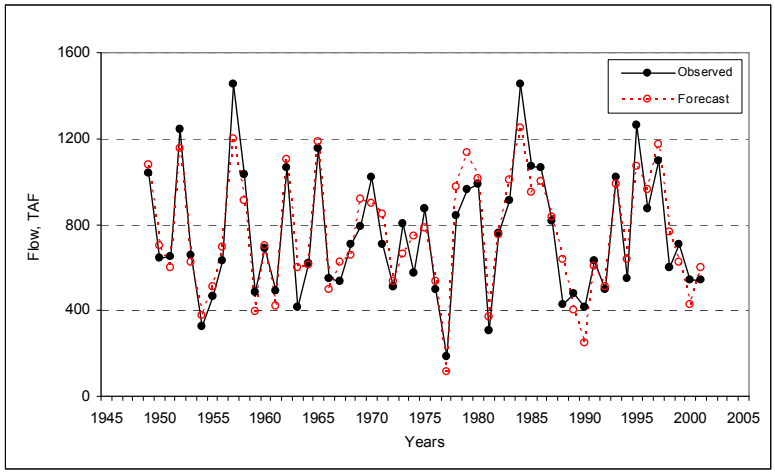

Fitting

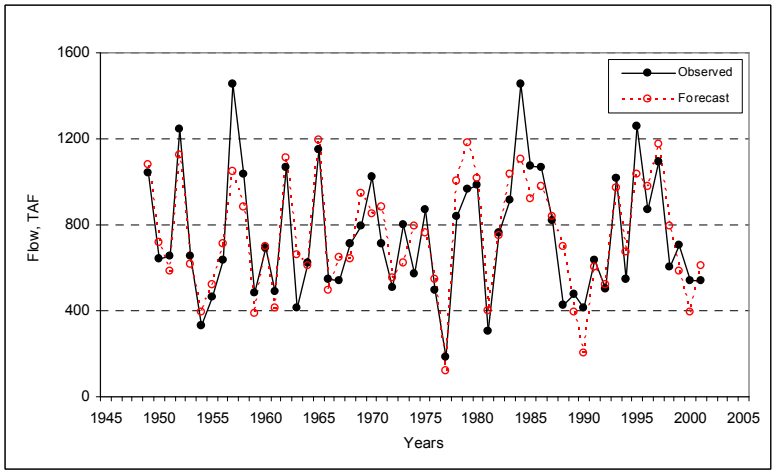

Drop one

Figure 16 Time series plots of forecasted streamflows by PCA model for the Gunnison River

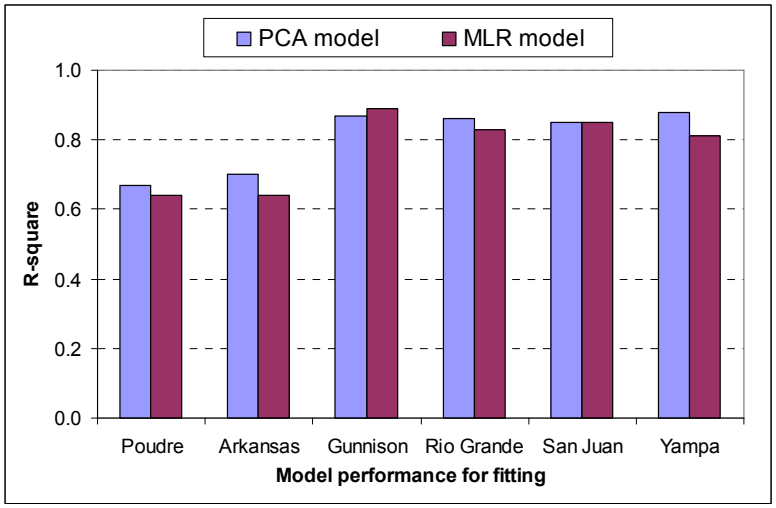

Fitting

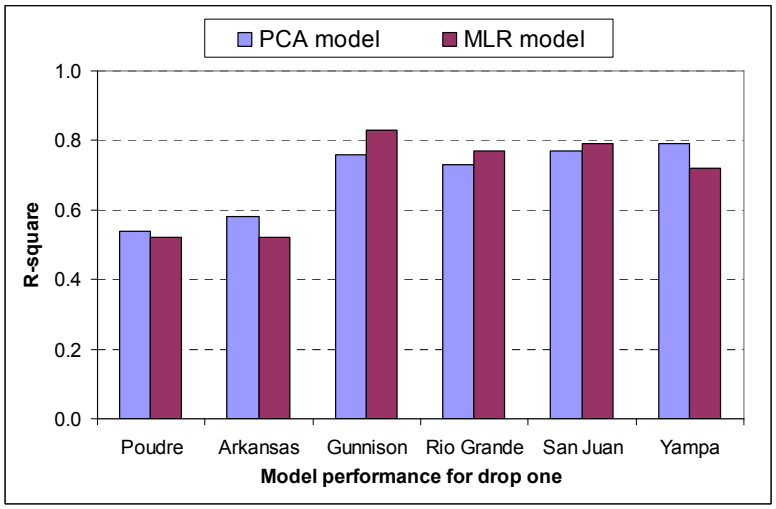

Drop one

Figure 17a Comparison of R^2 for the models in sections 6.3.1. and 6.3.2.

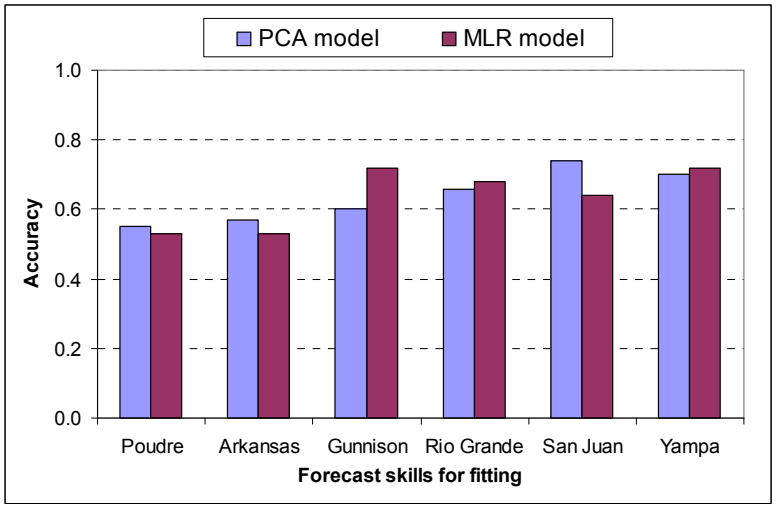

Fitting

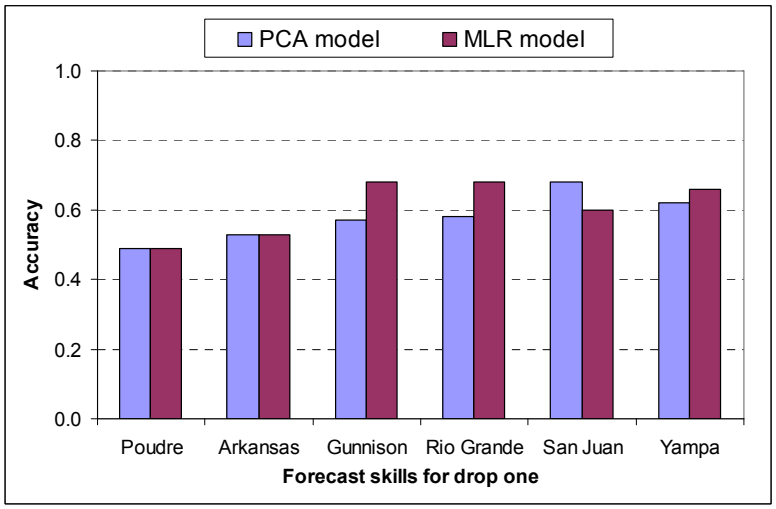

Drop one

Figure 17b Comparison of forecast skills for the models in sections 6.3.1 and 6.3.2

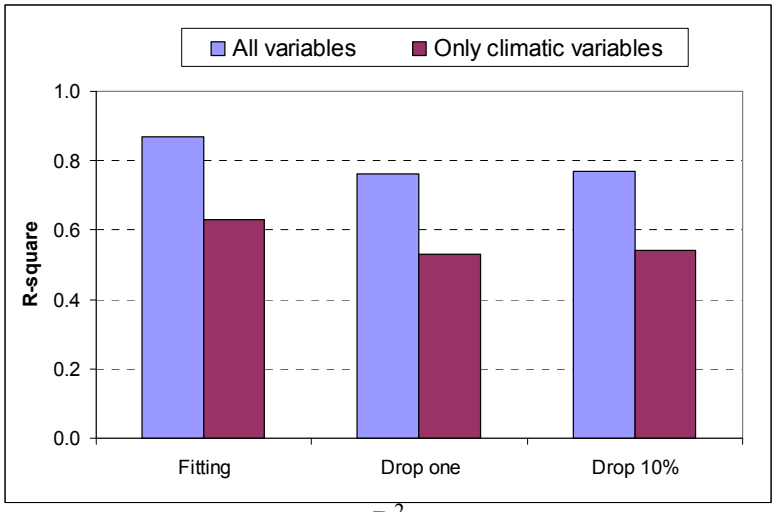

R^2

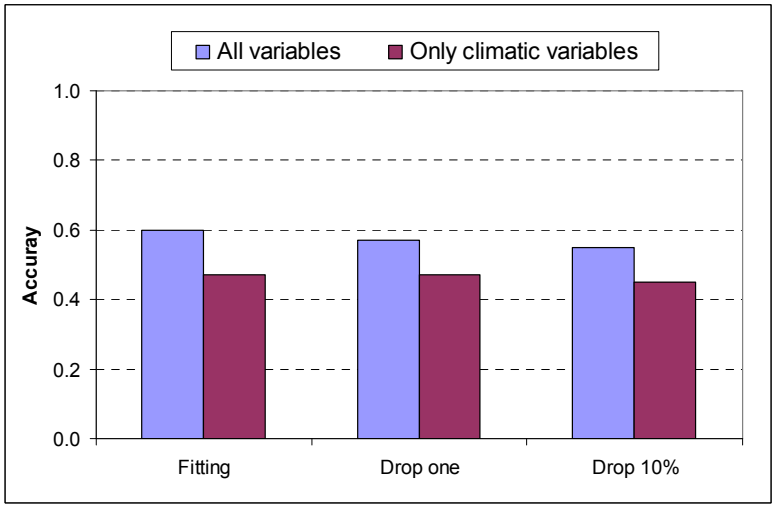

Accuracy

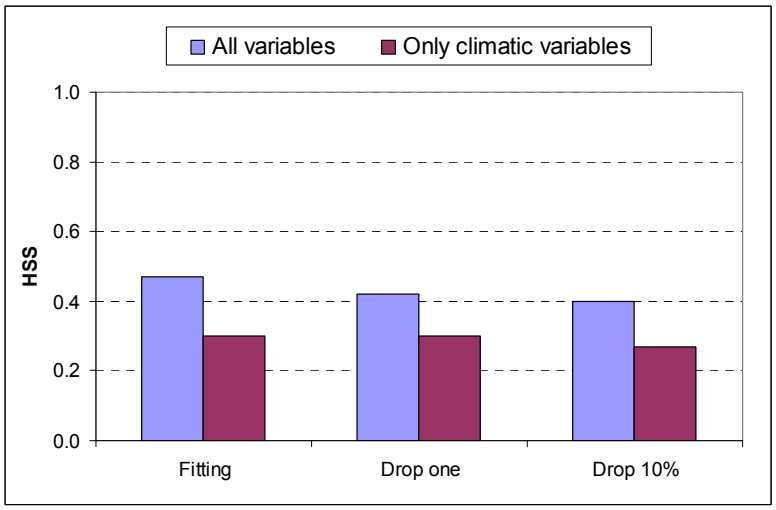

HSS

Figure 18. Comparison of R^2 for the models in sections 6.3.2 and 6.3.3

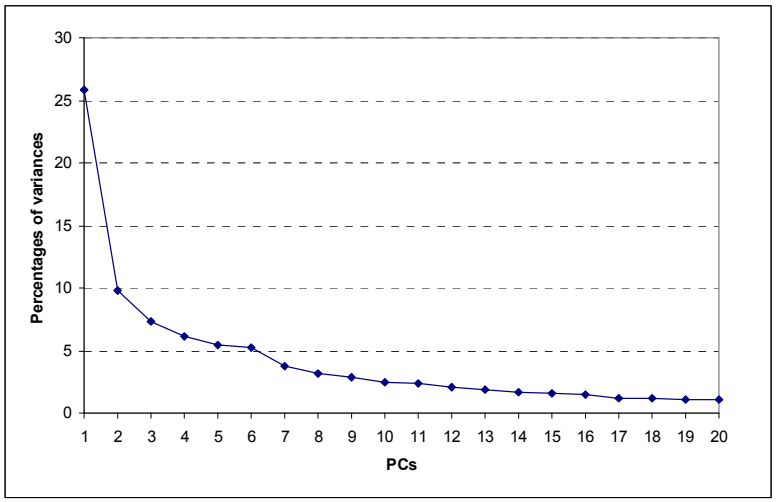

Figure 19. Variance of of the fist 20 PCs obtained from all of the potential predictors of 6 sites

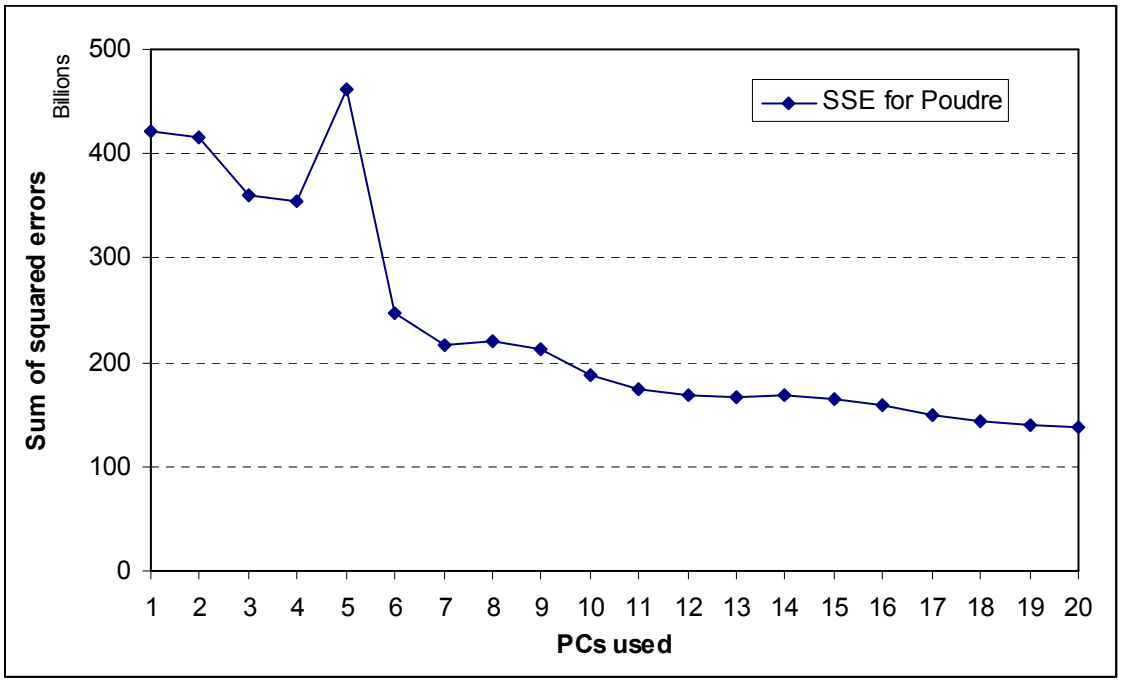

Figure 20. Sum of squared residuals of CCA model for the Poudre River using 20 PCs

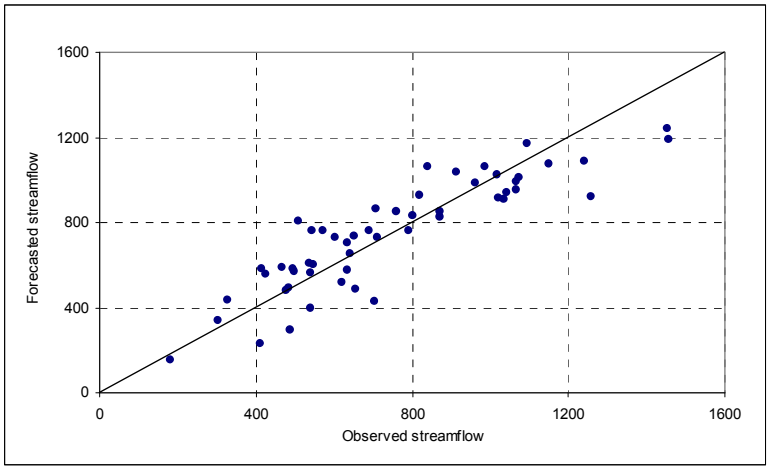

Fitting

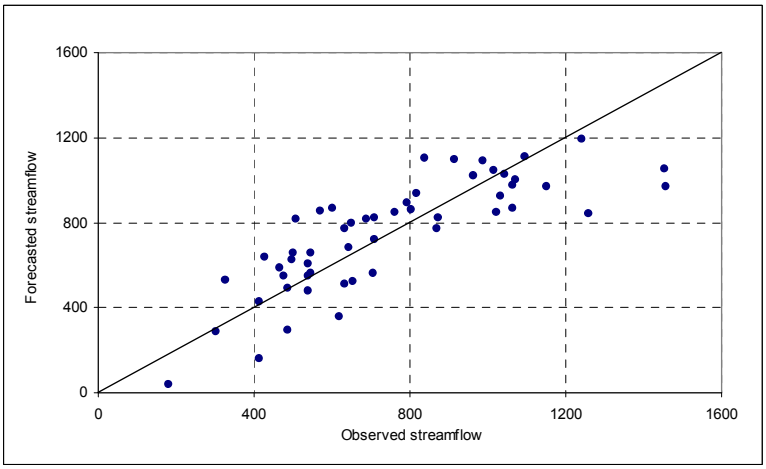

Drop one

Figure 21 Scatter plots of forecasted streamflows by CCA model for the Gunnison River

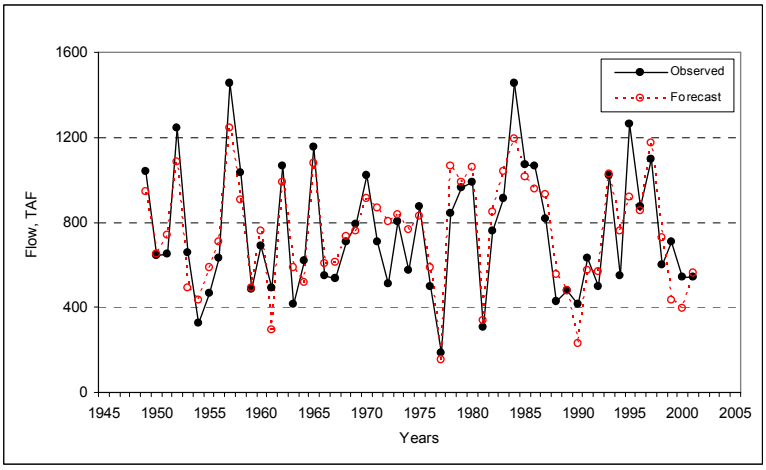

Fitting

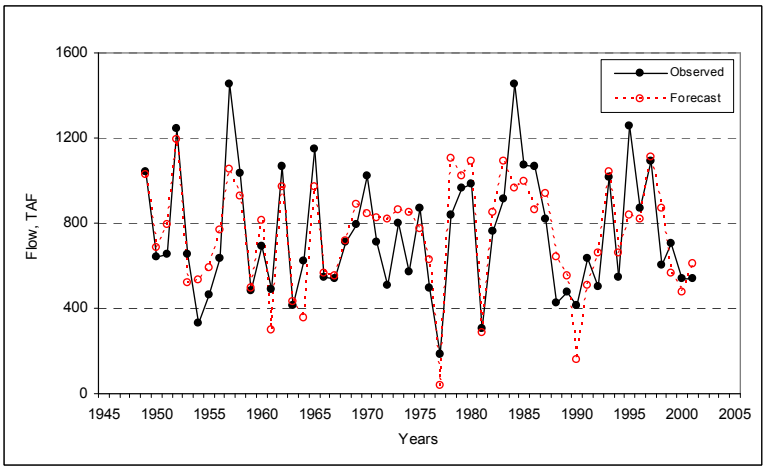

Drop one

Figure 22 Time series plots of forecasted streamflows by CCA model for the Gunnison River

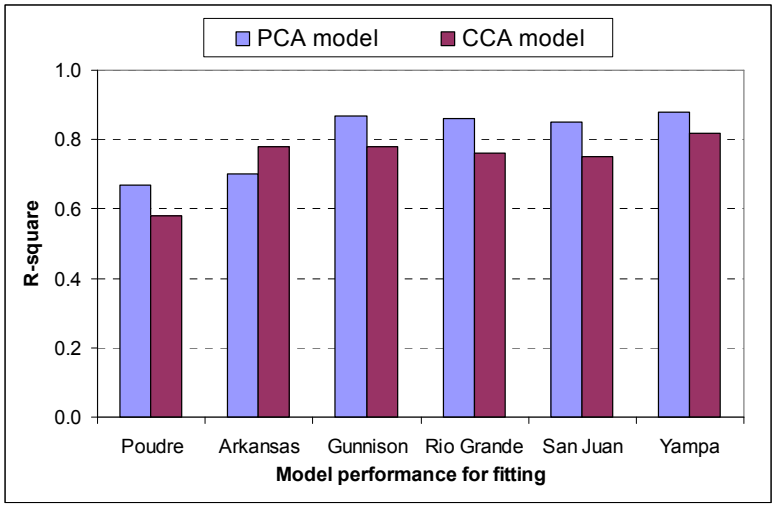

Fitting

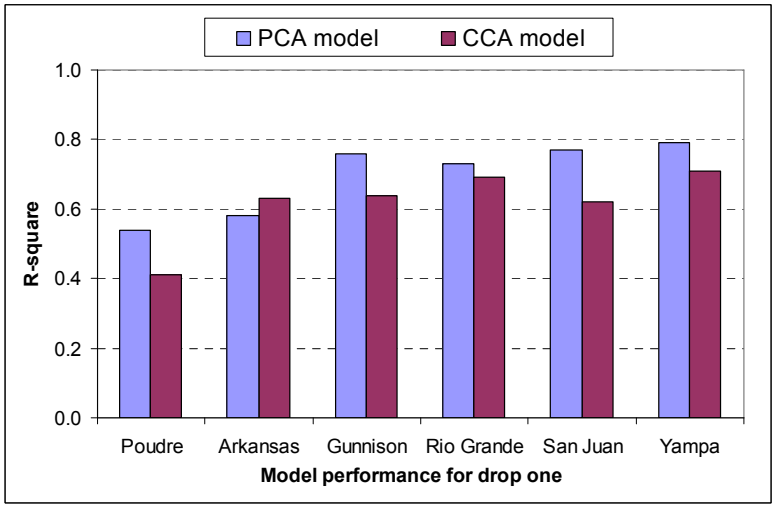

Drop one

Figure 23 Comparison of R^2 for the forecast models based on PCA and CCA for Gunnison River

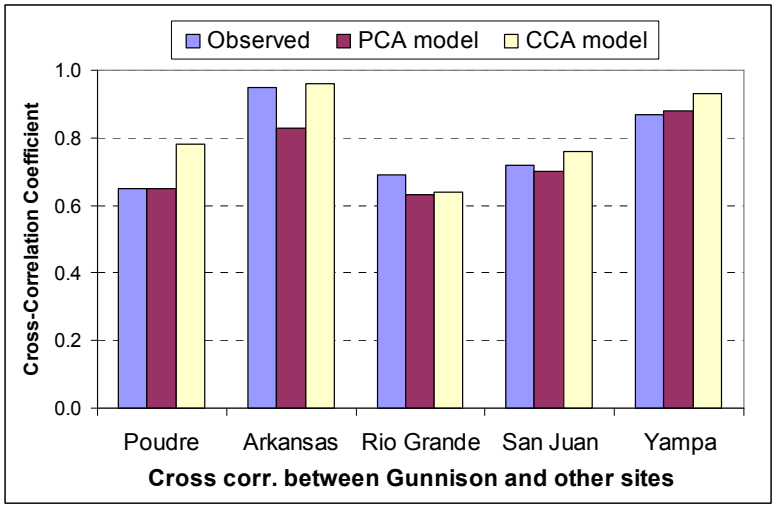

Fitting

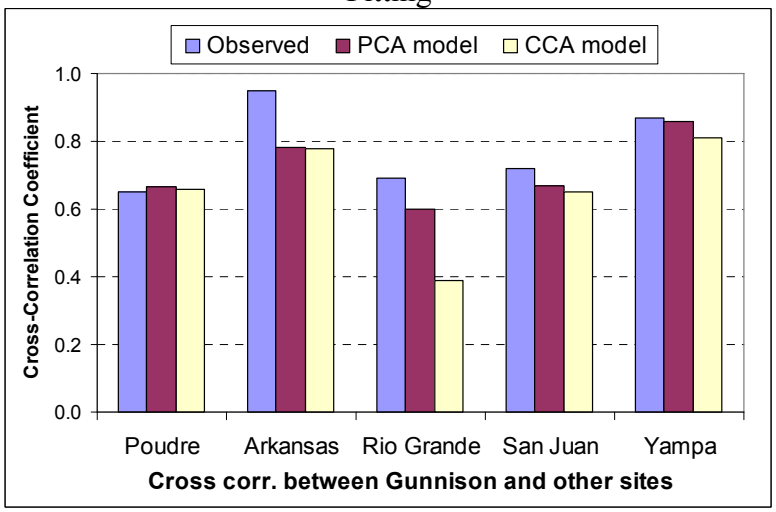

Drop one

Figure 24 Comparison of cross-correlation coefficient between the Gunnison River streamflows and those for the other sites obtained from historical and from PCA and CCA forecasts

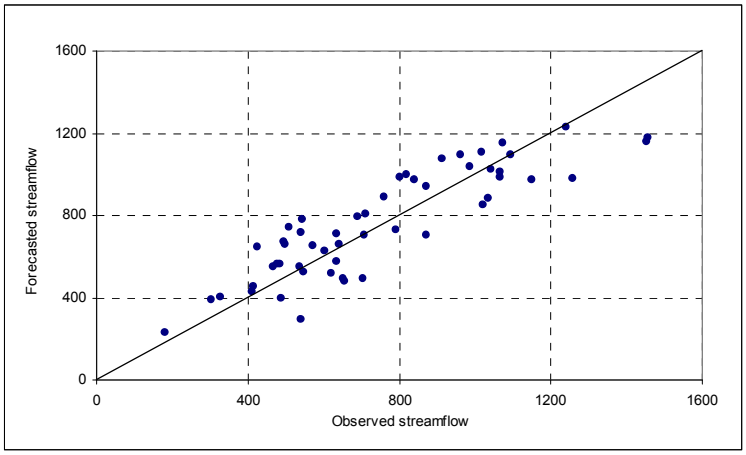

Fitting

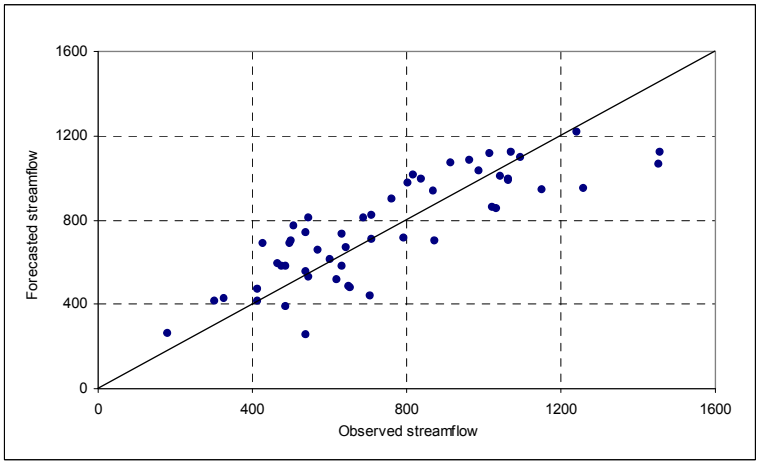

Drop one

Figure 25 Scatter plots of the forecast results by the aggregation – disaggregation model for Gunnison River

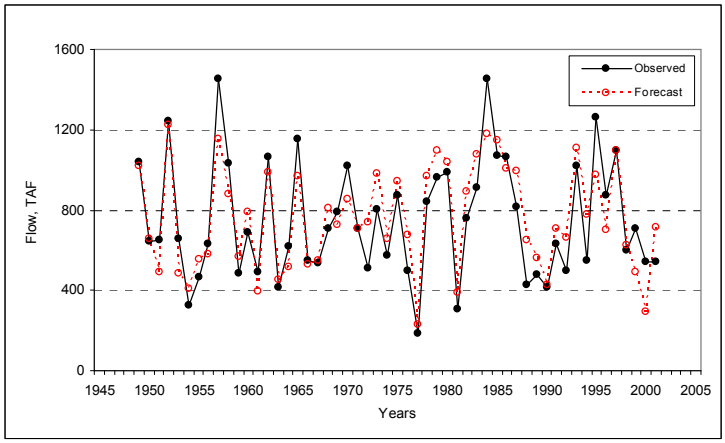

Fitting

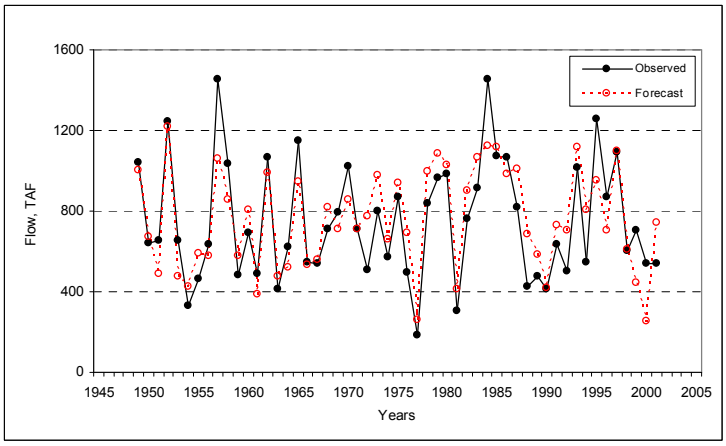

Drop one

Figure 26 Time series plots of the forecast results by the aggregation – disaggregation model for Gunnison River

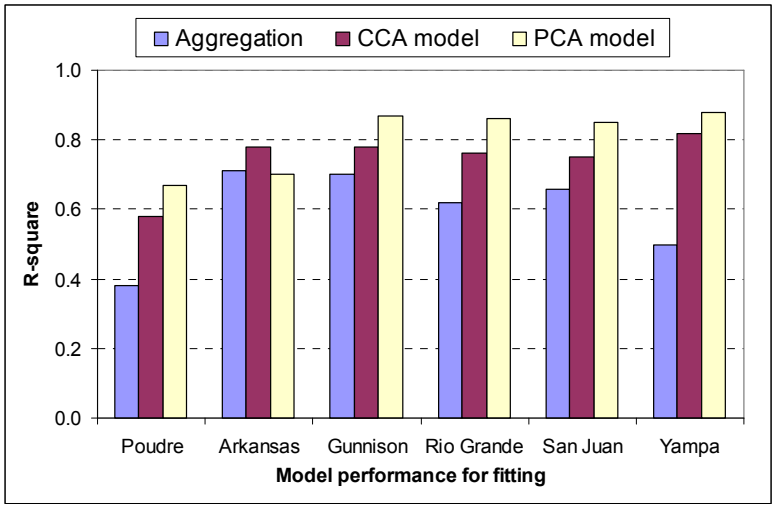

Fitting

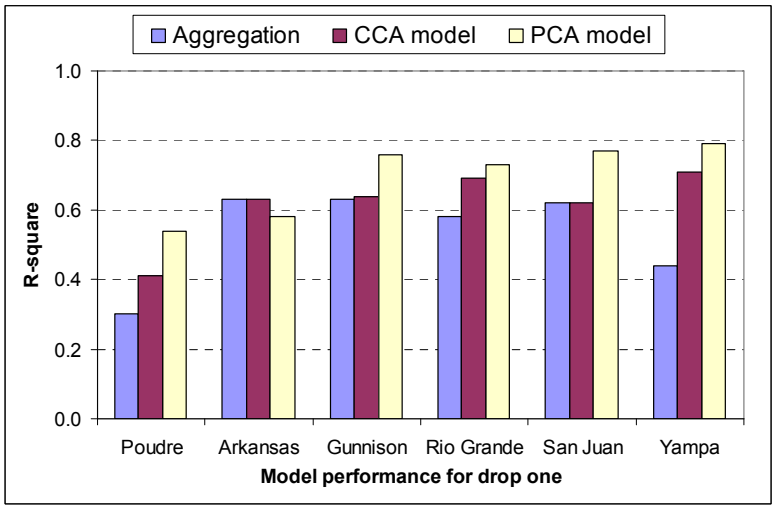

Drop one

Figure 27. Comparisons of R^2 for the Aggregation – Disaggregation, CCA and PCA models

A7: Potential predictors (for April-July)

Table A7.1 Potential predictors for Poudre River April-July Streamflow forecast

No	Name	Variable	Time	Location	General description	Corr. Coef
1	AF1	Accumulated flow of previous months	Prev. Apr-Mar		Accumulated flow for previous 12 months	0.15
2	SST1	Sea Surface Temperature	Jan-Mar	20°N-30°N 155°E-175°E	Northwest Pacific	-0.38
3	SST2	Sea Surface Temperature	Jan-Mar	6°S-15°S 100°W-120°W	Southeast Pacific	0.33
4	SST3	Sea Surface Temperature	Prev. Oct-Dec	23°N-28°N 160°E-165°E	Northwest Pacific	-0.42
5	SST4	Sea Surface Temperature	Prev. Jul-Sep	24°N-29°N 175°E-180°E	Northwest Pacific	-0.32
6	SST5	Sea Surface Temperature	Prev. Jul-Sep	30°N-40°N 20°W-30°W	Northeast Atlantic, west of Africa	-0.30
7	SST6	Sea Surface Temperature	Prev. Apr-Jun	20°N-26°N 160°E-170°E	Northwest Pacific	-0.31
8	SST7	Sea Surface Temperature	Prev. Apr-Jun	0°-5°S 160°E-170°E	Central west Pacific, east of Malaysia	0.35
9	SST8	Sea Surface Temperature	Prev. Apr-Jun	39°N-44°N 25°W-30°W	North central Atlantic	-0.29
10	GH1	Geopotential Height (700 mb)	Jan-Mar	35°N-45°N 120°W-180°W	Over north pacific	-0.45
11	GH2	Geopotential Height (700 mb)	Jan-Mar	68°N-76°N 175°E-175°W	Over western Canada and eastern Russia	0.34
12	GH3	Geopotential Height (700 mb)	Prev. Oct-Dec	32°N-52°N 100°W-125°W	Over western and central U.S.	-0.37
13	GH4	Geopotential Height (700 mb)	Prev. Oct-Dec	35°N-50°N 60°W-80°W	Over eastern U.S.	0.37
14	GH5	Geopotential Height (700 mb)	Prev. Oct-Dec	60°N-65°N 130°E-140°E	Over eastern Russia	-0.31
15	MW1	Meridional Wind (700 mb)	Prev. Oct-Dec	32°N-46°N 75°W-95°W	Eastern Canada and eastern U.S.	0.51
16	ZW1	Zonal Wind (700 mb)	Jan-Mar	25°N-30°N 170°W-125°W	Northern Pacific	0.40
17	ZW2	Zonal Wind (700 mb)	Jan-Mar	48°N-60°N 170°E-150°W	Northern Pacific	-0.41
18	ZW3	Zonal Wind (700 mb)	Jan-Mar	2°S-8°S 135°W-155°W	South Pacific near equator	0.41
19	ZW4	Zonal Wind (700 mb)	Prev. Jul-Sep	5°N-15°N 25°W-35°W	North Atlantic	-0.32
20	AT1	Air Temperature	Prev. Oct-Dec	40°N-50°N 115°W-125°W	Northwest U.S. and southwest Canada	-0..42
21	OLR1	Outgoing Long-Wave Radiation	Jan-Mar	30°N-35°N 150°W-165°W	Western states and west coast of U.S.	-0.39
22	OLR2	Outgoing Long-Wave Radiation	Prev. Oct-Dec	32°N-40°N 115°W-130°W	Western states and west coast of U.S.	-0.44
23	OLR3	Outgoing Long-Wave Radiation	Prev. Oct-Dec	20°N-26°N 150°W-165°W	Northwest Pacific	0.39
24	OLR4	Outgoing Long-Wave Radiation	Prev. Oct-Dec	5°N-2°S 118°W-130°W	East Pacific near equator	-0.33
25	RH1	Relative Humidity	Jan-Mar	38°N-45°N	Western mountain states	0.43

				117°W-122°W		
26	RH2	Relative Humidity	Jan-Mar	38°N-45°N 85°W-95°W	Eastern U.S.	0.42
27	NAO1	North Atlantic Oscillation	Jan			0.34
28	NOI1	Northern Oscillation Index	Jan-Mar			-0.42
29	PNA1	Pacific North America Index	Mar			0.38
30	PDO1	Pacific Decadal Oscillation	Mar			0.31
31	SOI1	Southern Oscillation Index	Jan-Mar			-0.28
32	PDSI1	Palmer Index	Jan-Mar		Climate Division	0.32
33	PDSI2	Palmer Index	Nov-Dec		Climate Division	0.28
34	SWE1	Snow Water Equivalent	Feb 1st		Basin average	0.46
35	SWE2	Snow Water Equivalent	Mar 1st		Basin average	0.49
36	SWE3	Snow Water Equivalent	Apr 1st		Basin average	0.65

Table A7.2 Potential predictors for Arkansas River April-July Flow

No	Name	Variable	Time	Location	General description	Corr. Coef
1	AF1	Accumulated flow of previous months	Prev. Apr-Mar		Accumulated flow volumes for previous 12 months	0.23
2	SST1	Sea Surface Temperature	Jan-Mar	25°N-30°N 160°E-165°E	Northwest Pacific	-0.46
3	SST2	Sea Surface Temperature	Prev. Oct-Dec	25°N-30°N 160°E-165°E	Northwest Pacific	-0.39
4	SST3	Sea Surface Temperature	Prev. Jul-Sep	25°N-35°N 20°W-30°W	Northwest Atlantic	-0.45
5	SST4	Sea Surface Temperature	Prev. Apr-Jun	35°N-45°N 20°W-25°W	Northwest Atlantic	-0.35
6	GH1	Geopotential Height (700 mb)	Prev. Oct-Dec	38°N-47°N 116°W-122°W	Western U.S.	-0.39
7	GH2	Geopotential Height (700 mb)	Prev. Oct-Dec	42°N-50°N 70°W-80°W	Eastern Canada and U.S.	0.47
8	GH3	Geopotential Height (700 mb)	Prev. Oct-Dec	28°N-33°N 172°E-180°E	North central Pacific	-0.31
9	MW1	Meridional Wind (700 mb)	Prev. Oct-Dec	45°N-55°N 130°W-135°W	Northeast U.S.	0.50
10	MW2	Meridional Wind (700 mb)	Prev. Oct-Dec	35°N-45°N 55°W-60°W	Eastern Canada and eastern U.S.	0.53
11	ZW1	Zonal Wind (700 mb)	Prev. Oct-Dec	48°N-57°N 105°W-118°W	Southern Canada	-0.42
12	ZW2	Zonal Wind (700 mb)	Prev. Oct-Dec	27°N-32°N 100°W-118°W	Southern U.S.	0.50
13	AT1	Air Temperature	Prev. Oct-Dec	35°N-48°N 115°W-130°W	Northwest U.S.	-0.41
14	OLR1	Outgoing Long-Wave Radiation	Prev. Oct-Dec	40°N-45°N 115°W-120°W	Western mountain states of U.S.	-0.29
15	RH1	Relative Humidity	Prev. Oct-Dec	40°N-45°N 117°W-122°W	Western mountain states	0.37
16	RH2	Relative Humidity	Prev. Oct-Dec	28°N-35°N 75°W-80°W	Southeast coast of U.S.	0.49
17	PDSI1	Palmer Index	Jan-Mar		Climate Division	0.35
18	PDSI2	Palmer Index	Prev. Nov-Dec		Climate Division	0.28
19	SWE1	Snow Water	Feb 1st		Basin average	0.56

		Equivalent				
20	SWE2	Snow Water Equivalent	Mar 1st		Basin average	0.56
21	SWE3	Snow Water Equivalent	Apr 1st		Basin average	0.60

Table A7.3 Potential predictors for Gunnison River April-July flow

No	Name	Variable	Time	Location	General description	Corr. Coef
1	AF1	Accumulated flow of previous months	Prev. Apr-Mar		Accumulated flow for previous 12 months	0.13
2	SST1	Sea Surface Temperature	Jan-Mar	50°N-53°N 155°W-165°W	Northern central Pacific, south of Alaska	0.35
3	SST2	Sea Surface Temperature	Jan-Mar	25°N-30°N 155°E-175°E	Northwest Pacific, southeast of Japan	-0.45
4	SST3	Sea Surface Temperature	Prev. Oct-Dec	50°N-53°N 158°W-168°W	Northern central Pacific, south of Alaska	0.32
5	SST4	Sea Surface Temperature	Prev. Oct-Dec	25°N-32°N 158°E-168°E	Northwest Pacific, southeast of Japan	-0.45
6	SST5	Sea Surface Temperature	Prev. Oct-Dec	30°N-35°N 54°W-59°W	Northern central Atlantic	-0.34
7	SST6	Sea Surface Temperature	Prev. Jul-Sep	28°N-34°N 20°W-30°W	Northeast Atlantic	-0.42
8	SST7	Sea Surface Temperature	Prev. Apr-Jun	46°N-53°N 158°E-168°E	Northwest Pacific, northeast of Japan	0.40
9	SST8	Sea Surface Temperature	Prev. Apr-Jun	25°N-30°N 165°E-170°E	Northwest Pacific, southeast of Japan	-0.32
10	SST9	Sea Surface Temperature	Prev. Apr-Jun	38°N-43°N 15°W-20°W	Northeast Atlantic	-0.31
11	SSST1	Seesaw SST	Jan-Mar		SST1-SST2	0.50
12	SSST2	Seesaw SST	Prev. Oct-Dec		SST3-SST4	0.53
13	GH1	Geopotential Height (700 mb)	Jan-Mar	30°N-40°N 130°E-160°E	Northwest Pacific, partly over Japan	-0.33
14	GH2	Geopotential Height (700 mb)	Prev. Oct-Dec	35°N-55°N 105°W-130°W	Over central and western U.S.	-0.38
15	GH3	Geopotential Height (700 mb)	Prev. Oct-Dec	40°N-60°N 60°W-75°W	Over eastern Canada and eastern U.S.	0.43
16	GH4	Geopotential Height (700 mb)	Prev. Oct-Dec	53°N-58°N 150°W-155°W	Southern Alaska	0.34
17	GH5	Geopotential Height (700 mb)	Prev. Oct-Dec	27°N-32°N 170°E-180°E	Northwest Pacific	-0.35
18	GH6	Geopotential Height (700 mb)	Prev. Jul-Sep	30°N-38°N 150°E-165°E	Northwest Pacific, east of Japan	-0.40
19	MW1	Meridional Wind (700 mb)	Prev. Oct-Dec	35°N-55°N 80°W-95°W	Eastern Canada and eastern U.S.	0.51
20	MW2	Meridional Wind (700 mb)	Prev. Oct-Dec	45°N-55°N 130°W-135°W	Northeast Pacific, west of Canada and U.S.	-0.43
21	MW3	Meridional Wind (700 mb)	Prev. Oct-Dec	30°N-55°N 40°W-65°W	Northwest Atlantic, east of CA and U.S.	-0.44
22	ZW1	Zonal Wind (700 mb)	Jan-Mar	48°N-55°N 110°W-125°W	Southwest Canada	-0.33
23	ZW2	Zonal Wind (700 mb)	Jan-Mar	20°N-28°N 130°E-160°E	Western Pacific, east of China	0.34
24	ZW3	Zonal Wind (700 mb)	Prev. Oct-Dec	25°N-35°N 100°W-120°W	Southern U.S.	0.44
25	ZW4	Zonal Wind (700 mb)	Prev. Oct-Dec	50°N-56°N 115°W-125°W	Southwest Canada and northwest U.S.	-0.39
26	AT1	Air Temperature	Prev. Oct-Dec	45°N-55°N 105°W-110°W	Western mountain states	-0.44
27	OLR1	Outgoing Long-Wave Radiation	Jan-Mar	34°N-44°N 90°W-105°W	Central states and western mountain states	-0.37

28	OLR2	Outgoing Long-Wave Radiation	Prev. Oct-Dec	31°N-46°N 105°W-120°W	Central states and western mountain states	-0.44
29	RH1	Relative Humidity	Jan-Mar	38°N-45°N 115°W-120°W	Western mountain states	0.30
30	RH2	Relative Humidity	Prev. Oct-Dec	38°N-45°N 115°W-120°W	Western mountain states	0.35
31	RH3	Relative Humidity	Prev. Oct-Dec	30°N-35°N 70°W-80°W	Southeast U.S.	0.48
32	RH4	Relative Humidity	Prev. Oct-Dec	27°N-32°N 155°W-170°W	Northern central Pacific	0..36
33	AO1	Arctic Oscillation	Mar			-0.30
34	SWMR1	South-West Monsoon Rainfall	Jan-Mar		Arizona and New Mexico rainfall	0.37
35	PDSI1	Palmer Index	Jan-Mar		Climate Division	0.70
36	PDSI2	Palmer Index	Prev. Oct-Dec		Climate Division	0.43
37	SWE1	Snow Water Equivalent	Feb 1st		Basin average	0.73
38	SWE2	Snow Water Equivalent	Mar 1st		Basin average	0.76
39	SWE3	Snow Water Equivalent	Apr 1st		Basin average	0.85

Table A7.4 Potential predictors for Rio Grande (near Taos) April-July flow

No	Name	Variable	Time	Location	General description	Corr. Coef
1	AF1	Accumulated flow of previous months	Prev. Apr-Mar		Accumulated flow for previous 12 months	0.25
2	SST1	Sea Surface Temperature	Jan-Mar	47°N-55°N 148°W-158°W	Northeast Pacific, south of Alaska	0.49
3	SST2	Sea Surface Temperature	Jan-Mar	22°N-29°N 148°W-158°W	North central Pacific	-0.41
4	SST3	Sea Surface Temperature	Jan-Mar	12°N-18°N 152°E-160°E	Northwest Pacific	-0.38
5	SST4	Sea Surface Temperature	Jan-Mar	11°S-18°S 105°W-115°W	Southeast Pacific	0.38
6	SST5	Sea Surface Temperature	Jan-Mar	50°N-68°N 25°W-38°W	North Atlantic	-0.41
7	SST6	Sea Surface Temperature	Prev. Oct-Dec	42°N-48°N 145°W-160°W	Northeast Pacific, south of Canada	0.43
8	SST7	Sea Surface Temperature	Prev. Oct-Dec	29°N-34°N 169°E-179°E	Northwest Pacific, southeast of Japan	-0.42
9	SST8	Sea Surface Temperature	Prev. Oct-Dec	13°S-18°S 105°W-115°W	Southeastern Pacific	0.39
10	SST9	Sea Surface Temperature	Prev. Oct-Dec	55°N-60°N 30°W-38°W	North central Atlantic	-0.46
11	SST10	Sea Surface Temperature	Prev. Oct-Dec	3°N-12°N 45°W-55°W	Northwestern Atlantic	-0.41
12	SST11	Sea Surface Temperature	Prev. Jul-Sep	25°-30°N 150°E-155°E	Northwest Pacific	-0.40
13	SST12	Sea Surface Temperature	Prev. Jul-Sep	10°N-16°N 78°W-85°W	Caribbean Sea	-0.32
14	SST13	Sea Surface Temperature	Prev. Jul-Sep	8°N-16°N 48°W-58°W	Northwestern Atlantic	-0.42
15	SST14	Sea Surface Temperature	Prev. Jul-Sep	13°N-23°N 22°E-30°E	Northeast Atlantic	-0.33
16	SST15	Sea Surface Temperature	Prev. Apr-Jun	24°N-30°N 160°E-170°E	Northwest Pacific	-0.38

17	SST16	Sea Surface Temperature	Prev. Apr-Jun	52°N-59°N 25°W-35°W	North Atlantic	-0.45
18	SST17	Sea Surface Temperature	Prev. Apr-Jun	35°N-45°N 10°W-20°W	Northeast Atlantic	-0.45
19	SSST1	Seesaw SST	Jan-Mar		SST1-SST2	0.54
20	SSST2	Seesaw SST	Prev. Oct-Dec		SST6-SST7	0.52
21	GH1	Geopotential Height (700 mb)	Jan-Mar	29°N-39°N 120°W-130°W	West coast of U.S.	-0.39
22	GH2	Geopotential Height (700 mb)	Prev. Oct-Dec	30°N-40°N 110°W-120°W	Southwest U.S.	-0.46
23	GH3	Geopotential Height (700 mb)	Prev. Oct-Dec	28°N-38°N 70°W-80°W	Southeast U.S.	0.61
24	GH4	Geopotential Height (700 mb)	Prev. Oct-Dec	46°N-56°N 140°W-150°W	Northeast Pacific	0.50
25	GH5	Geopotential Height (700 mb)	Prev. Oct-Dec	60°N-70°N 90°W-105°W	Northeast Canada	-0.44
26	GH6	Geopotential Height (700 mb)	Prev. Oct-Dec	52°N-62°N 28°W-38°W	Northern Atlantic	-0.51
27	GH7	Geopotential Height (700 mb)	Prev. Jul-Sep	30°N-40°N 160°E-170°E	Northwest Pacific	-0.35
28	MW1	Meridional Wind (700 mb)	Prev. Oct-Dec	44°N-54°N 132°W-124°W	Northwestern U.S. and southwest coast of Canada	-0.57
29	MW2	Meridional Wind (700 mb)	Prev. Oct-Dec	28°N-44°N 80°W-100°W	Eastern U.S.	0.61
30	MW3	Meridional Wind (700 mb)	Prev. Oct-Dec	44°N-50°N 50°W-60°W	East coast of Canada	-0.52
31	ZW1	Zonal Wind (700 mb)	Jan-Mar	40°N-50°N 108°W-122°W	Northwest U.S.	-0.45
32	ZW2	Zonal Wind (700 mb)	Jan-Mar	20°N-30°N 110°W-120°W	Northeastern Pacific, west of Mexico	0.46
33	ZW3	Zonal Wind (700 mb)	Prev. Oct-Dec	20°N-30°N 100°W-120°W	South of U.S.	0.61
34	ZW4	Zonal Wind (700 mb)	Prev. Oct-Dec	22°N-28°N 60°W-85°W	Caribbean Sea	-0.47
35	ZW5	Zonal Wind (700 mb)	Prev. Jul-Sep	7°N-15°N 50°W-58°W	Northwest Atlantic	-0.45
36	ZW6	Zonal Wind (700 mb)	Prev. Jul-Sep	22°N-30°N 35°W-60°W	Central north Atlantic	0.41
37	AT1	Air Temperature	Prev. Oct-Dec	32°N-50°N 105°W-120°W	Western U.S.	-0.67
38	OLR1	Outgoing Long-Wave Radiation	Jan-Mar	32°N-40°N 105°W-115°W	Southwestern U.S.	-0.49
39	OLR2	Outgoing Long-Wave Radiation	Prev. Oct-Dec	30°N-42°N 100°W-112°W	Southwestern U.S.	-0.61
40	RH1	Relative Humidity	Jan-Mar	33°N-40°N 105°W-115°W	Southwestern U.S.	0.53
41	RH2	Relative Humidity	Prev. Oct-Dec	30°N-40°N 105°W-118°W	Southwestern U.S.	0.60
42	RH3	Relative Humidity	Prev. Oct-Dec	32°N-40°N 89°W-109°W	Central east U.S.	0.59
43	PDO1	Pacific Decadal Oscillation	Mar			0.40
44	PDSI1	Palmer Index	Jan-Mar		Climate Division	0.51
45	PDSI2	Palmer Index	Prev. Nov-Dec		Climate Division	0.36
46	SWE1	Snow Water Equivalent	Feb 1st		Basin average	0.46

47	SWE2	Snow Water Equivalent	Mar 1st		Basin average	0.49
48	SWE3	Snow Water Equivalent	Apr 1st		Basin average	0.65

Table A7.5 Potential predictors for San Juan River April-July flow

No	Name	Variable	Time	Location	General description	Corr. Coef
1	AF1	Accumulated flow of previous months	Prev. Apr-Mar		Accumulated flow of previous 12 months	-0.08
2	SST1	Sea Surface Temperature	Jan-Mar	40°N-50°N 145°W-155°W	Northeast Pacific	0.40
3	SST2	Sea Surface Temperature	Jan-Mar	12°S-20°S 105°W-115°W	Southeast Pacific	0.32
4	SST3	Sea Surface Temperature	Prev. Oct-Dec	42°N-48°N 160°W-170°W	North central Pacific, south of Alaska	0.31
5	SST4	Sea Surface Temperature	Prev. Oct-Dec	28°N-33°N 170°E-175°E	Northwest Pacific, southeast of Japan	-0.48
6	SST5	Sea Surface Temperature	Prev. Jul-Sep	18°N-30°N 20°W-25°W	North central Atlantic	-0.43
7	SST6	Sea Surface Temperature	Prev. Apr-Jun	25°N-30°N 150°E-170°E	Northwest Pacific	-0.35
8	SST7	Sea Surface Temperature	Prev. Apr-Jun	30°N-46°N 15°W-20°W	Northeast Atlantic	-0.41
9	GH1	Geopotential Height (700 mb)	Jan-Mar	30°N-35°N 115°W-125°W	West coast of U.S.	-0.59
10	GH2	Geopotential Height (700 mb)	Prev. Oct-Dec	30°N-35°N 110°W-120°W	Southwest U.S.	-0.46
11	GH3	Geopotential Height (700 mb)	Prev. Oct-Dec	31°N-36°N 70°W-75°W	Southeast U.S.	0.40
12	GH4	Geopotential Height (700 mb)	Prev. Oct-Dec	45°N-55°N 145°W-150°W	Northeast Pacific	0.42
13	GH5	Geopotential Height (700 mb)	Prev. Oct-Dec	28°N-33°N 175°E-180°E	North central Pacific	-0.42
14	MW1	Meridional Wind (700 mb)	Prev. Oct-Dec	32°N-45°N 80°W-92°W	Eastern U.S.	0.49
15	MW2	Meridional Wind (700 mb)	Prev. Oct-Dec	33°N-45°N 120°W-128°W	West coast of U.S.	-0.50
16	MW3	Meridional Wind (700 mb)	Prev. Oct-Dec	45°N-50°N 50°W-60°W	Northwest Atlantic	-0.40
17	ZW1	Zonal Wind (700 mb)	Jan-Mar	45°N-50°N 110°W-120°W	Northern U.S.	-0.43
18	ZW2	Zonal Wind (700 mb)	Jan-Mar	22°N-29°N 115°W-122°W	Northeast Pacific	0.54
19	ZW3	Zonal Wind (700 mb)	Prev. Oct-Dec	22°N-29°N 115°W-122°W	Northeast Pacific	0.50
20	AT1	Air Temperature	Prev. Oct-Dec	35°N-46°N 115°W-120°W	Western U.S.	-0.54
21	AT2	Air Temperature	Prev. Oct-Dec	28°N-33°N 80°W-85°W	Southeast U.S.	0.38
22	OLR1	Outgoing Long-Wave Radiation	Jan-Mar	33°N-40°N 110°W-115°W	Central U.S.	-0.58
23	OLR2	Outgoing Long-Wave Radiation	Prev. Oct-Dec	33°N-40°N 110°W-115°W	Central U.S.	-0.48
24	RH1	Relative Humidity	Jan-Mar	28°N-33°N 110°W-115°W	Southwest U.S.	0.57
25	RH2	Relative Humidity	Prev. Oct-Dec	28°N-33°N 110°W-115°W	Southwest U.S.	0.48
26	NOI1	Northern Oscillation Index	Jan-Mar			-0.31
27	SWMR1	Southwest Monsoon	Jan-Mar		Arizona and New Mexico	0.60

		Rainfall			rainfall	
28	PDSI1	Palmer Index	Jan-Mar		Climate Division	0.64
29	PDSI2	Palmer Index	Prev. Nov-Dec		Climate Division	0.38
30	SWE1	Snow Water Equivalent	Feb 1st		Basin average	0.62
31	SWE2	Snow Water Equivalent	Mar 1st		Basin average	0.67
32	SWE3	Snow Water Equivalent	Apr 1st		Basin average	0.85

Table A7.6 Potential predictors for Yampa River April-July flow

No	Name	Variable	Time	Location	General description	Corr. Coef
1	AF1	Accumulated flow of previous months	Prev. Apr-Mar		Accumulated flow for previous 12 months	0.22
2	SST1	Sea Surface Temperature	Jan-Mar	45°N-50°N 170°W-175°W	Northern central Pacific, south of Alaska	0.42
3	SST2	Sea Surface Temperature	Jan-Mar	25°N-30°N 160°E-165°E	Northwest Pacific, southeast of Japan	-0.52
4	SST3	Sea Surface Temperature	Prev. Jul-Sep	29°N-34°N 20°W-30°W	Northeast Atlantic	-0.45
5	SST4	Sea Surface Temperature	Prev. Apr-Jun	30°N-35°N 170°W-180°W	Northern central Pacific	-0.37
6	GH1	Geopotential Height (700 mb)	Jan-Mar	30°N-35°N 155°E-160°E	Northwest Pacific	-0.43
7	GH2	Geopotential Height (700 mb)	Prev. Oct-Dec	35°N-50°N 100°W-120°W	Northern U.S.	-0.53
8	GH3	Geopotential Height (700 mb)	Prev. Oct-Dec	53°N-58°N 60°W-65°W	Eastern Canada	0.38
9	MW1	Meridional Wind (700 mb)	Prev. Oct-Dec	45°N-55°N 85°W-95°W	Eastern Canada and eastern U.S.	0.54
10	MW2	Meridional Wind (700 mb)	Prev. Oct-Dec	45°N-56°N 135°W-145°W	West coast of Canada	-0.43
11	MW3	Meridional Wind (700 mb)	Prev. Oct-Dec	35°N-45°N 57°W-62°W	Northwest Atlantic	-0.41
12	ZW1	Zonal Wind (700 mb)	Jan-Mar	31°N-36°N 115°W-120°W	West coast of U.S.	0.42
13	ZW2	Zonal Wind (700 mb)	Jan-Mar	52°N-57°N 115°W-120°W	Southern Canada	-0.36
14	ZW3	Zonal Wind (700 mb)	Jan-Mar	22°N-28°N 150°E-160°E	Northwest Pacific	0.41
15	ZW4	Zonal Wind (700 mb)	Jan-Mar	42°N-48°N 155°E-165°E	Northwest Pacific	-0.38
16	ZW5	Zonal Wind (700 mb)	Prev. Oct-Dec	30°N-35°N 105°W-120°W	Southern U.S.	0.56
17	ZW6	Zonal Wind (700 mb)	Prev. Oct-Dec	55°N-60°N 110°W-122°W	Southern Canada	-0.52
18	AT1	Air Temperature	Prev. Oct-Dec	48°N-55°N 110°W-122°W	Western Canada	-0.56
19	OLR1	Outgoing Long-Wave Radiation	Jan-Mar	33°N-38°N 116°W-121°W	Southwest U.S.	-0.34
20	OLR2	Outgoing Long-Wave Radiation	Jan-Mar	38°N-43°N 90°W-100°W	Eastern U.S.	-0.38
21	OLR3	Outgoing Long-Wave Radiation	Prev. Oct-Dec	33°N-40°N 115°W-120°W	Southwest U.S.	-0.49
22	RH1	Relative Humidity	Jan-Mar	33°N-38°N 115°W-120°W	Western U.S.	0.35
23	RH2	Relative Humidity	Jan-Mar	32°N-37°N 87°W-92°W	Southeast U.S.	0.37

24	RH3	Relative Humidity	Prev. Oct-Dec	33°N-38°N 115°W-120°W	Western U.S.	0.36
25	PDO1	Pacific Decadal Oscillation	Mar			0.30
26	SWMR1	South-West Monsoon Rainfall	Jan		Arizona and New Mexico rainfall	0.30
27	PDSI1	Palmer Index	Jan-Mar		Climate Division	0.66
28	PDSI2	Palmer Index	Prev. Nov-Dec		Climate Division	0.40
29	SWE1	Snow Water Equivalent	Feb 1st		Basin average	0.54
30	SWE2	Snow Water Equivalent	Mar 1st		Basin average	0.57
31	SWE3	Snow Water Equivalent	Apr 1st		Basin average	0.51

A8: Potential predictors for yearly

Table A8.1 Potential predictors for Poudre River April-March flow

No	Name	Variable	Time	Location	General description	Corr. Coef
1	Log-1	Lag-1 flow	Prev. Apr-Mar			0.20
2	SST1	Sea Surface Temperature	Jan-Mar	20°N-28°N 160°E-170°E	Northwest Pacific	-0.42
3	SST2	Sea Surface Temperature	Jan-Mar	5°S-15°S 110°W-120°W	Southeast Pacific	0.33
4	SST3	Sea Surface Temperature	Oct-Dec	24°N-30°N 160°E-170°E	Northwest Pacific	-0.43
5	SST4	Sea Surface Temperature	Oct-Dec	5°S-20°S 85°W-110°W	Southeast Pacific	0.30
6	SST5	Sea Surface Temperature	Jul-Sep	23°N-29°N 172°E-180°W	Northwest Pacific	-0.33
7	SST6	Sea Surface Temperature	Jul-Sep	30°N-36°N 22°W-30°W	Northeast Atlantic	-0.35
8	SST7	Sea Surface Temperature	Apr-Jun	20°N-25°N 160°E-170°E	Northwest Pacific	-0.33
9	SST8	Sea Surface Temperature	Apr-Jun	33°N-38°N 25°W-30°W	Northeast Atlantic	-0.29
10	SSST1	Seesaw SST	Jan-Mar		SST2 – SST1	0.52
11	SSST2	Seesaw SST	Oct-Dec		SST4 – SST3	0.46
12	GH1	Geopotential Height (700 mb)	Jan-Mar	32°N-45°N 170°E-150°W	North Pacific	-0.41
13	GH2	Geopotential Height (700 mb)	Oct-Dec	40°N-50°N 105°W-120°W	West U.S.	-0.38
14	GH3	Geopotential Height (700 mb)	Oct-Dec	40°N-50°N 60°W-70°W	East U.S.	0.38
15	GH4	Geopotential Height (700 mb)	Jul-Sep	15°N-20°N 25°W-32°W	East Atlantic	0.30
16	MW1	Meridional Wind (700 mb)	Jan-Mar	14°N-19°N 120°W-125°W	Northeast Pacific	-0.44
17	MW2	Meridional Wind (700 mb)	Oct-Dec	35°N-45°N 80°E-90°W	Northwest U.S. and southwest Canada	0.52
18	ZW1	Zonal Wind (700 mb)	Jan-Mar	50°N-60°N 170°E-180°E	Northwest Pacific	-0.45
19	ZW2	Zonal Wind (700 mb)	Jan-Mar	25°N-30°N 170°E-175°W	Central north Pacific	0.33
20	ZW3	Zonal Wind (700 mb)	Oct-Dec	53°N-58°N 108°W-120°W	South Canada	-0.38
21	ZW4	Zonal Wind (700 mb)	Jul-Sep	5°N-15°N 25°W-40°W	Northeast Atlantic	-0.34

22	AT1	Air Temperature	Oct-Dec	42°N-55°N 110°W-125°W	Northwest U.S. and southwest Canada	-0.45
23	AT2	Air Temperature	Jul-Sep	58°N-65°N 30°W-45°W	South Greenland	-0.38
24	OLR1	Outgoing Long-Wave Radiation	Oct-Dec	33°N-45°S 110°W-125°W	West U.S.	-0.45
25	RH1	Relative Humidity	Jan-Mar	35°N-40°N 90°W-95°W	Central U.S.	0.47
26	EA1	East Atlantic Oscillation	Jun			0.38
27	MEI1	Multivariate ENSO Index	Mar			0.31
28	NAO1	North Atlantic Oscillation	Jan			0.34
29	NOI1	Northern Oscillation Index	Jan-Mar			-0.42
30	PDO1	Pacific Decadal Oscillation	Mar			0.33
31	PNA1	Pacific North American Index	Mar			0.35
32	PNA2	Pacific North American Index	Oct-Dec			-0.33
33	SOI1	Southern Oscillation Index	Feb			-0.32
34	SWM1	Southwest Monsoon Rainfall	Jan-Mar			0.36
35	PDSI1	Palmer Index	Mar		Climate Division	0.48
36	PDSI2	Palmer Index	Feb		Climate Division	0.37
37	PDSI3	Palmer Index	Jan		Climate Division	0.36
38	SWE	Snow Water Equivalent	Feb 1st		Basin average	0.49
39	SWE	Snow Water Equivalent	Mar 1st		Basin average	0.44
40	SWE	Snow Water Equivalent	Apr 1st		Basin average	0.63

Table A8.2 Potential predictors for Poudre River October-September flow

No	Name	Variable	Time	Location	General description	Corr. Coef
1	Lag-1	Lag-1 flow	Prev. Oct-Sep			0.16
2	SST1	Sea Surface Temperature	Jul-Sep	23°N-28°N 172°E-179°E	Central North Pacific	-0.37
3	SST2	Sea Surface Temperature	Jul-Sep	25°N-30°N 85°W-90°W	Southeast Pacific, west of Peru	0.31
4	SST3	Sea Surface Temperature	Jul-Sep	30°N-35°N 14°W-28°W	Northeast Atlantic	-0.33
5	SST4	Sea Surface Temperature	Apr-Jun	22°N-29°N 172°W-179°W	Central North Pacific	-0.33
6	SST5	Sea Surface Temperature	Apr-Jun	32°N-38°N 21°W-32°W	Northeast Atlantic	-0.35
7	SST6	Sea Surface Temperature	Jan-Mar	31°N-36°N 69°W-74°W	Northeast Atlantic	-0.29
8	SST7	Sea Surface Temperature	Oct-Dec	31°N-38°N 55°W-62°W	Northeast Atlantic	-0.32
9	GH1	Geopotential Height (700 mb)	Jul-Sep	12°N-20°N 20°W-30°W	Northeast Atlantic	0.31
10	GH2	Geopotential Height (700 mb)	Apr-Jun	44°N-50°N 120°W-1130°W	Northwest U.S. and southwest Canada	0.30
11	GH3	Geopotential Height (700 mb)	Apr-Jun	1°N-6°N 22°W-30°W	North Atlantic near equator	0.29

12	GH4	Geopotential Height (700 mb)	Oct-Dec	50°N-56°N 10°W-18°W	Northeast Atlantic	-0.30
13	MW1	Meridional Wind (700 mb)	Apr-Jun	41°N-48°N 98°W-108°W	Central North U.S.	-0.38
14	MW2	Meridional Wind (700 mb)	Apr-Jun	22°N-30°N 160°W-168°W	Central North Pacific	-0.36
15	MW3	Meridional Wind (700 mb)	Jan-Mar	72°N-78°N 120°W-112°W	South Arctic near Canada	-0.35
16	ZW1	Zonal Wind (700 mb)	Jul-Sep	4°N-16°N 25°W-45°W	North Atlantic near equator	-0.33
17	ZW2	Zonal Wind (700 mb)	Apr-Jun	45°N-50°N 126°W-132°W	Northwest Canada	0.34
18	ZW3	Zonal Wind (700 mb)	Apr-Jun	12°N-18°N 161°E-167°E	Central North Pacific	0.37
19	AT1	Air Temperature (surface)	Jul-Sep	60°N-68°N 40°W-50°W	South Greenland	-0.38
20	AT2	Air Temperature (surface)	Apr-Jun	38°N-44°N 89°W-96°W	Central U.S.	-0.30
21	AT3	Air Temperature (surface)	Apr-Jun	36°N-42°N 20°W-26°W	Northeast Atlantic	-0.31
22	AT4	Air Temperature (surface)	Jan-Mar	51°N-57°N 110°W-118°W	Central West U.S.	-0.29
23	OLR1	Outgoing Long-Wave Radiation	Apr-Jun	25°N-33°N 132°W-142°W	Northeast Pacific near U.S. and Mexico	-0.32
24	OLR2	Outgoing Long-Wave Radiation	Jan-Mar	30°N-37°N 97°W-112°W	Central U.S.	-0.29
25	EA1	East Atlantic (oscillation)	Feb			0.31
26	EA2	East Atlantic (oscillation)	Jun			0.37
27	NOI1	North Atlantic Oscillation	Dec-Jan			-0.29

Table A8.3 Potential predictors for Gunnison River April-March flow

No	Name	Variable	Time	Location	General description	Corr. Coef
1	Lag-1	Lag-1 flow	Prev. Apr-Mar			0.15
2	SST1	Sea Surface Temperature	Jan-Mar	46°N-51°N 160°W-170°W	Northeast Pacific	0.48
3	SST2	Sea Surface Temperature	Jan-Mar	25°N-30°N 165°E-175°E	Northwestl Pacific	-0.39
4	SST3	Sea Surface Temperature	Prev. Oct-Dec	43°N-48°N 170°W-175°W	Northeast Pacific	0.41
5	SST4	Sea Surface Temperature	Prev. Oct-Dec	26°N-31°N 165°E-170°E	Northwest Pacific	-0.41
6	SST5	Sea Surface Temperature	Prev. Jul-Sep	27°N-32°N 25°W-30°W	Northeast Atlantic	-0.42
7	SSST1	Seesaw SST	Jan-Mar		SST1-SST2	0.49
8	SSST2	Seesaw SST	Prev. Oct-Dec		SST3-SST4	0.52
9	GH1	Geopotential Height (700 mb)	Jan-Mar	30°N-40°N 130°E-140°E	Northwest Pacific	-0.32
10	GH2	Geopotential Height (700 mb)	Prev. Oct-Dec	32°N-50°N 110°W-120°W	Over U.S.	-0.40
11	GH3	Geopotential Height (700 mb)	Prev. Oct-Dec	45°N-52°N 66°W-75°W	Southeast Canada	0.44
12	GH4	Geopotential Height (700 mb)	Prev. Oct-Dec	27°N-32°N 175°E-180°E	North central Pacific	-0.35
13	GH5	Geopotential Height (700 mb)	Prev. Jul-Sep	30°N-35°N 160°E-165°E	North central Pacific	-0.36

14	GH6	Geopotential Height (700 mb)	Prev. Apr-Jun	50°N-60°N 80°W-85°W	Northwest PAcific	-0.29
15	PR1	Precipitation Rate	Jan-Mar	35°N-41°N 115°W-120°W	West U.S.	0.31
16	PR2	Precipitation Rate	Jan-Mar	24°N-29°N 88°W-93°W	Gulf of Mexico	0.36
17	PR3	Precipitation Rate	Jan-Mar	17°N-22°N 170°E-175°E	Northwest Pacific	-0.28
18	PR4	Precipitation Rate	Prev. Oct-Dec	40°N-45°N 115°W-120°W	West U.S.	0.48
19	PR5	Precipitation Rate	Prev. Oct-Dec	28°N-33°N 170°W-175°W	Northwest Pacific	0.32
20	PW1	Precipitable Water	Jan-Mar	30°N-35°N 105°W-110°W	South U.S.	0.37
21	PW2	Precipitable Water	Prev. Oct-Dec	32°N-40°N 75°W-90°W	Southwest U.S.	0.48
22	PW3	Precipitable Water	Prev. Oct-Dec	43°N-48°N 120°W-125°W	Southwest Canada	-0.29
23	PW4	Precipitable Water	Prev. Jul-Sep	25°N-30°N 115°W-121°W	West coast of Mexico	0.35
24	PW5	Precipitable Water	Prev. Jul-Sep	15°N-20°N 25°W-30°W	Northeast Atlantic	-0.33
25	MW1	Meridional Wind (700 mb)	Prev. Oct-Dec	42°N-47°N 85°W-95°W	Northeast U.S.	0.49
26	MW2	Meridional Wind (700 mb)	Prev. Oct-Dec	45°N-50°N 125°W-130°W	West coast of Canada	-0.33
27	MW3	Meridional Wind (700 mb)	Prev. Oct-Dec	38°N-47°N 55°W-60°W	Northwest Atlantic	-0.38
28	ZW1	Zonal Wind (700 mb)	Jan-Mar	23°N-28°N 130°E-140°E	Northwest Pacific	0.38
29	ZW2	Zonal Wind (700 mb)	Prev. Oct-Dec	28°N-33°N 105°W-115°W	South U.S.	0.44
30	ZW3	Zonal Wind (700 mb)	Prev. Oct-Dec	50°N-55°N 110°W-115°W	South Canada	-0.39
31	AT1	Air Temperature	Prev. Oct-Dec	47°N-52°N 110°W-120°W	Northwest U.S.	-0.49
32	AT2	Air Temperature	Prev. Jul-Sep	26°N-31°N 115°W-120°W	West coast of Mexico	0.32
33	AT3	Air Temperature	Prev. Apr-Jun	47°N-52°N 70°W-85°W	Southeast Canada	-0.32
34	OLR1	Outgoing Long-Wave Radiation	Prev. Oct-Dec	35°N-44°N 110°W-120°W	Southwest U.S.	-0.44
35	OLR2	Outgoing Long-Wave Radiation	Prev. Apr-Jun	41°N-46°N 85°W-95°W	Northeast U.S.	-0.32
36	RH1	Relative Humidity	Prev. Oct-Dec	40°N-45°N 11°W-120°W	West U.S.	0.39
37	RH2	Relative Humidity	Prev. Oct-Dec	30°N-35°N 75°W-80°W	Southeast U.S.	0.51
38	RH3	Relative Humidity	Prev. Oct-Dec	27°N-32°N 160°W-165°W	Northeast Pacific	0.35
39	SWMR1	Southwest Monsoon Rainfall	Jan-Mar		Arizona and New Mexico rainfall	0.33
40	SWE1	Snow Water Equivalent	Feb 1st		Basin average	0.71
41	SWE2	Snow Water Equivalent	Mar 1st		Basin average	0.73
42	SWE3	Snow Water Equivalent	Apr 1st		Basin average	0.82

Table A8.4 Potential predictors for Gunnison River October-September flow

No	Name	Variable	Time	Location	General description	Corr. Coef
1	Lag-1	Lag-1 flow	Prev. Oct-Sep			0.15
2	SST1	Sea Surface Temperature	Jul-Sep	35°N-40°N 155°E-175°E	North-west Pacific, east of Japan	-0.34
3	SST2	Sea Surface Temperature	Jul-Sep	11°S-16°S 85°W-115°W	South-east Pacific, west of Peru	0.28
4	SST3	Sea Surface Temperature	Apr-Jun	35°N-40°N 155°E-160°E	North-west Pacific, east of Japan	-0.35
5	SST4	Sea Surface Temperature	Apr-Jun	31°N-36°N 45°W-55°W	Central northern Atlantic, east of U.S.	-0.38
6	SST5	Sea Surface Temperature	Jan-Mar	47°N-52°N 165°W-170°W	North-east Pacific, south of Alaska	0.51
7	SST6	Sea Surface Temperature	Jan-Mar	21°N-26°N 155°E-165°E	North-west Pacific, east of Japan	-0.41
8	SSST1	Seesaw SST	Jul-Sep		SST1-SST2	0.36
9	SSST2	Seesaw SST	Jan-Mar		SST5-SST6	0.52
10	GH1	Geopotential Height (700 mb)	Jul-Sep	35°N-45°N 160°E-175°E	North-west Pacific, east of Japan	-0.35
11	GH2	Geopotential Height (700 mb)	Jul-Sep	28°N-35°N 50°W-60°W	Northern central Atlantic	-0.29
12	GH3	Geopotential Height (700 mb)	Apr-Jun	27°N-32°N 95°W-105°W	Southern states	-0.40
13	GH4	Geopotential Height (700 mb)	Apr-Jun	30°N-40°N 40°W-60°W	Northern central Atlantic	-0.35
14	GH5	Geopotential Height (1000 mb)	Jul-Sep	55°N-65°N 57°W-105°W	Eastern Canada	-0.31
15	GH6	Geopotential Height (1000 mb)	Jul-Sep	25°N-30°N 120°E-130°E	Western Pacific near China	0.32
16	GH7	Geopotential Height (1000 mb)	Apr-Jun	25°N-35°N 50°W-60°W	Northern central Atlantic	-0.40
17	PR1	Precipitation Rate	Jan-Mar	17°N-22°N 165°E-175°E	Western Pacific, north of Marshall Islands	-0.30
18	MW1	Meridional Wind (700 mb)	Jul-Sep	28°N-35°N 150°E-155°E	Western Pacific, south-east of Japan	-0.45
19	MW2	Meridional Wind (700 mb)	Apr-Jun	25°N-28°N 110°W-118°W	East Pacific, near CA and Mexico	-0.37
20	MW3	Meridional Wind (surface)	Jul-Sep	25°N-31°N 150°E-155°E	Western Pacific, east of Japan	-0.34
21	ZW1	Zonal Wind (700 mb)	Jul-Sep	48°N-53°N 170°E-175°E	North-west Pacific, north-east of Japan	-0.28
22	ZW2	Zonal Wind (700 mb)	Jul-Sep	27°N-32°N 160°E-165°E	Western Pacific, east of Japan	0.43
23	ZW3	Zonal Wind (700 mb)	Jul-Sep	49°N-54°N 28°W-35°W	Central northern Atlantic, east of Canada	-0.29
24	AT1	Air Temperature	Jul-Sep	41°N-46°N 105°W-110°W	Western mountain states	-0.28
25	AT2	Air Temperature	Apr-Jun	35°N-40°N 100°W-105°W	Western mountain states	-0.42
26	OLR1	Outgoing Long-Wave Radiation	Apr-Jun	35°N-45°N 90°W-110°W	Central states and western mountain states	-0.43
27	AO1	Arctic Oscillation	Mar-May			-0.38
28	PDO1	Pacific Decadal Oscillation	Mar			0.29
29	PDO2	Pacific Decadal Oscillation	Sep			0.28
30	PNA1	Pacific/ North American Teleconnection Pattern	Mar-Apr			0.38

31	SWM1	South-West Monsoon Rainfall	Jan-Mar		Arizona and New Mexico rainfall	0.33
31	SWE4	Snow Water Equivalent	May 1st		Basin average	0.33

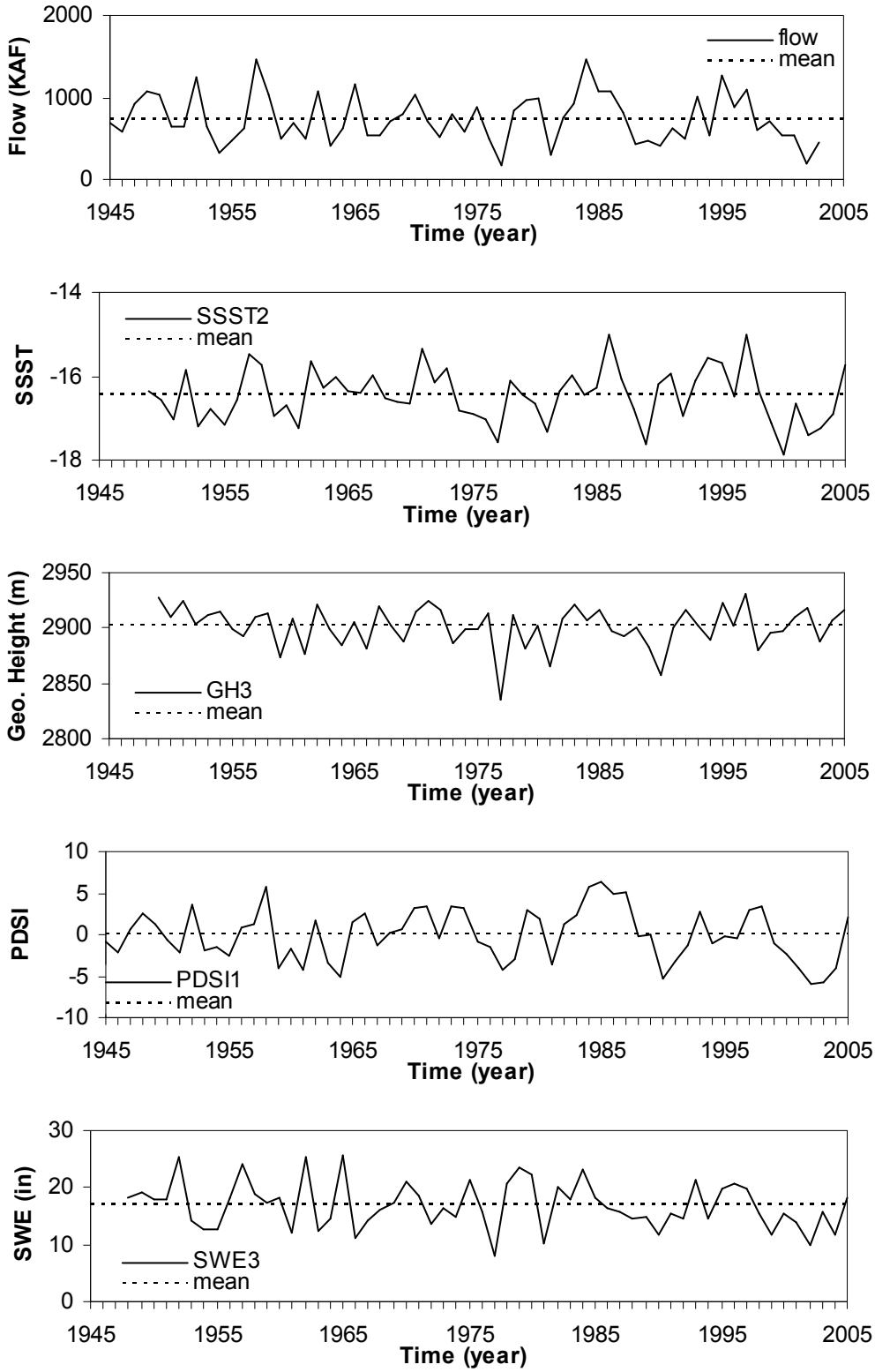

Figure A9.3 Time series of April-July streamflows and potential predictors for Gunnison River

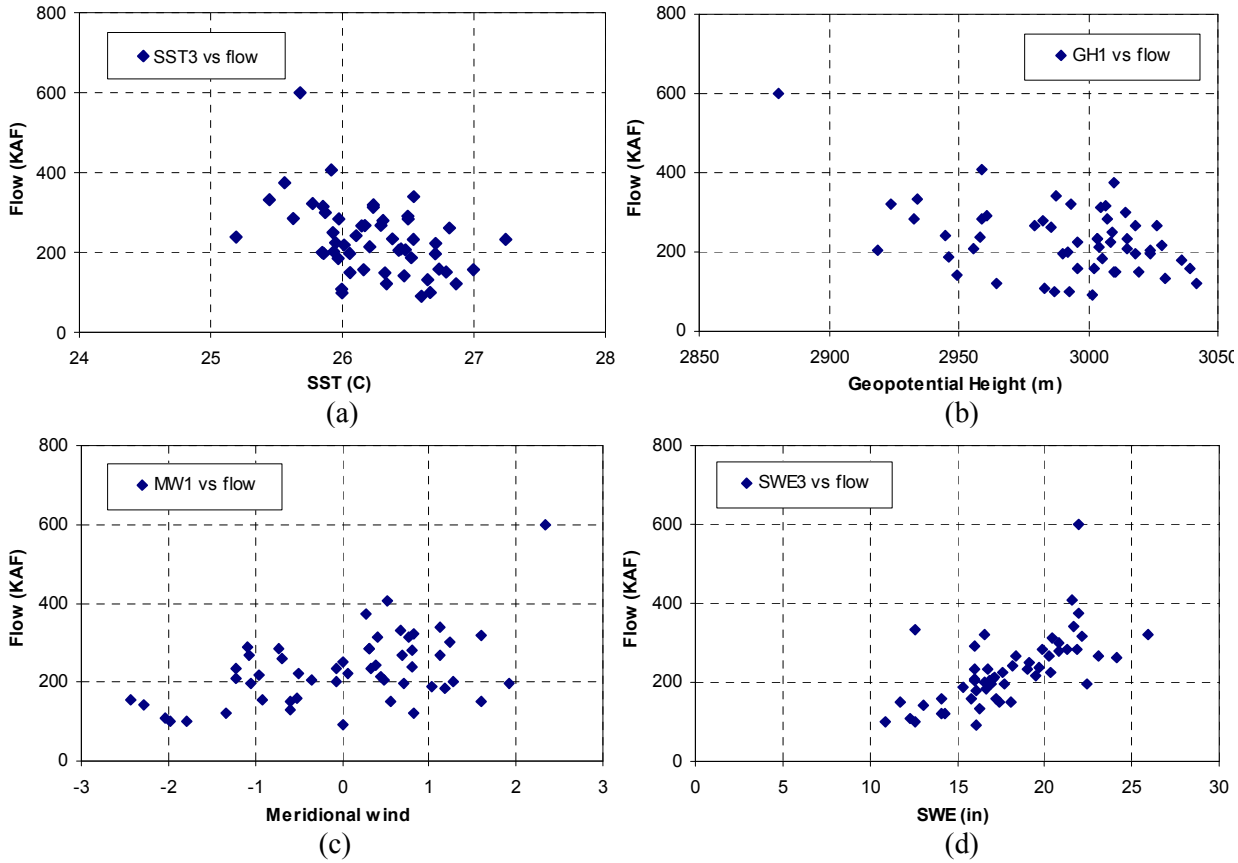

Figure A9.7 Potential predictor for Poudre River April-July streamflow: (a) SST3, (b) GH1, (c) MW1, and (d) SWE3

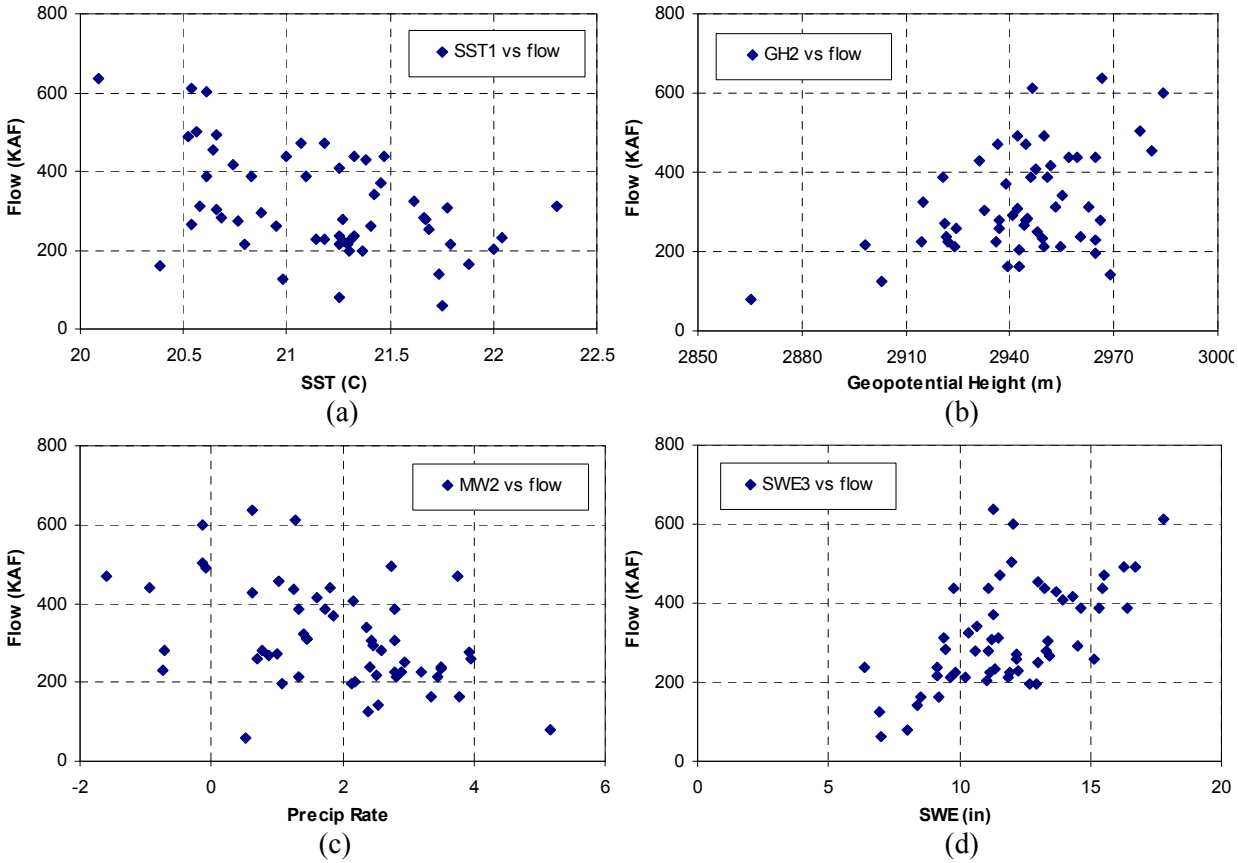

Figure A9.8 Potential predictor for Arkansas River April-July streamflow: (a) SST1, (b) GH2, (c) MW2, and (d) SWE3

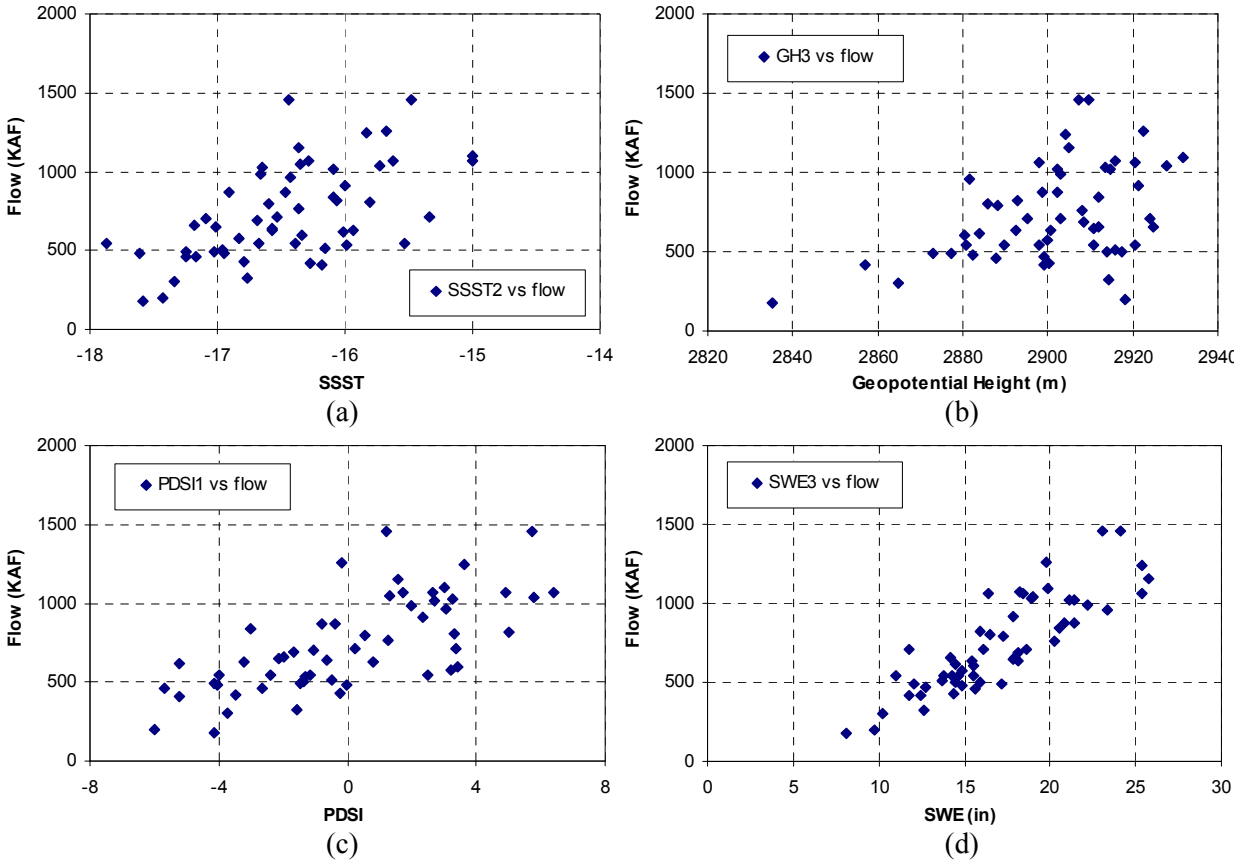

Figure A9.9 Potential predictor vs. Gunnison River April-July streamflow: (a) SSST2, (b) GH3, (c) PDSI1, and (d) SWE3

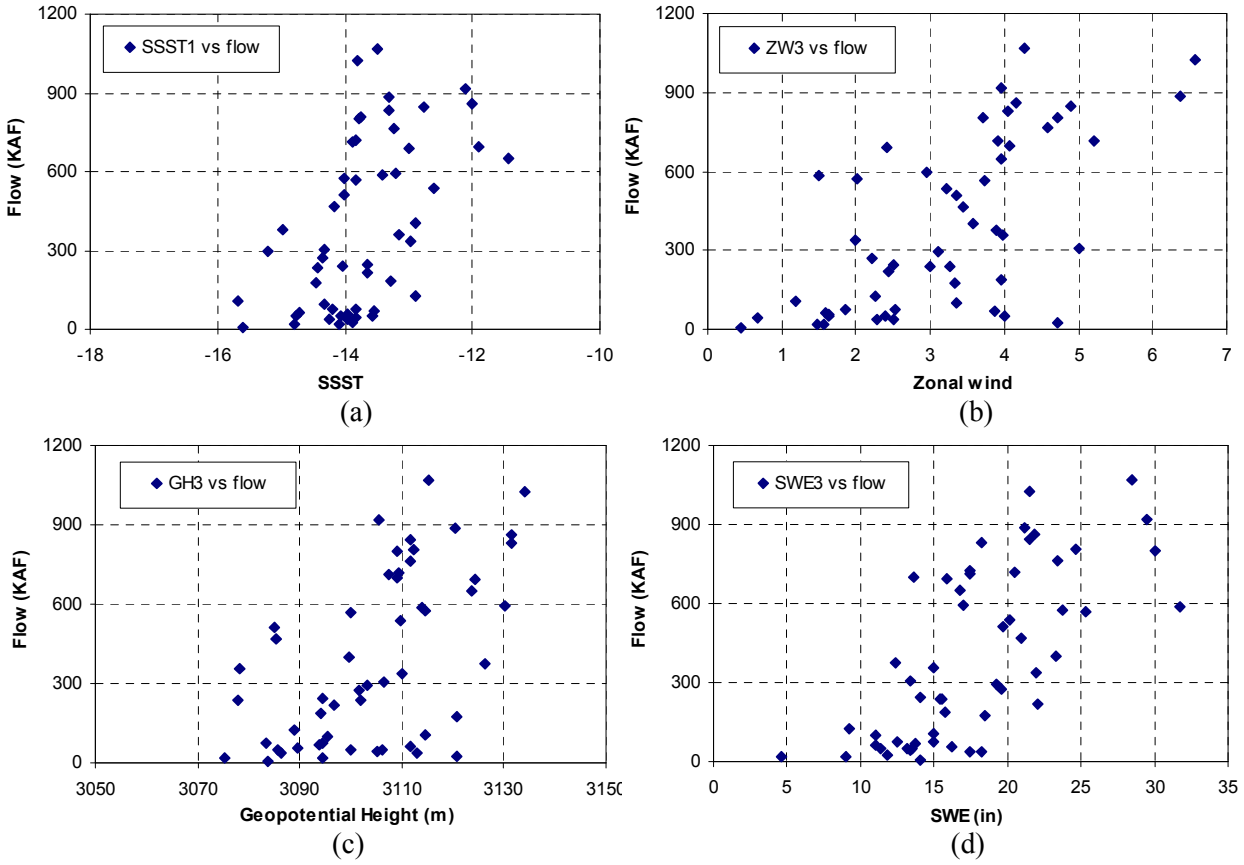

Figure A9.10 Potential predictor vs. Rio Grande April-July streamflow: (a) SSST1, (b) ZW3, (c) GH3, and (d) SWE3

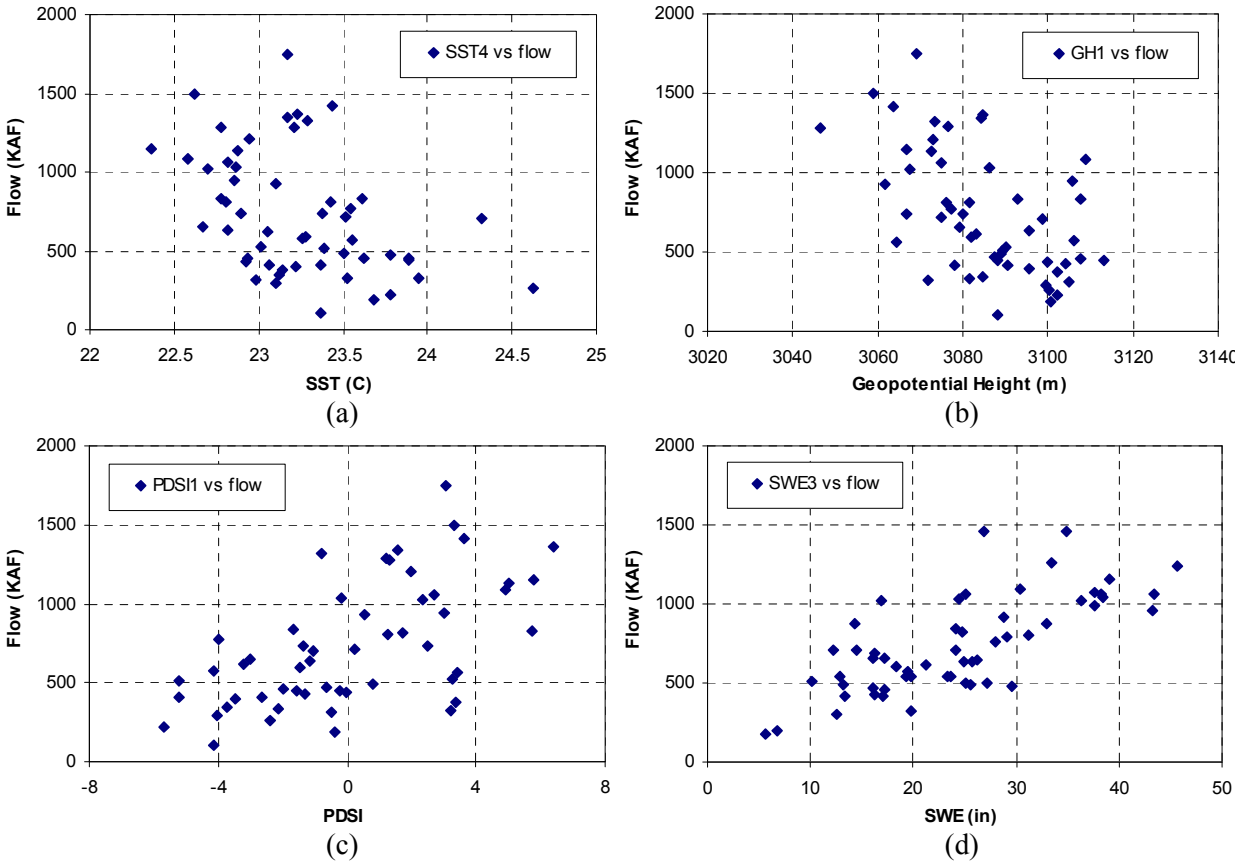

Figure A9.11 Potential predictor vs. San Juan River April-July streamflow: (a) SST4, (b) GH1, (c) PDSI1, and (d) SWE3

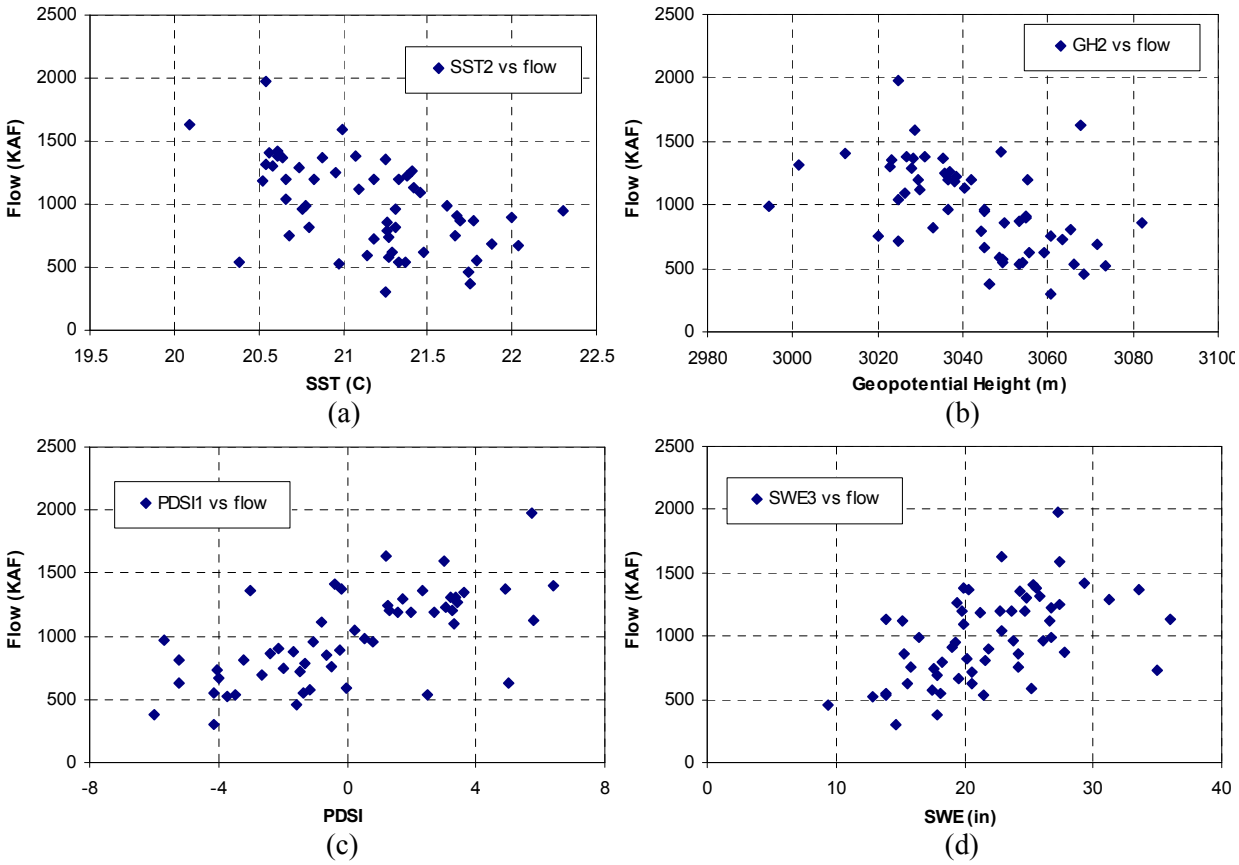

Figure A9.12 Potential predictor vs. Yampa River April-July streamflow: (a) SST2, (b) GH2, (c) PDS1, and (d) SWE3

Appendix B: Results of PCA and CCA

B1: Results of PCA on the potential predictors for each site

Table B1.1 Variances of PCs for Poudre River

PCs	Variance	%	Accum %	PCs	Variance	%	Accum %
1	10.05	27.9	27.9	19	0.31	0.9	95.1
2	4.95	13.7	41.7	20	0.29	0.8	95.9
3	2.66	7.4	49.1	21	0.27	0.7	96.6
4	2.35	6.5	55.6	22	0.24	0.7	97.3
5	2.08	5.8	61.4	23	0.18	0.5	97.8
6	1.70	4.7	66.1	24	0.14	0.4	98.2
7	1.57	4.4	70.4	25	0.13	0.4	98.6
8	1.28	3.6	74.0	26	0.11	0.3	98.9
9	1.17	3.3	77.3	27	0.10	0.3	99.1
10	1.12	3.1	80.4	28	0.08	0.2	99.4
11	0.97	2.7	83.0	29	0.07	0.2	99.5
12	0.76	2.1	85.2	30	0.05	0.1	99.7
13	0.73	2.0	87.2	31	0.04	0.1	99.8
14	0.66	1.8	89.0	32	0.03	0.1	99.9
15	0.55	1.5	90.5	33	0.02	0.1	99.9
16	0.51	1.4	92.0	34	0.01	0.0	100.0
17	0.44	1.2	93.2	35	0.01	0.0	100.0
18	0.38	1.1	94.2	36	0.00	0.0	100.0

Table B1.2 Variances of PCs for Arkansas River

PCs	Variance	%	Accum %	PCs	Variance	%	Accum %
1	7.71	36.7	36.7	11	0.29	1.4	94.2
2	2.57	12.2	49.0	12	0.25	1.2	95.4
3	2.26	10.7	59.7	13	0.23	1.1	96.5
4	1.73	8.2	67.9	14	0.19	0.9	97.4
5	1.48	7.0	75.0	15	0.16	0.8	98.2
6	1.10	5.3	80.2	16	0.13	0.6	98.8
7	0.79	3.8	84.0	17	0.10	0.5	99.3
8	0.71	3.4	87.3	18	0.06	0.3	99.5
9	0.64	3.0	90.4	19	0.05	0.2	99.8
10	0.50	2.4	92.8	20	0.03	0.1	99.9

Table B1.3 Variances of PCs for Gunnison River

PCs	Variance	%	Accum %	PCs	Variance	%	Accum %
1	11.50	29.5	29.5	21	0.25	0.6	96.5
2	3.77	9.7	39.2	22	0.23	0.6	97.1
3	3.09	7.9	47.1	23	0.21	0.5	97.7
4	2.77	7.1	54.2	24	0.17	0.4	98.1
5	2.40	6.2	60.3	25	0.14	0.4	98.5
6	2.12	5.4	65.8	26	0.12	0.3	98.8
7	1.69	4.3	70.1	27	0.11	0.3	99.0

8	1.44	3.7	73.8	28	0.09	0.2	99.3
9	1.30	3.3	77.1	29	0.07	0.2	99.5
10	1.17	3.0	80.1	30	0.06	0.2	99.6
11	0.99	2.5	82.7	31	0.04	0.1	99.7
12	0.89	2.3	85.0	32	0.04	0.1	99.8
13	0.74	1.9	86.9	33	0.03	0.1	99.9
14	0.67	1.7	88.6	34	0.02	0.1	99.9
15	0.63	1.6	90.2	35	0.01	0.0	100.0
16	0.61	1.6	91.8	36	0.01	0.0	100.0
17	0.55	1.4	93.2	37	0.00	0.0	100.0
18	0.45	1.1	94.3	38	0.00	0.0	100.0
19	0.34	0.9	95.2	39	0.00	0.0	100.0
20	0.27	0.7	95.9				

Table B1.4 Variances of PCs for Rio Grande

PCs	Variance	%	Accum %	PCs	Variance	%	Accum %
1	14.48	30.8	30.8	25	0.17	0.4	97.7
2	6.15	13.1	43.9	26	0.14	0.3	98.0
3	4.50	9.6	53.5	27	0.14	0.3	98.3
4	3.25	6.9	60.4	28	0.12	0.2	98.6
5	2.95	6.3	66.7	29	0.10	0.2	98.8
6	1.95	4.1	70.8	30	0.09	0.2	99.0
7	1.78	3.8	74.6	31	0.08	0.2	99.2
8	1.53	3.3	77.8	32	0.07	0.2	99.3
9	1.17	2.5	80.3	33	0.06	0.1	99.5
10	1.02	2.2	82.5	34	0.06	0.1	99.6
11	0.93	2.0	84.5	35	0.05	0.1	99.7
12	0.89	1.9	86.3	36	0.03	0.1	99.8
13	0.79	1.7	88.0	37	0.03	0.1	99.8
14	0.64	1.4	89.4	38	0.03	0.1	99.9
15	0.56	1.2	90.6	39	0.02	0.0	99.9
16	0.49	1.0	91.6	40	0.01	0.0	99.9
17	0.46	1.0	92.6	41	0.01	0.0	100.0
18	0.44	0.9	93.5	42	0.01	0.0	100.0
19	0.40	0.8	94.4	43	0.01	0.0	100.0
20	0.35	0.8	95.1	44	0.00	0.0	100.0
21	0.34	0.7	95.8	45	0.00	0.0	100.0
22	0.28	0.6	96.4	46	0.00	0.0	100.0
23	0.27	0.6	97.0	47	0.00	0.0	100.0
24	0.18	0.4	97.4				

Table B1.5 Variances of PCs for San Juan River

PCs	Variance	%	Accum %	PCs	Variance	%	Accum %
1	10.61	33.2	33.2	17	0.27	0.8	95.1
2	4.34	13.6	46.7	18	0.26	0.8	95.9
3	2.77	8.6	55.4	19	0.21	0.7	96.5
4	1.86	5.8	61.2	20	0.20	0.6	97.1
5	1.80	5.6	66.8	21	0.18	0.6	97.7
6	1.56	4.9	71.7	22	0.15	0.5	98.2
7	1.21	3.8	75.4	23	0.13	0.4	98.6
8	1.02	3.2	78.6	24	0.12	0.4	98.9

9	0.97	3.0	81.7	25	0.09	0.3	99.2
10	0.85	2.7	84.4	26	0.07	0.2	99.4
11	0.77	2.4	86.8	27	0.05	0.2	99.6
12	0.67	2.1	88.8	28	0.04	0.1	99.7
13	0.52	1.6	90.5	29	0.03	0.1	99.8
14	0.48	1.5	92.0	30	0.03	0.1	99.9
15	0.41	1.3	93.3	31	0.02	0.1	100.0
16	0.31	1.0	94.2	32	0.01	0.0	100.0

Table B1.6 Variances of PCs for Yampa River

PCs	Variance	%	Accum %	PCs	Variance	%	Accum %
1	9.08	29.3	29.3	17	0.28	0.9	95.7
2	3.73	12.0	41.3	18	0.24	0.8	96.5
3	3.11	10.0	51.4	19	0.21	0.7	97.2
4	2.87	9.2	60.6	20	0.19	0.6	97.8
5	2.09	6.7	67.4	21	0.13	0.4	98.2
6	1.49	4.8	72.2	22	0.12	0.4	98.6
7	1.44	4.7	76.8	23	0.10	0.3	98.9
8	1.13	3.7	80.5	24	0.07	0.2	99.1
9	0.94	3.0	83.5	25	0.06	0.2	99.4
10	0.82	2.6	86.1	26	0.05	0.2	99.5
11	0.56	1.8	87.9	27	0.05	0.2	99.7
12	0.53	1.7	89.7	28	0.03	0.1	99.8
13	0.50	1.6	91.3	29	0.03	0.1	99.9
14	0.42	1.4	92.6	30	0.02	0.1	99.9
15	0.38	1.2	93.9	31	0.02	0.1	100.0
16	0.30	1.0	94.8				

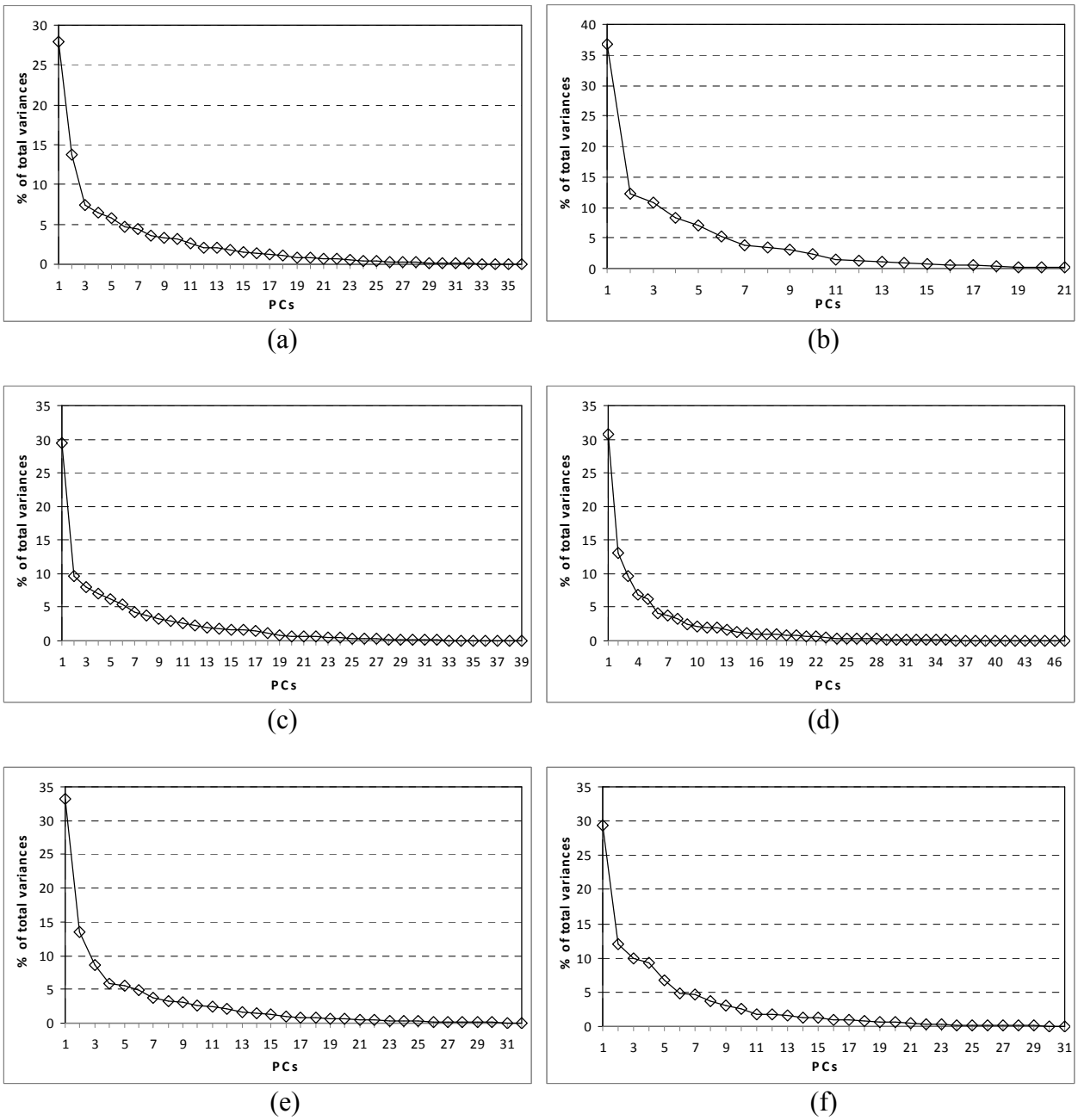

Figure B1.1 Plot of variances the PCs: (a) Poudre River, (b) Arkansas River, (c) Gunnison River, (d) Rio Grande, (e) San Juan River, and (f) Yampa River

B2: Results of PCA on the potential predictors for all sites

Table B2.1 Variances of PCs obtained from all of the potential predictors for 6 sites

PCs	Variance	%	Accumulated %	PCs	Variance	%	Accumulated %	PCs	Variance	%	Accumulated %
1	51.7	25.1	25.1	26	1.4	0.7	92.5	52	0.2	0.1	100.0
2	23.4	11.4	36.5	27	1.2	0.6	93.1	53 ~ 206	0.0	0.0	100.0
3	15.0	7.3	43.7	28	1.2	0.6	93.7				
4	12.1	5.9	49.6	29	1.1	0.5	94.2				
5	11.4	5.6	55.2	30	1.0	0.5	94.7				
6	9.9	4.8	60.0	31	1.0	0.5	95.2				
7	7.8	3.8	63.8	32	1.0	0.5	95.6				
8	6.5	3.1	66.9	33	0.9	0.4	96.1				
9	5.9	2.9	69.8	34	0.8	0.4	96.5				
10	5.1	2.5	72.3	35	0.7	0.4	96.8				
11	4.7	2.3	74.5	36	0.7	0.3	97.1				
12	4.0	1.9	76.5	37	0.7	0.3	97.5				
13	3.8	1.8	78.3	38	0.6	0.3	97.7				
14	3.4	1.7	80.0	39	0.6	0.3	98.0				
15	3.2	1.6	81.5	40	0.5	0.2	98.3				
16	2.9	1.4	83.0	41	0.5	0.2	98.5				
17	2.6	1.3	84.2	42	0.4	0.2	98.7				
18	2.4	1.2	85.4	43	0.4	0.2	98.9				
19	2.3	1.1	86.5	44	0.4	0.2	99.1				
20	2.1	1.0	87.5	45	0.3	0.2	99.2				
21	2.0	1.0	88.5	46	0.3	0.1	99.4				
22	1.9	0.9	89.4	47	0.3	0.1	99.5				
23	1.8	0.9	90.3	48	0.3	0.1	99.7				
24	1.6	0.8	91.0	49	0.2	0.1	99.8				
25	1.6	0.8	91.8	50	0.2	0.1	99.8				

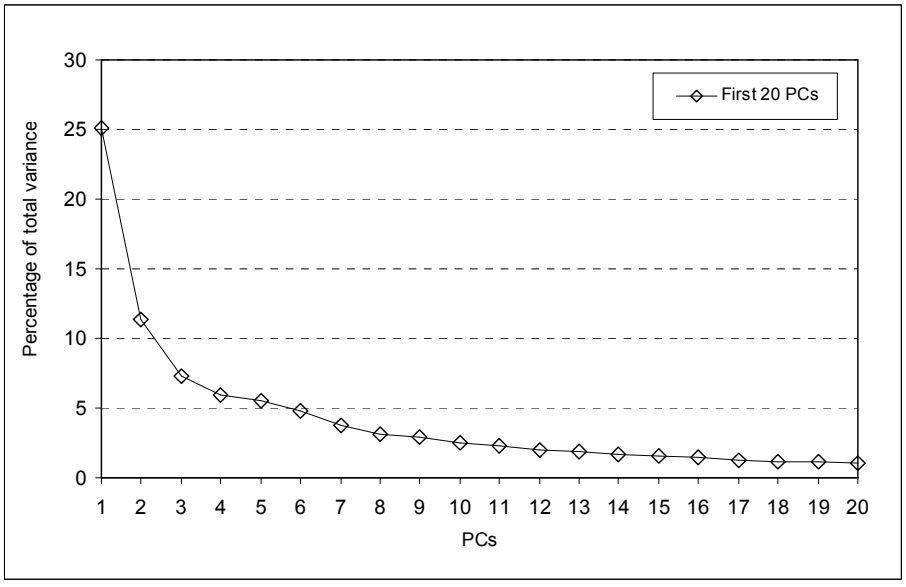

Figure B2.1 Plot of vairance of of the fist 20 PCs obtained fron all of the potential predictors of 6 sites

B3: Result of CCA

Table B3.1 ***a*** matrix

0.0943	0.0219	0.0473	-0.0237	0.0305	0.015
-0.0339	0.095	0.0022	0.0348	-0.0006	-0.0268
-0.0059	-0.1231	-0.0054	0.0382	0.0242	0.0899
-0.0694	0.0375	0.1038	-0.0223	0.0213	0.0045
-0.0239	0.057	0.0042	-0.0991	-0.0647	0.0586
0.0094	0.0389	-0.1019	0.0784	0.0797	0.0314
-0.0693	0.0175	0.0479	-0.0233	0.1109	0.0484
-0.0342	0.0695	-0.0725	-0.0837	0.0784	0.011
0.1175	0.1079	-0.0199	0.0321	-0.108	0.0313
0.0334	0.0157	-0.0633	0.0597	-0.0203	-0.0009
-0.0332	-0.0073	-0.0945	-0.1367	0.108	-0.06
0.0845	-0.0499	-0.0457	-0.0666	0.0578	-0.0679
0.0111	0.0203	-0.0624	-0.016	0.0729	-0.0859
-0.0414	0.1318	-0.0293	0.0113	0.0957	0.0528
0.03	-0.0718	0.0956	-0.0089	-0.0214	-0.0381
-0.0492	-0.0441	0.0327	-0.0982	-0.0492	-0.1793
0.016	0.0048	-0.0444	0.0244	-0.0885	0.0957
0.0441	0.03	-0.1108	-0.0422	-0.0112	-0.1319
0.0297	0.0052	-0.036	-0.0267	-0.0297	0.0015
-0.014	-0.0798	0.0167	0.0085	-0.1177	-0.127
-0.0113	-0.0161	0.0105	-0.121	-0.0867	-0.1374
-0.0073	-0.049	0.131	0.029	0.031	-0.0988
0.0435	-0.0436	-0.0084	0.1104	-0.0465	-0.177
-0.0309	-0.0239	0.1267	-0.0794	0.0761	0.0368
0.0191	-0.0049	-0.0299	-0.1278	0.0495	-0.0682
-0.083	0.0105	0.1061	0.0228	0.156	-0.0059
-0.0098	-0.0884	-0.0573	0.0753	0.0541	0.0278
-0.0528	-0.0641	-0.042	-0.2432	-0.0046	-0.0196
-0.0418	0.0981	-0.0602	0.0049	-0.0648	0.1066
0.1095	-0.0174	-0.2407	-0.0309	0.1657	-0.0777
0.0728	-0.0798	-0.0507	-0.0073	0.1729	-0.0615
-0.0025	0.065	0.1863	0.3467	0.2018	-0.2754
-0.1306	0.0587	0.0947	0.0177	0.0056	0.0775
0.0747	0.012	-0.0251	0.0727	0.0413	-0.1434
-0.0268	0.0133	0.1342	0.0313	-0.0669	-0.1206
-0.0185	-0.0997	0.0939	-0.0626	0.215	-0.0297

Table B3.2 ***b*** matrix

-0.111	0.436	0.052	1.075	-0.168	1.142
0.539	-0.193	0.074	-0.089	-1.385	-1.199
-0.394	-0.815	1.691	1.606	2.031	0.422
-0.414	0.989	-1.010	0.582	0.144	-1.580
-0.586	-0.299	0.677	-1.469	-0.737	1.369
0.095	-0.515	-1.883	-1.453	-0.531	-0.236

Appendix C: Model performances

C1: Yearly streamflow forecast models

Table C1.1 Model performance for April – March streamflow forecast of Poudre River

Method	Values of R^2		Values of skill scores	
	Item	Values	Item	Values
Fitting	R^2	0.62	*Accuracy*	0.53
	adj. R^2	0.59	*HSS*	0.37
Drop one	R^2	0.44	*Accuracy*	0.51
	adj. R^2	0.39	*HSS*	0.35

Table C1.2 Model performance for October – September streamflow forecast of Poudre River

Method	Values of R^2		Values of skill scores	
	Item	Values	Item	Values
Fitting	R^2	0.65	*Accuracy*	0.55
	adj. R^2	0.62	*HSS*	0.40
Drop one	R^2	0.54	*Accuracy*	0.47
	adj. R^2	0.50	*HSS*	0.30

Appendix D: Plot of results

D1: Time series plots for single-site models (MLR model)

Poudre River

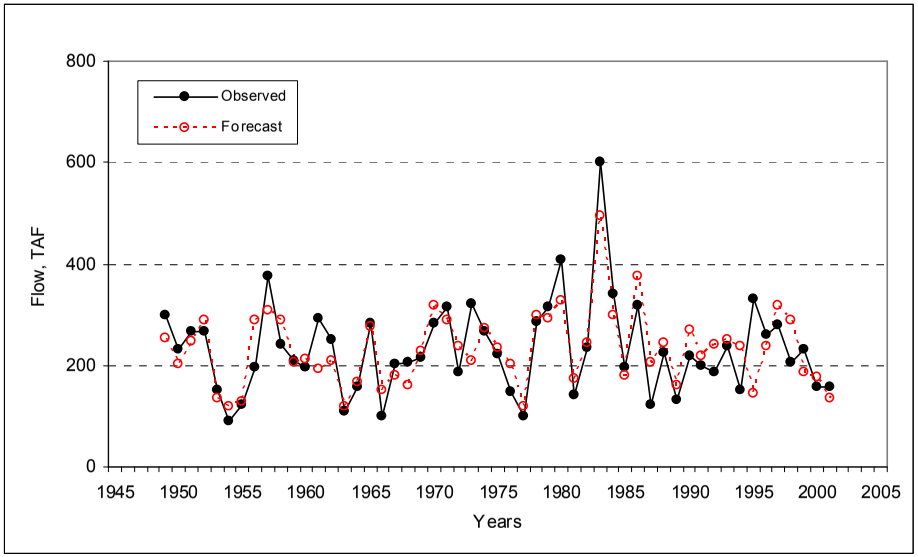

Fitting

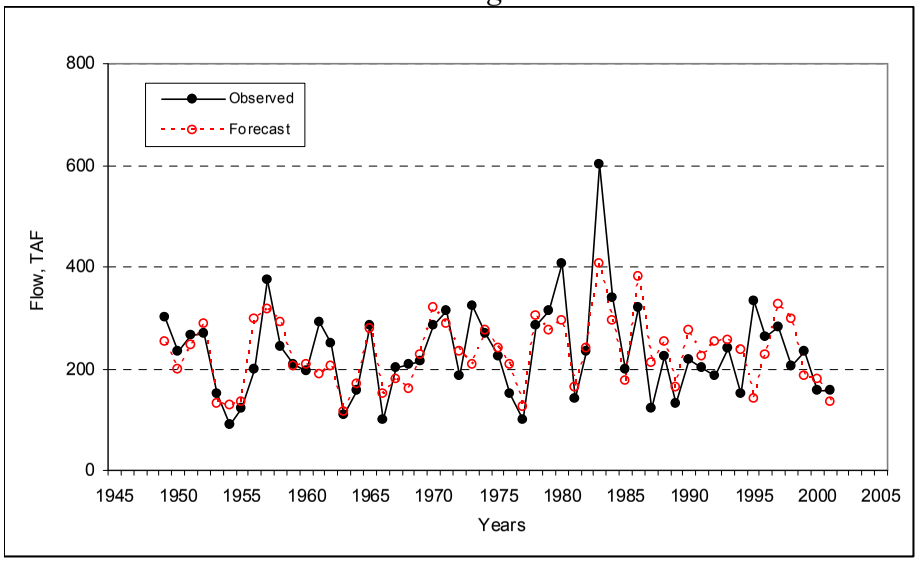

Drop-10%

Fig. D1.1 Comparison of forecast results for Poudre River

Arkansas River

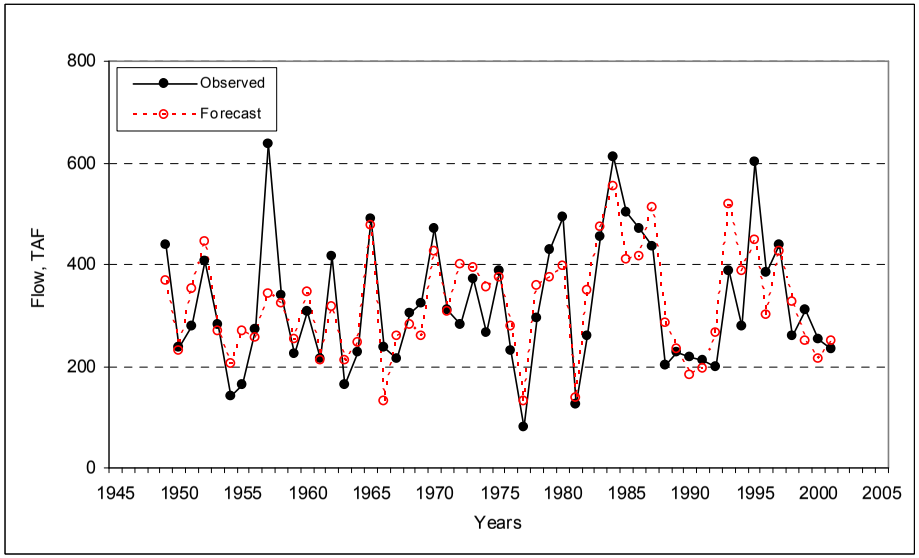

Fitting

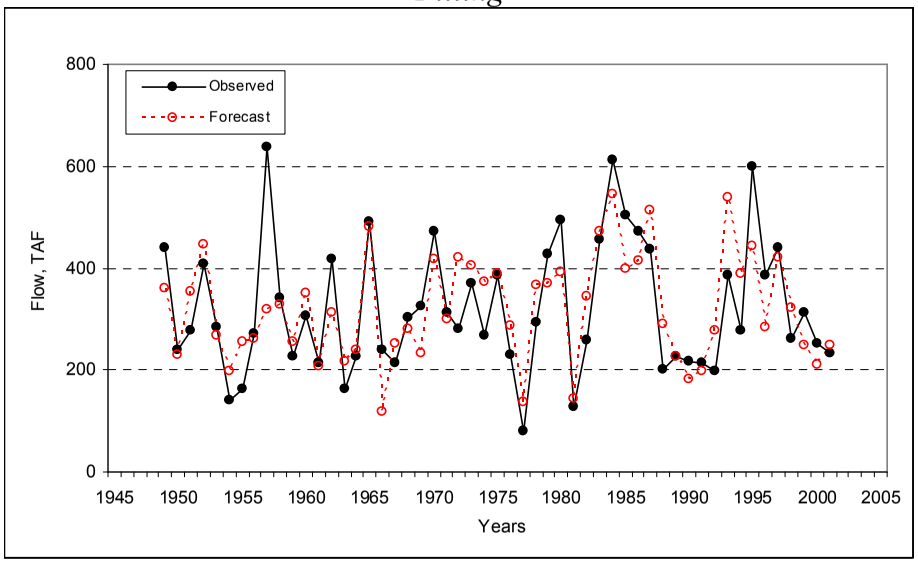

Drop-10%

Fig. D1.2 Comparison of forecast results for Arkansas River

Gunnison River

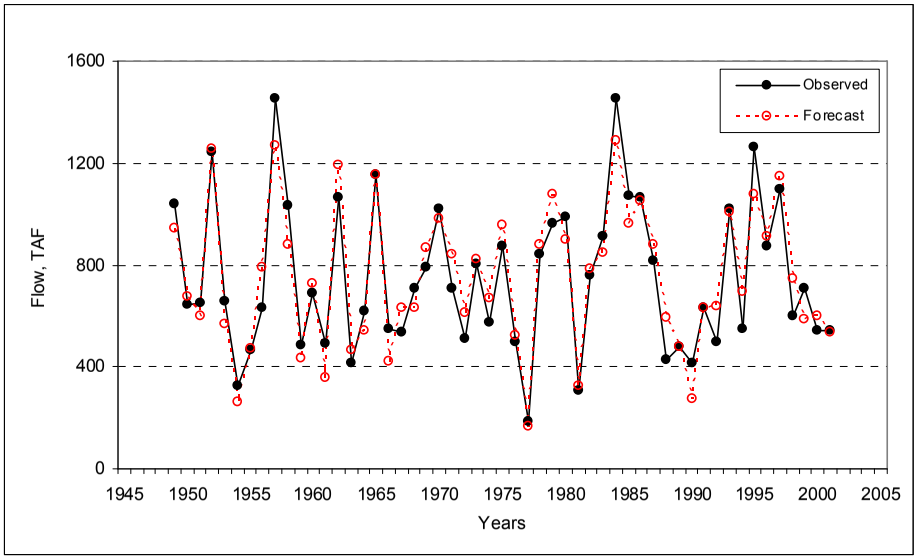

Fitting

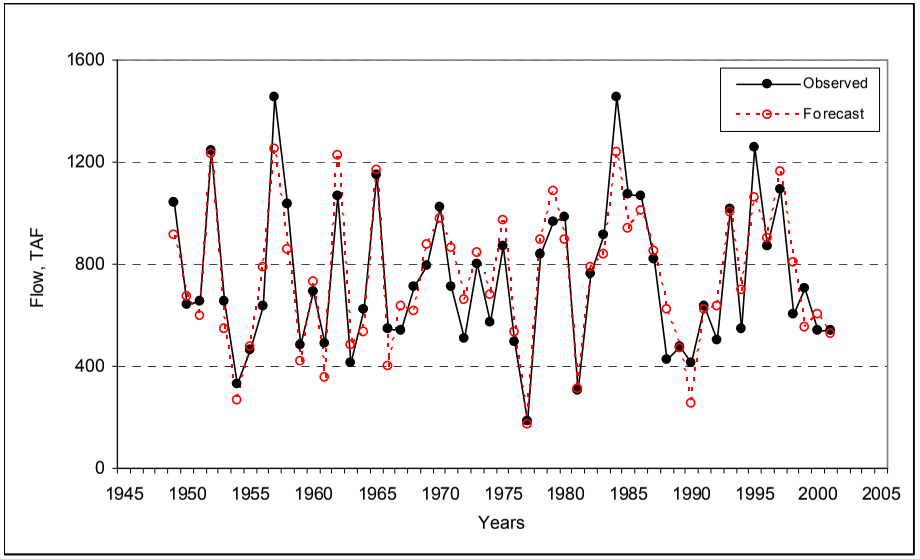

Drop-10%

Fig. D1.3 Comparison of forecast results for Gunnison River

Rio Grande

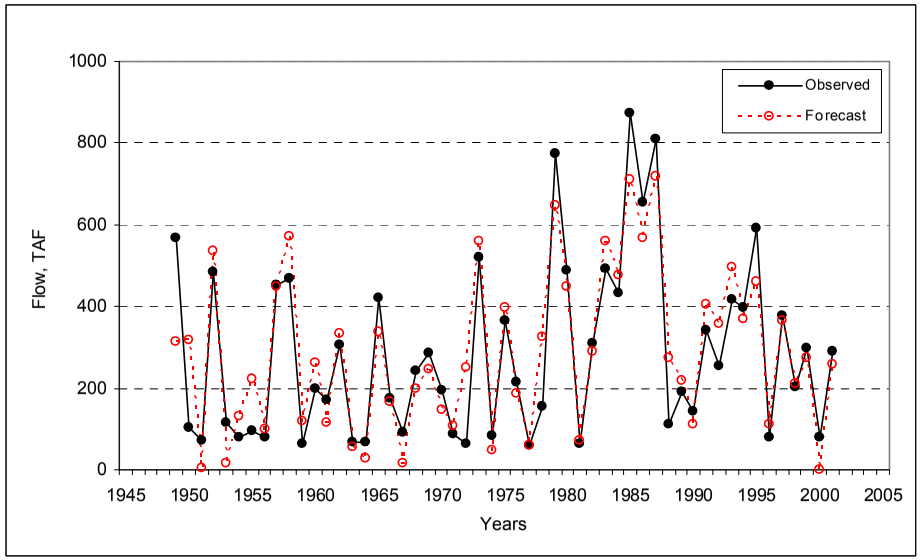

Fitting

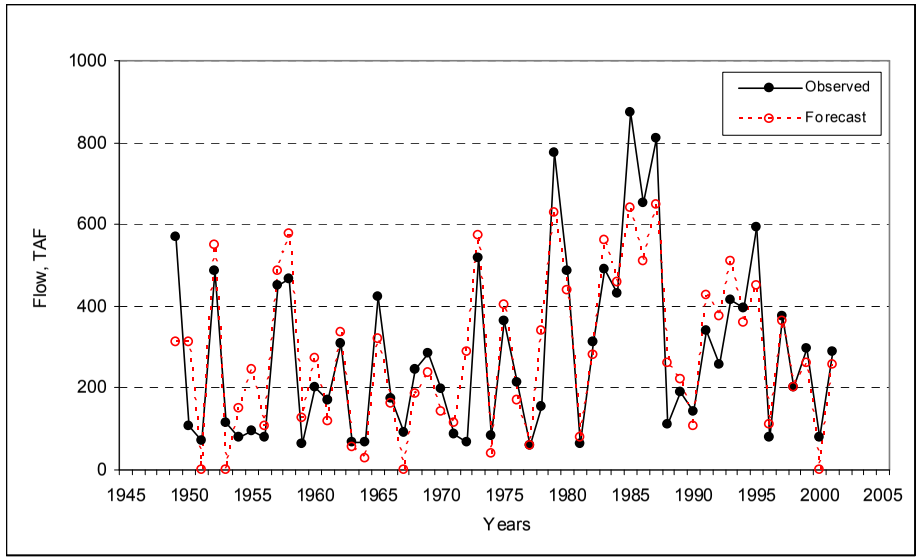

Drop-10%

Fig. D1.4 Comparison of forecast results Rio Grande

San Juan River

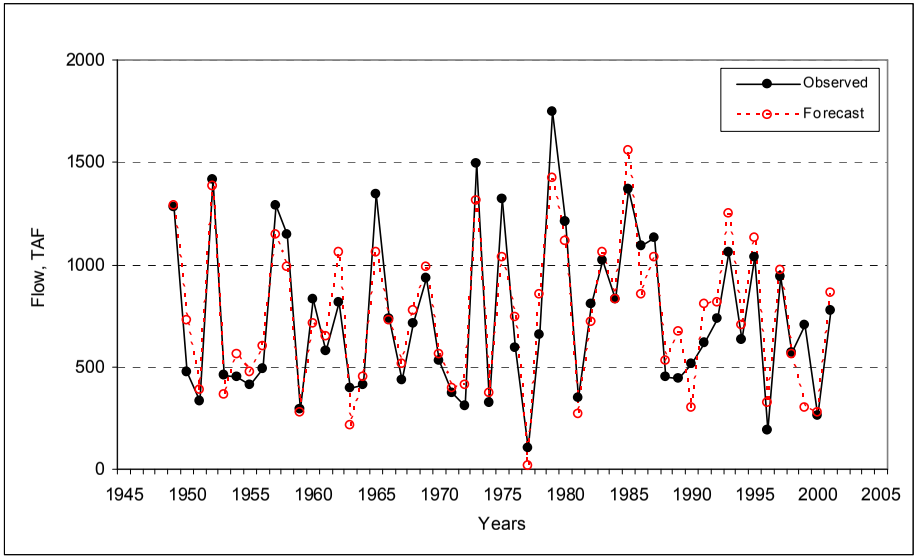

Fitting

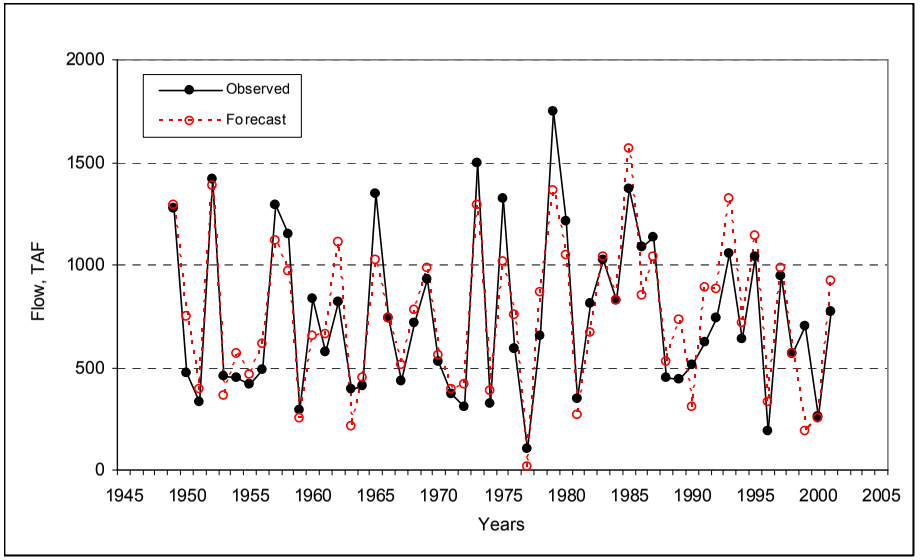

Drop-10%

Fig. D1.5 Comparison of forecast results for San Juan River

Yampa River

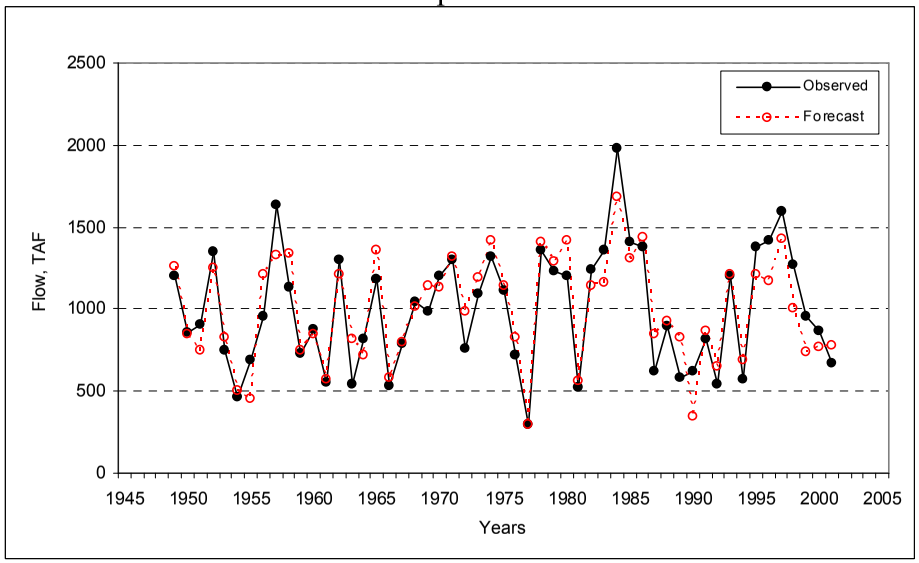

Fitting

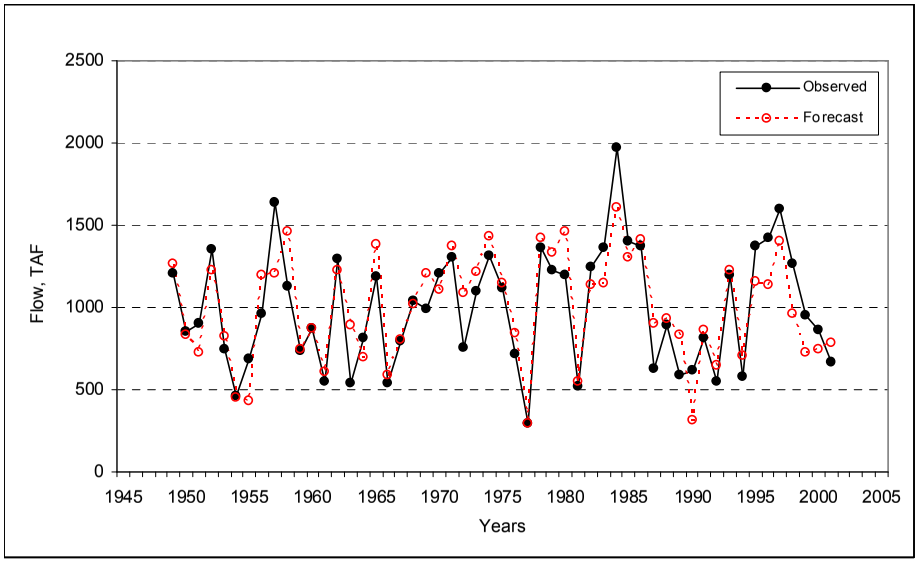

Drop-10%

Fig. D1.6 Comparison of forecast results for Yampa River

D2: Comparison of single –site models (PCA) and CCA model

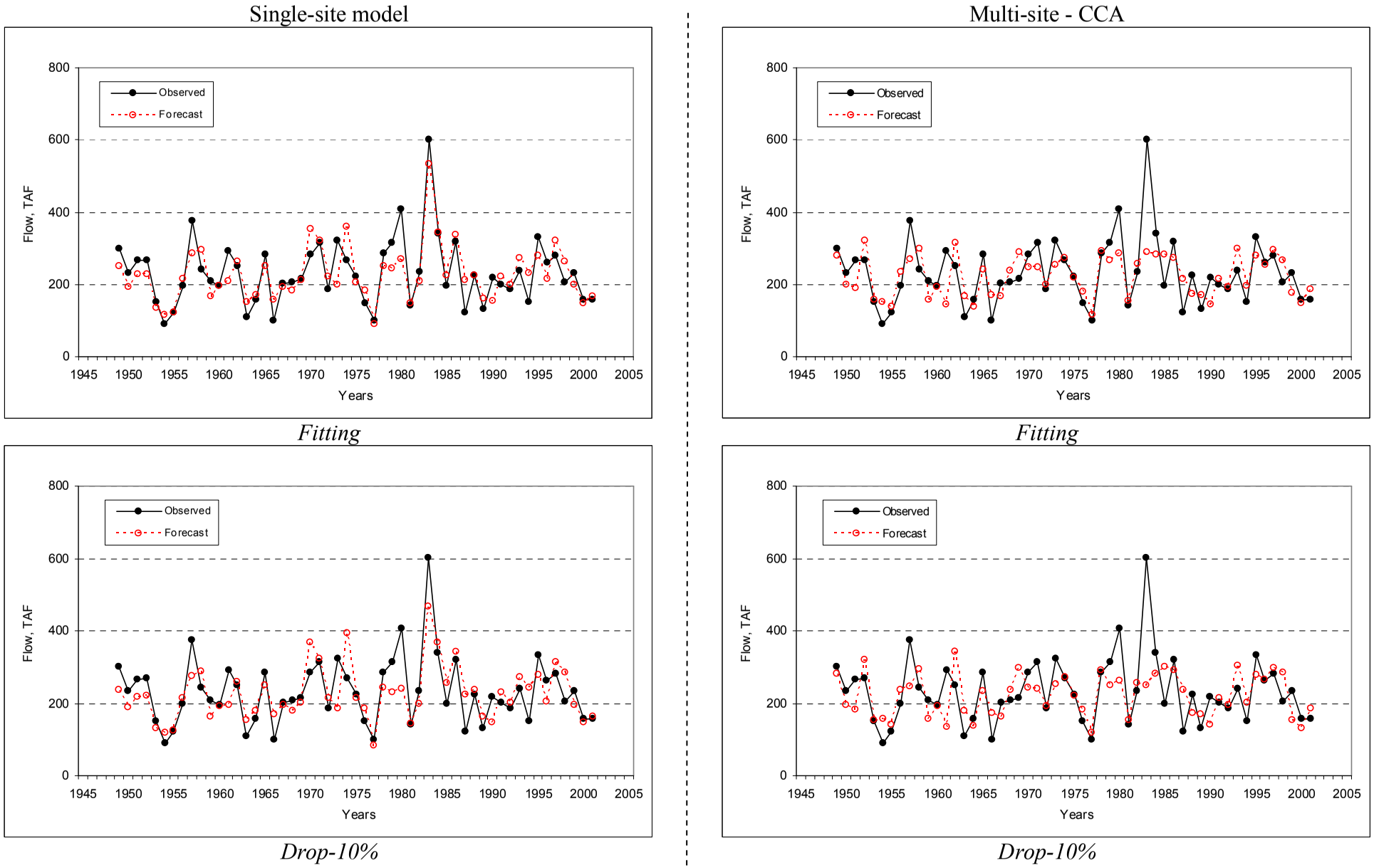

Fig. D2.1 Comparison of forecast results for Poudre River

Single-site model

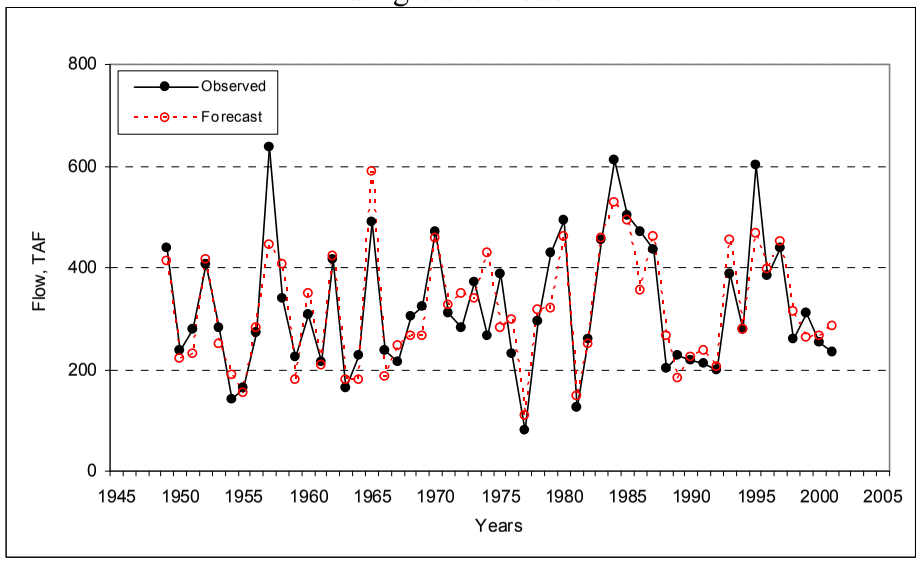

Fitting

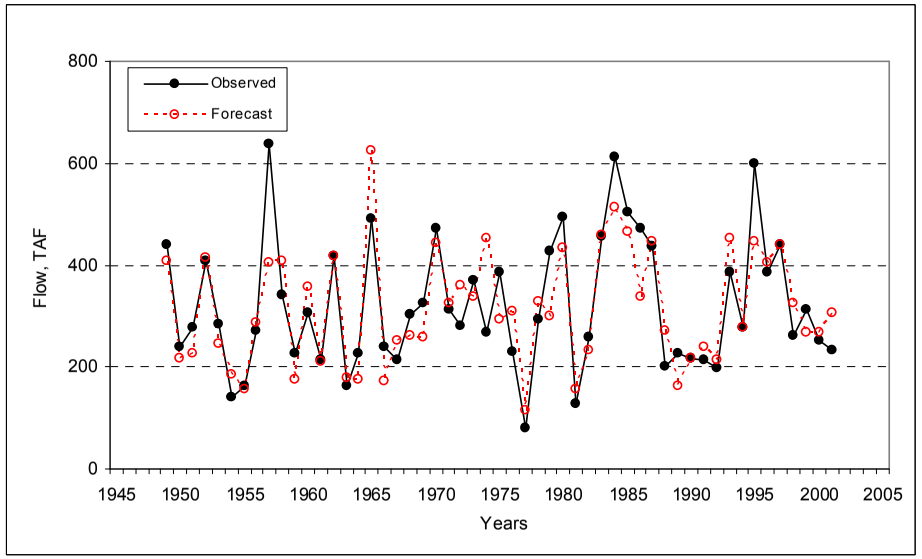

Drop-10%

Multi-site – CCA

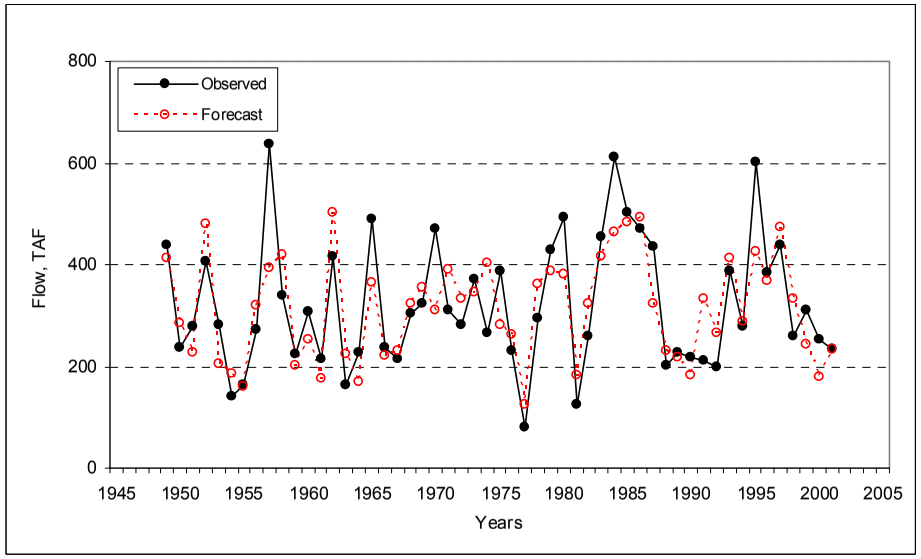

Fitting

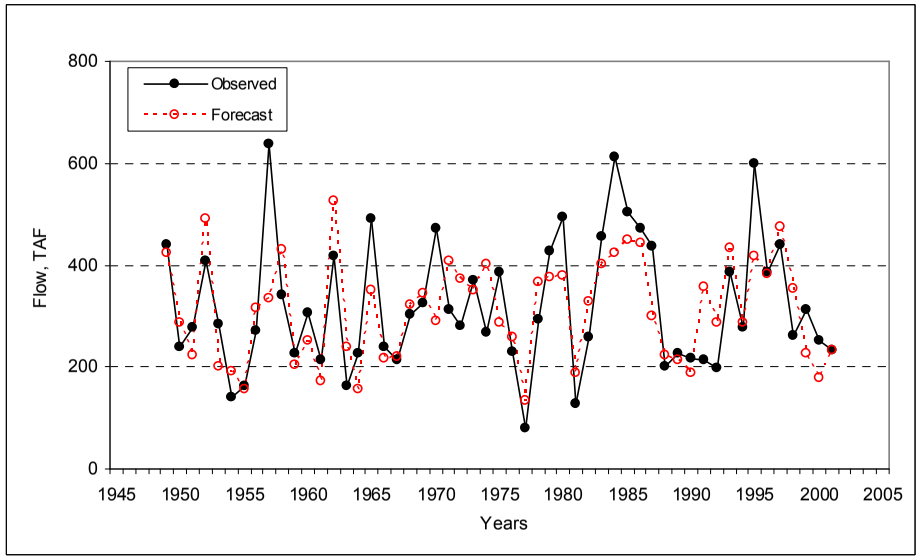

Drop-10%

Fig. D2.2 Comparison of forecast results for Arkansas River

Single-site model

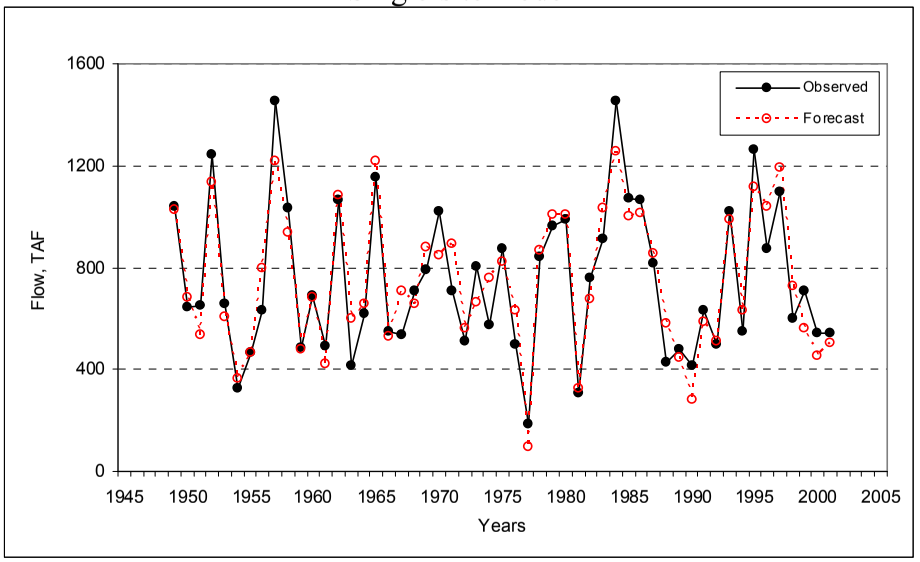

Fitting

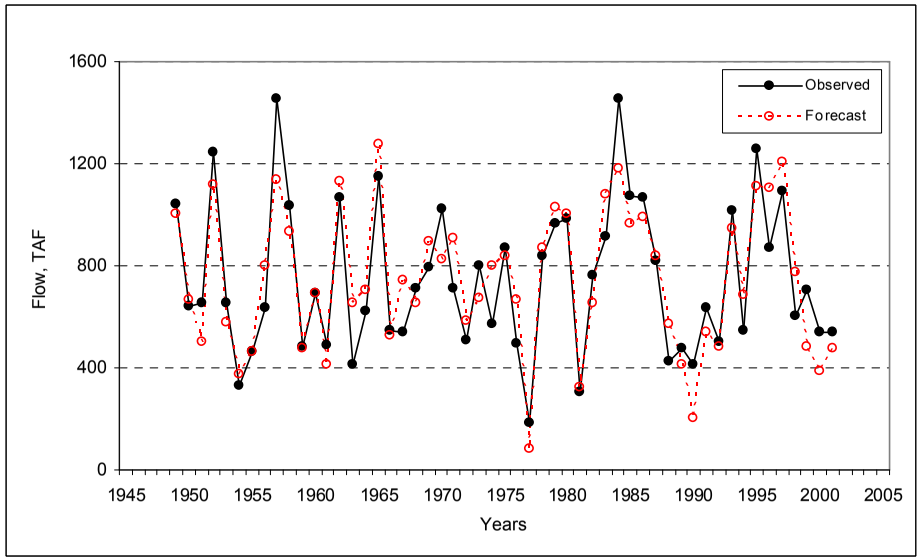

Drop-10%

Multi-site – CCA

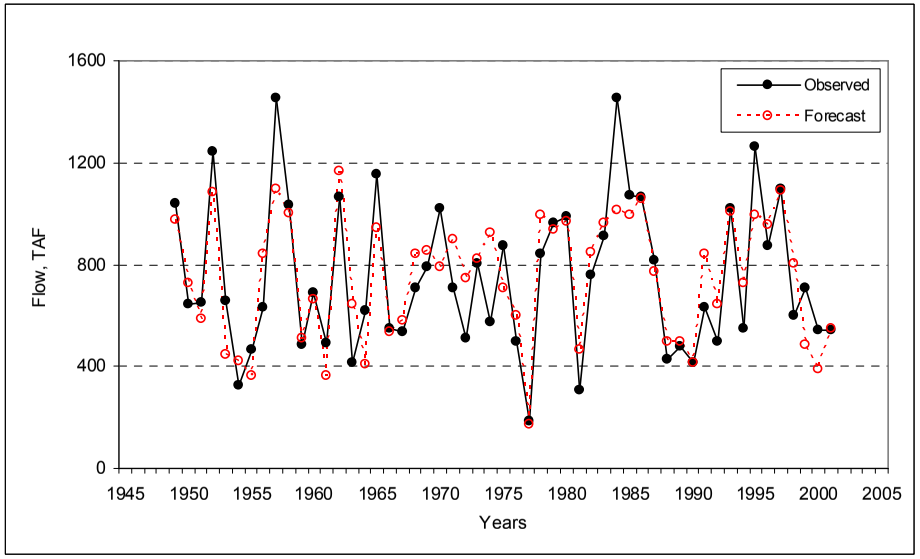

Fitting

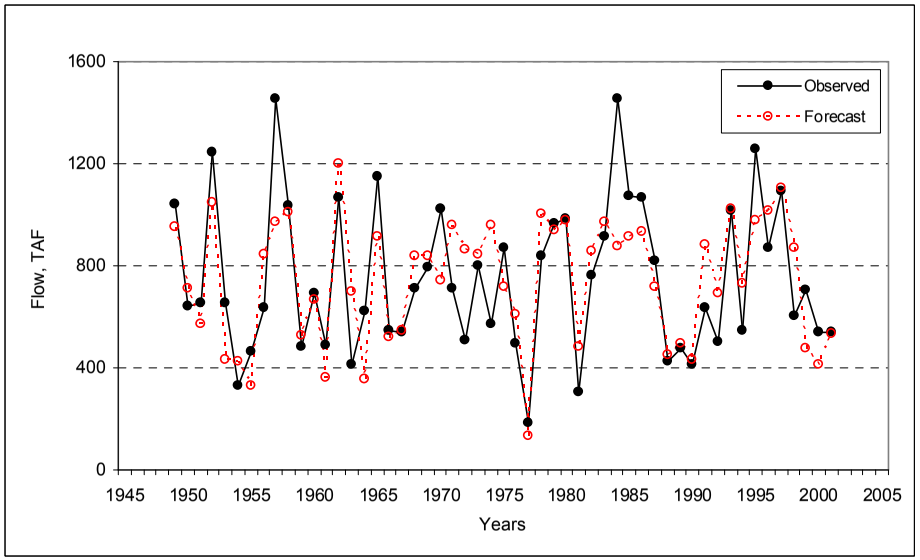

Drop-10%

Fig. D2.3 Comparison of forecast results for Gunnison River

Single-site model

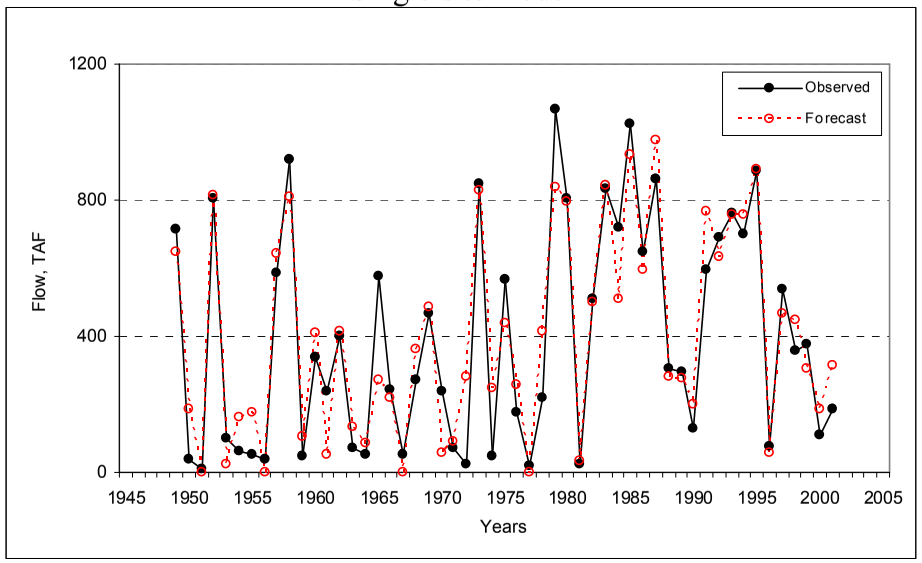

Fitting

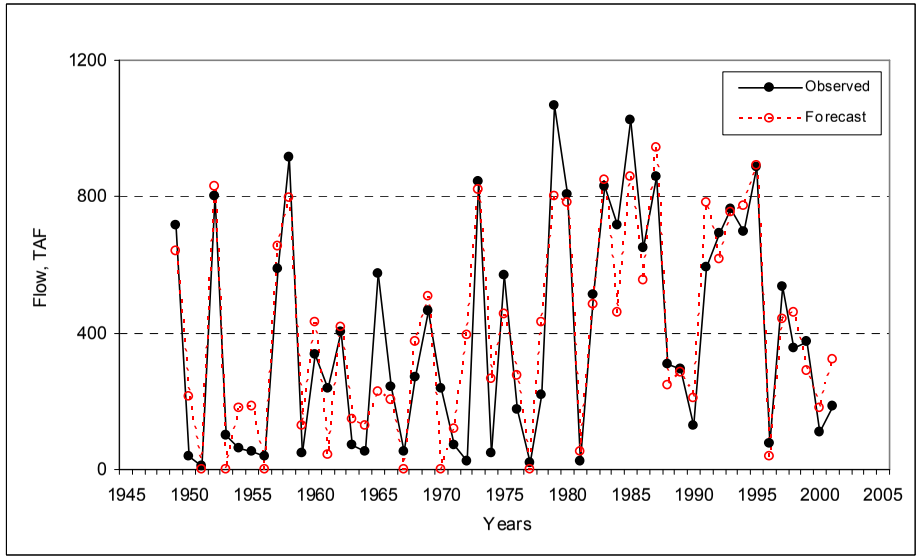

Drop-10%

Multi-site – CCA

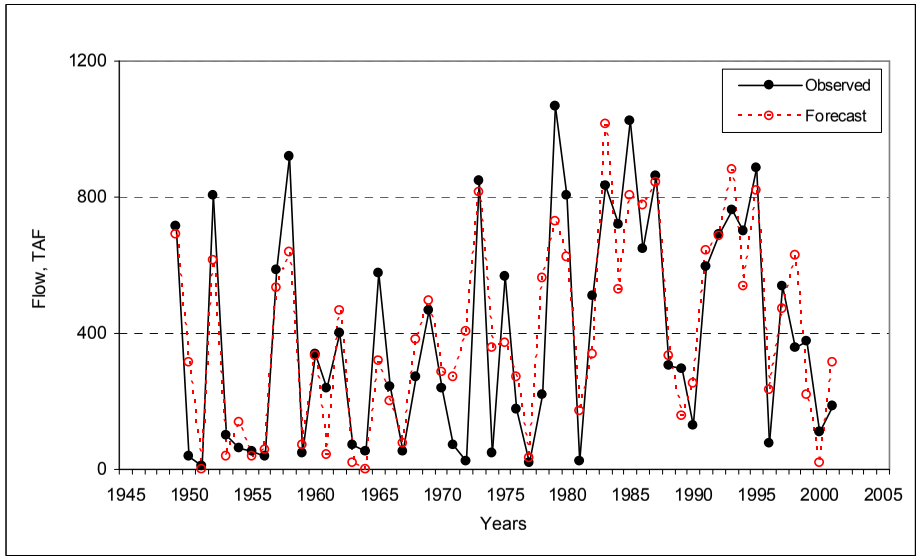

Fitting

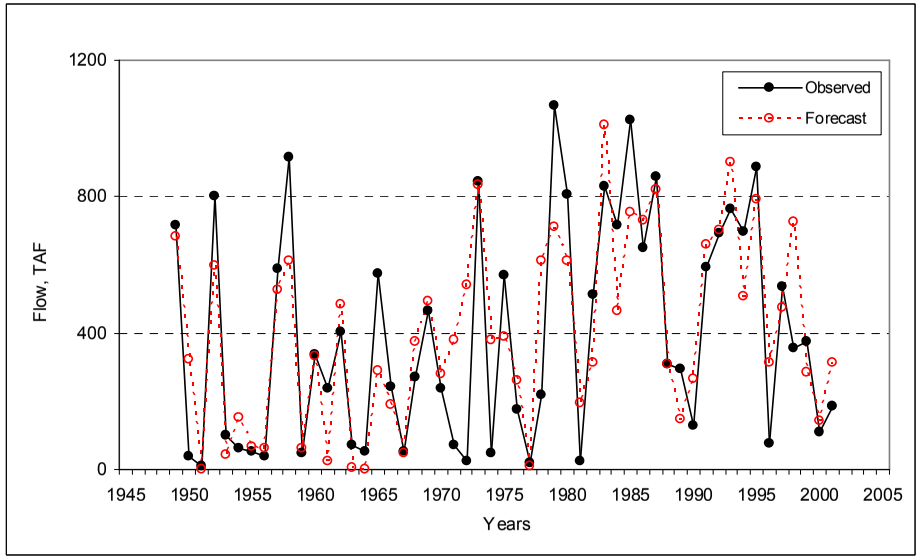

Drop-10%

Fig. D2.4 Comparison of forecast results for Rio Grande

Single-site model

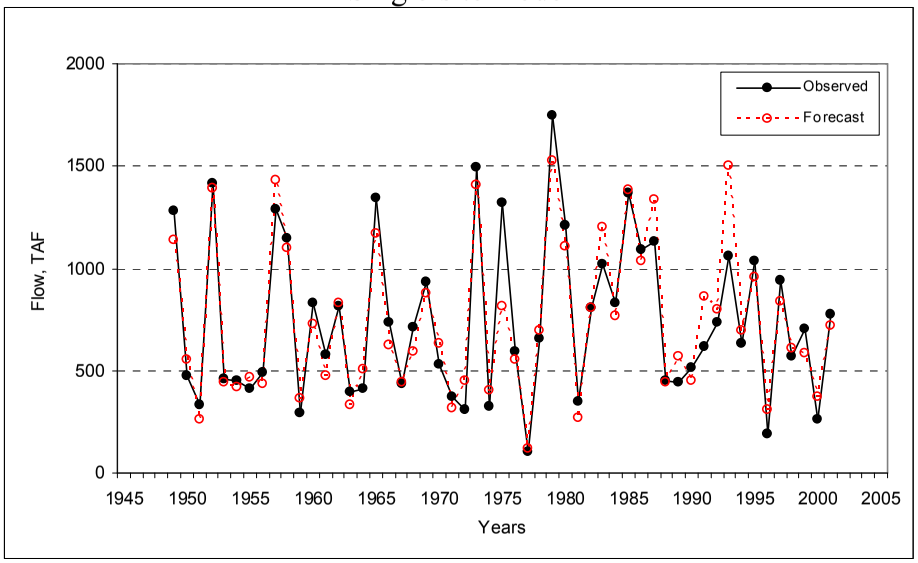

Fitting

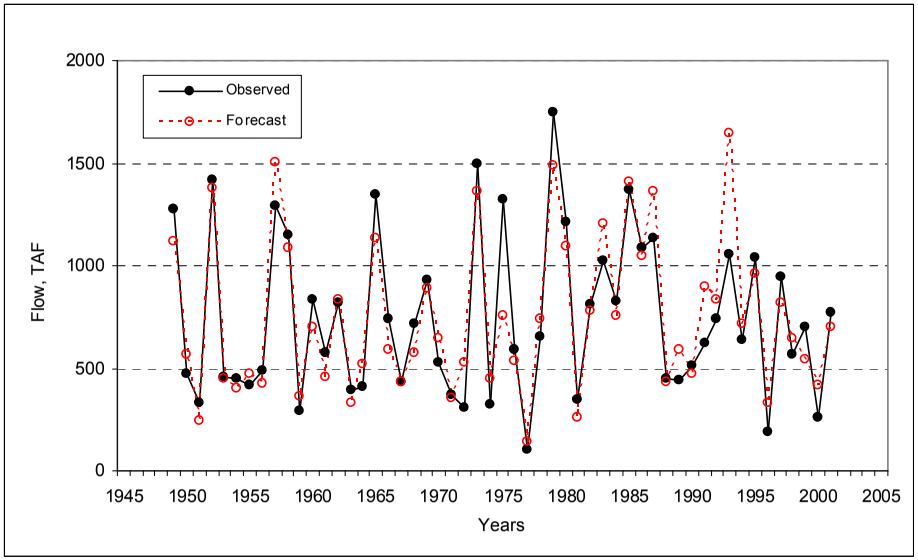

Drop-10%

Multi-site – CCA

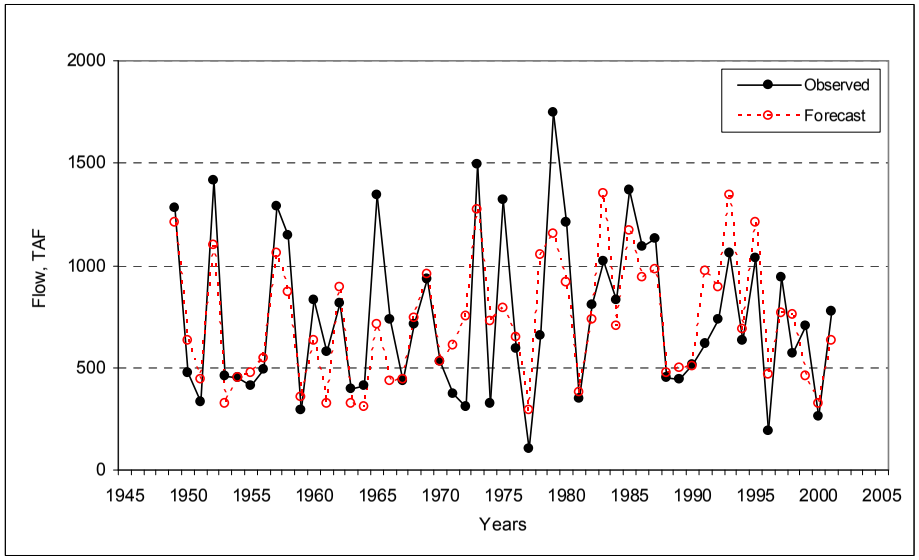

Fitting

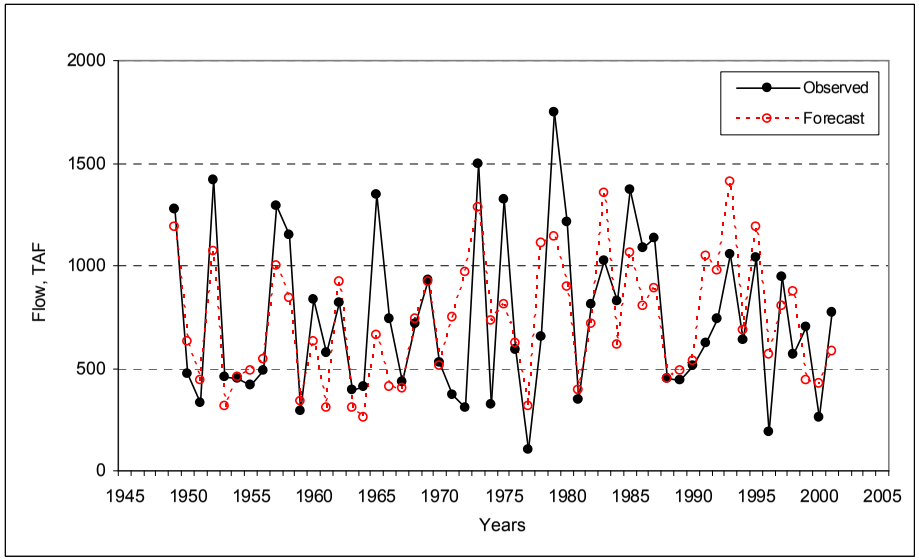

Drop-10%

Fig. D2.5 Comparison of forecast results for San Juan River

Single-site model

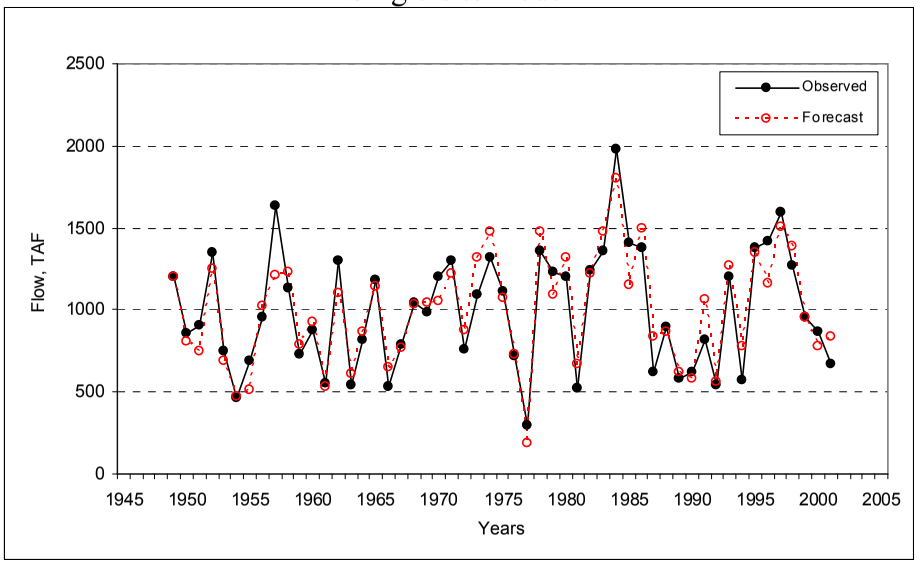

Fitting

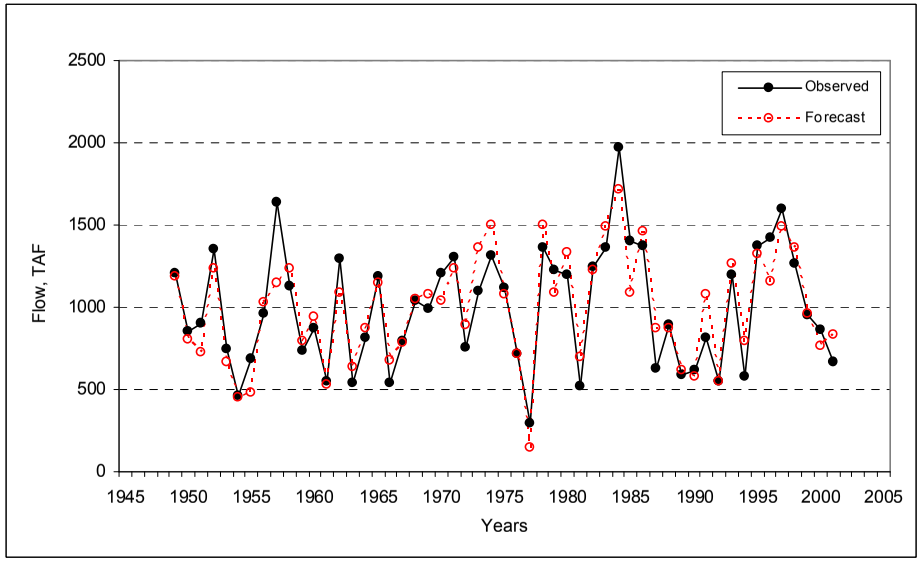

Drop-10%

Multi-site – CCA

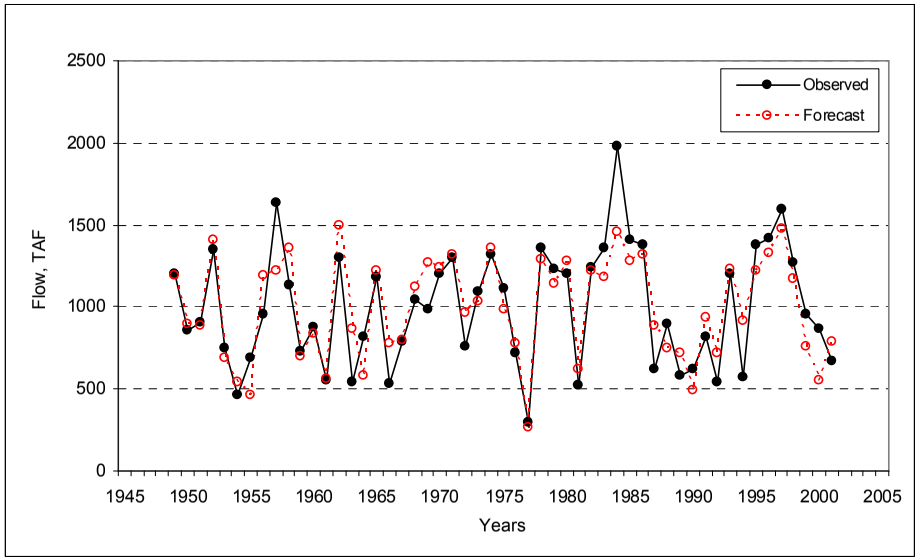

Fitting

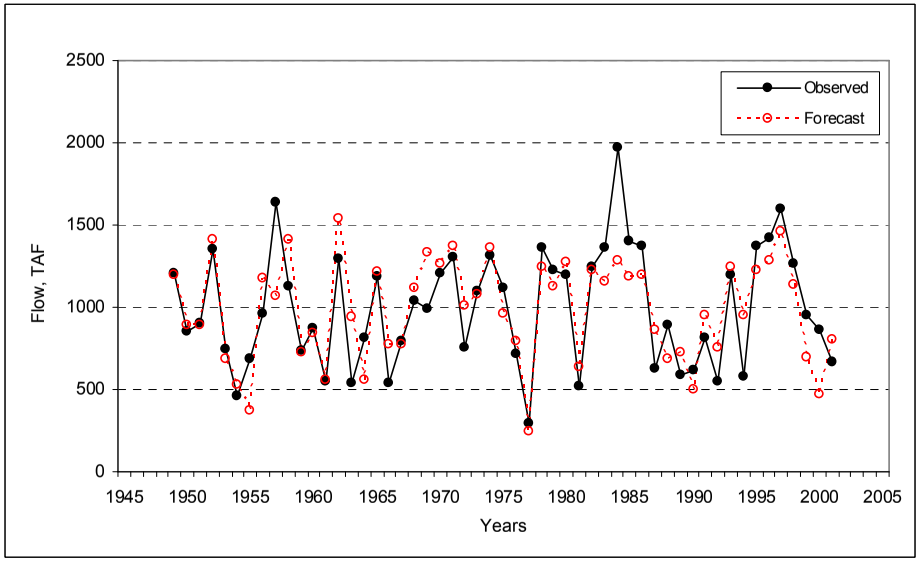

Drop-10%

Fig. D2.6 Comparison of forecast results for Yampa River

D3: Scatter plots for single-site models (MLR model)

Poudre River

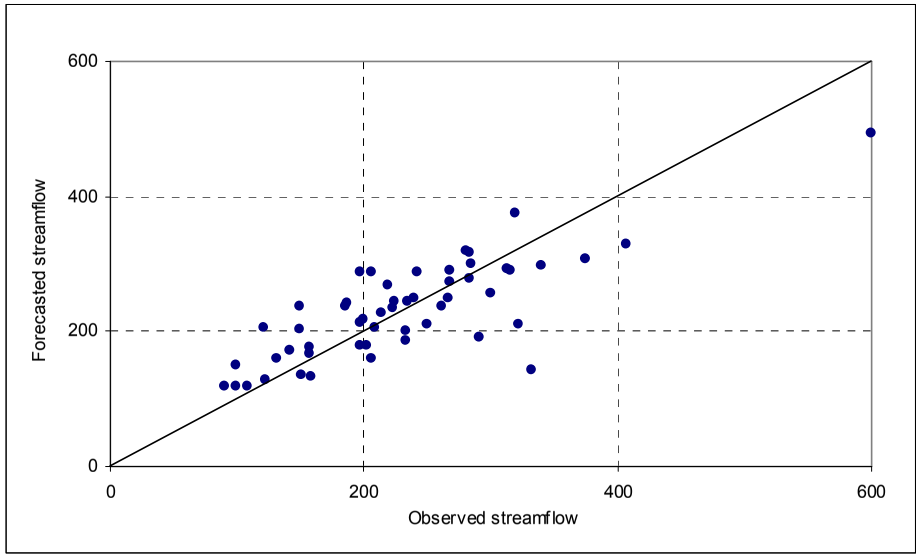

Fitting

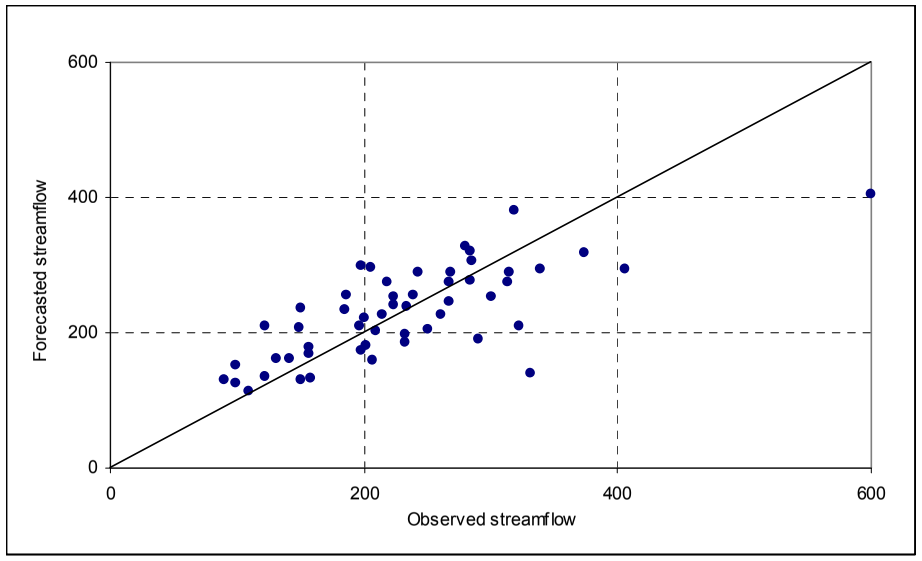

Drop-10%

Fig. D3.1 Comparison of forecast results for Poudre River

Arkansas River

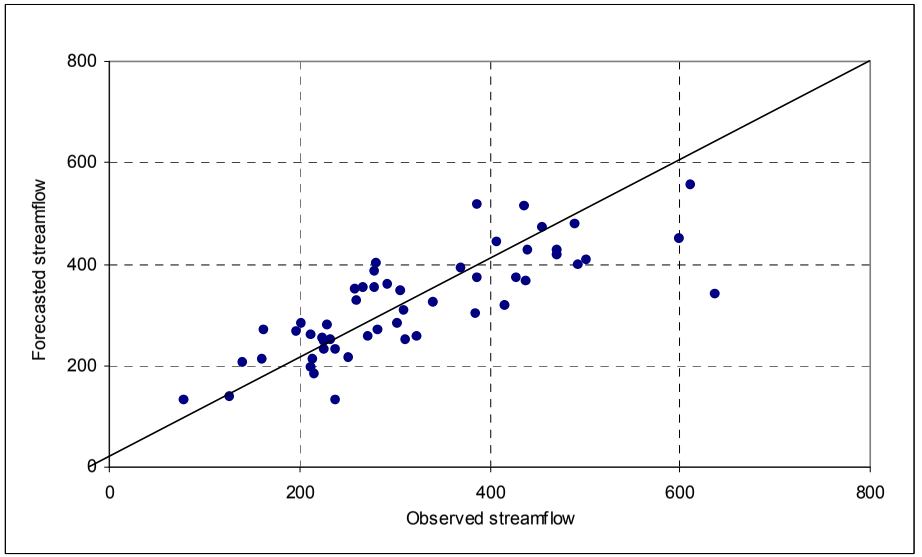

Fitting

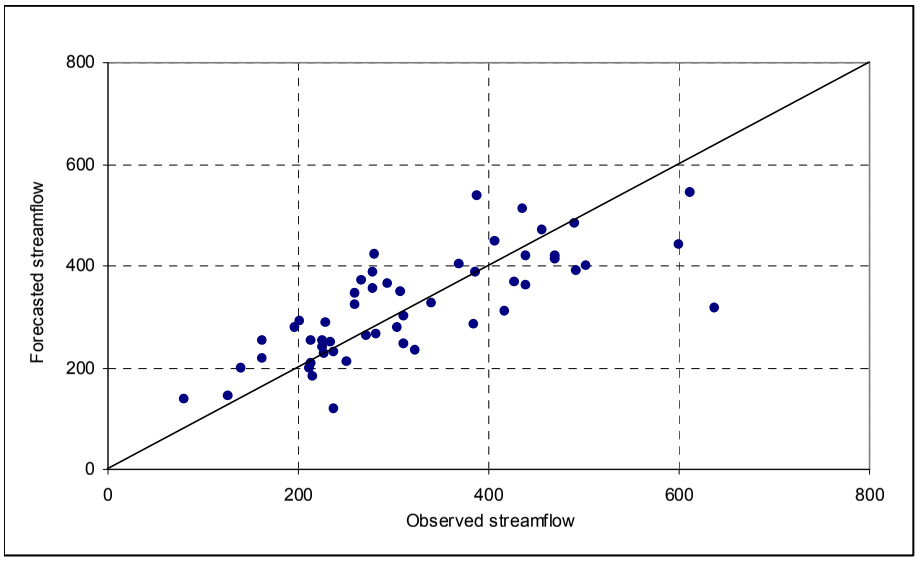

Drop-10%

Fig. D3.2 Comparison of forecast results for Arkansas River

Gunnison River

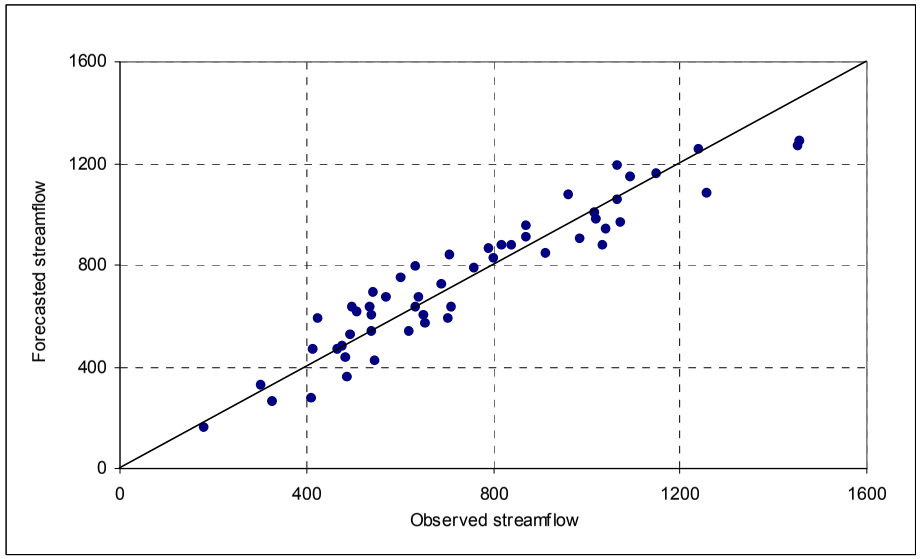

Fitting

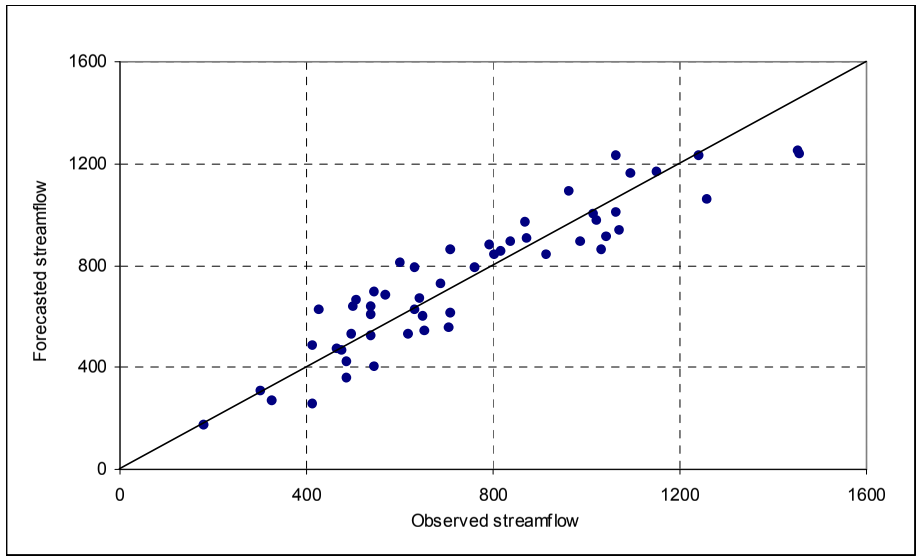

Drop-10%

Fig. D3.3 Comparison of forecast results for Gunnison River

Rio Grande

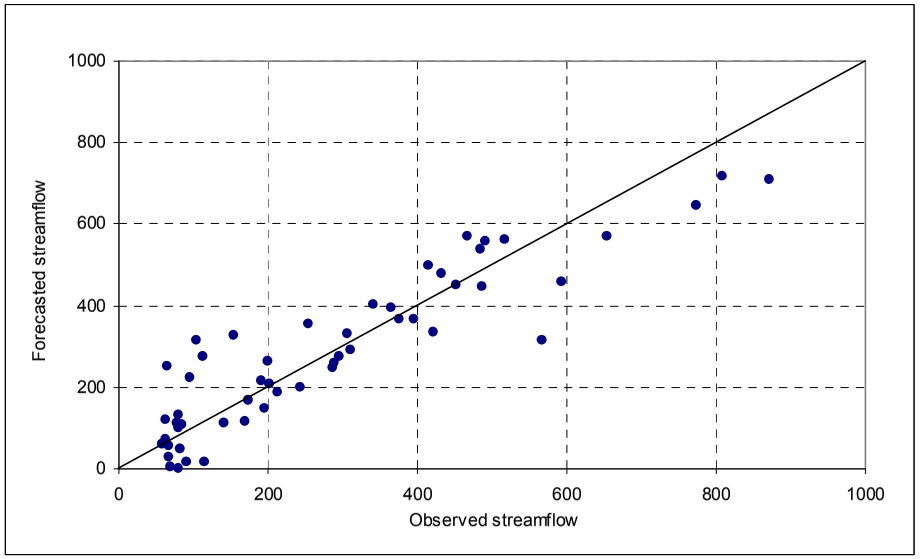

Fitting

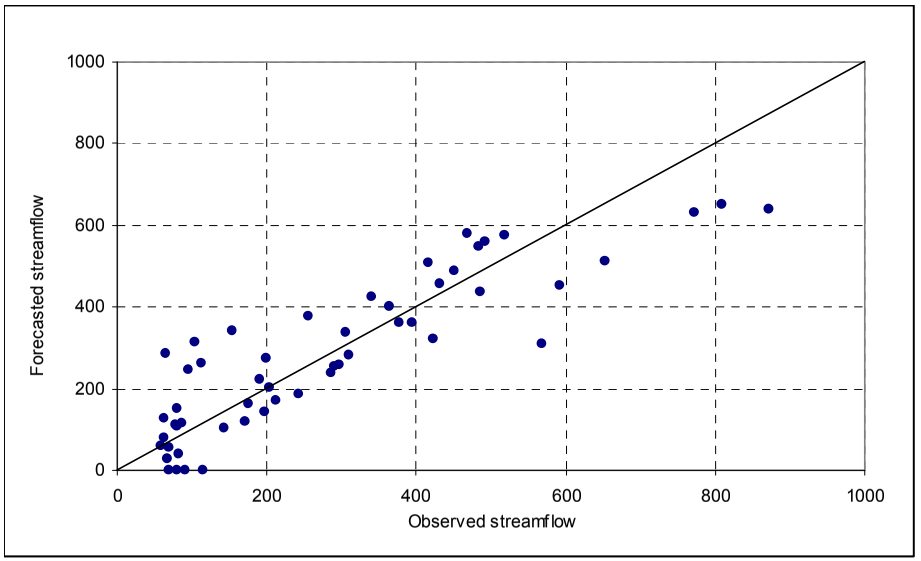

Drop-10%

Fig. D3.4 Comparison of forecast results Rio Grande

San Juan River

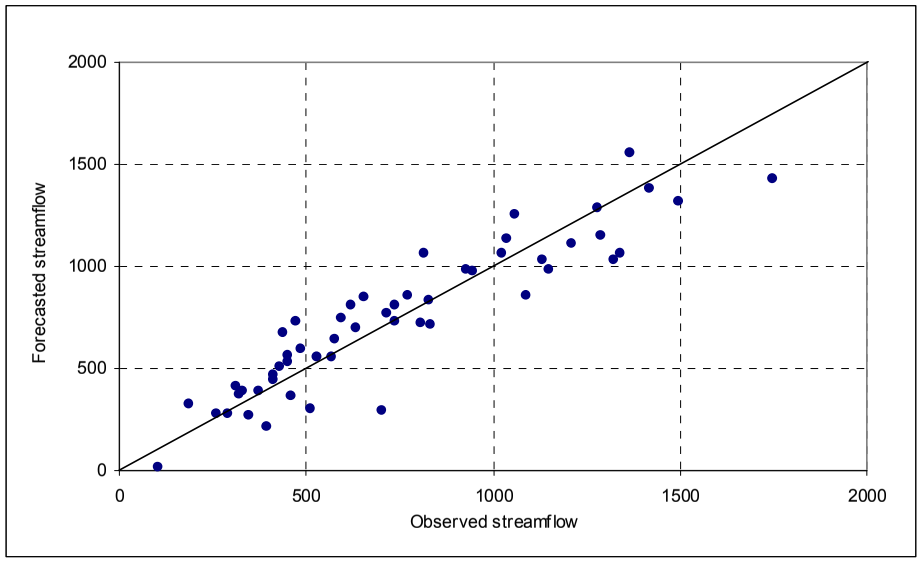

Fitting

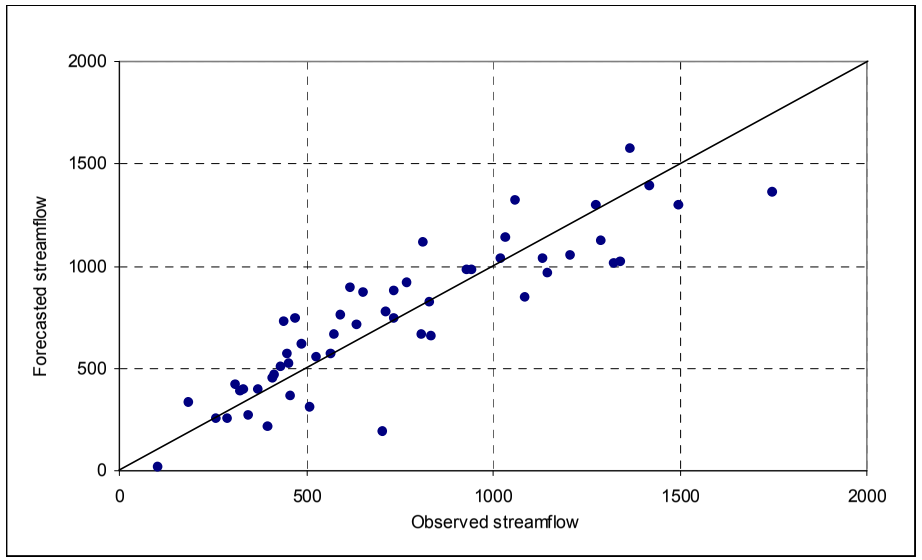

Drop-10%

Fig. D3.5 Comparison of forecast results for San Juan River

Yampa River

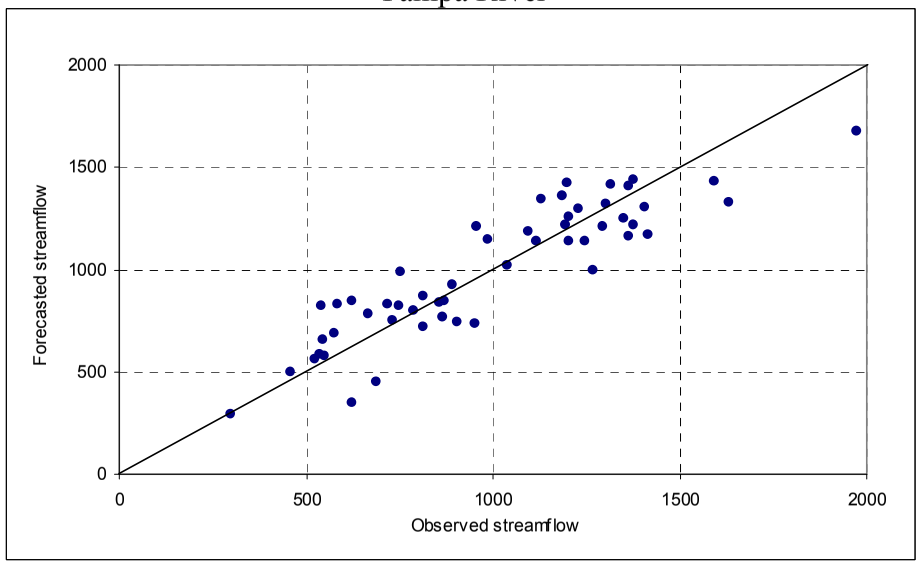

Fitting

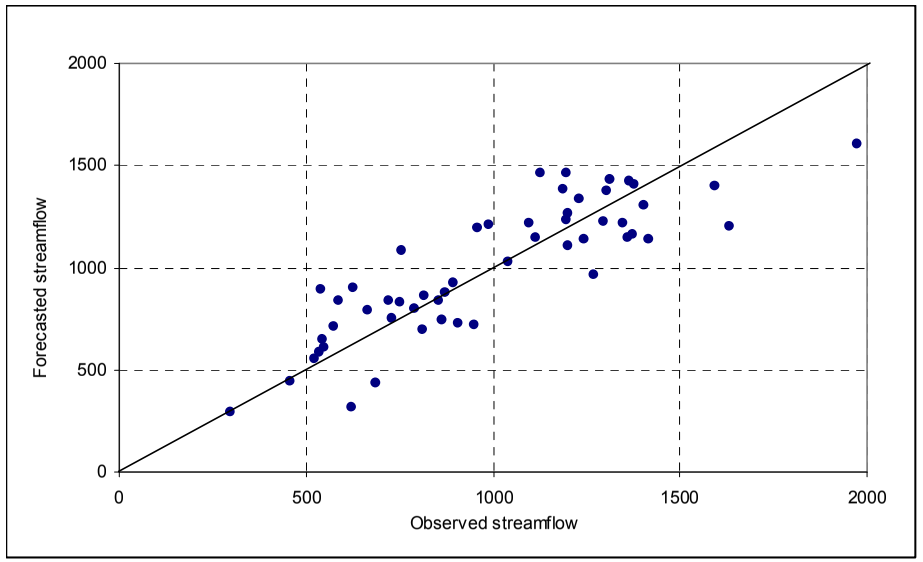

Drop-10%

Fig. D3.6. Comparison of forecast results for Yampa River

D4: Comparison of single –site models (PCA) and CCA model

Single-site model

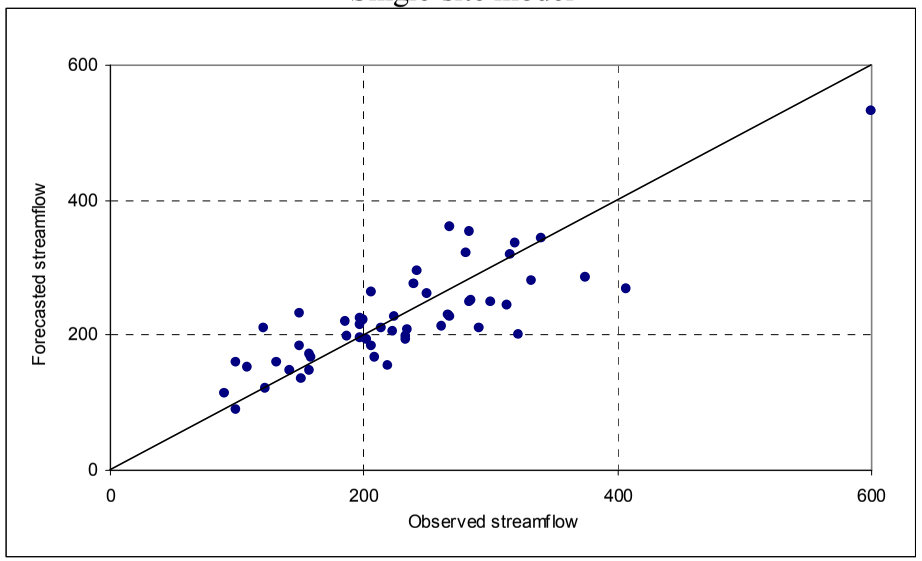

Fitting

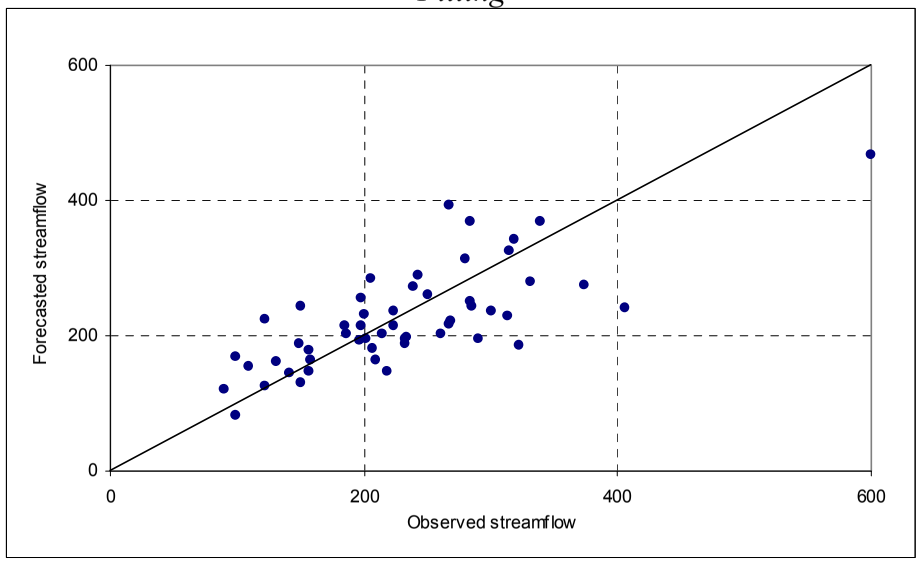

Drop-10%

Multi-site - CCA

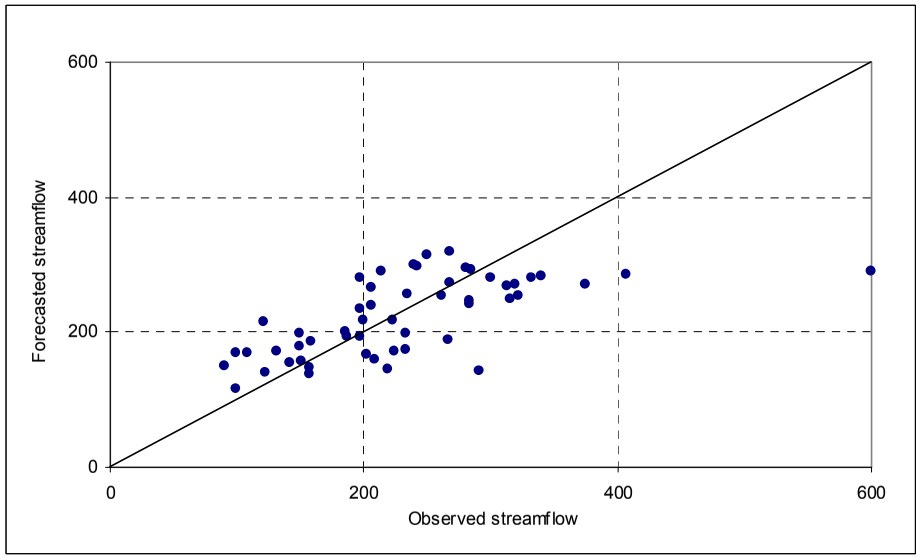

Fitting

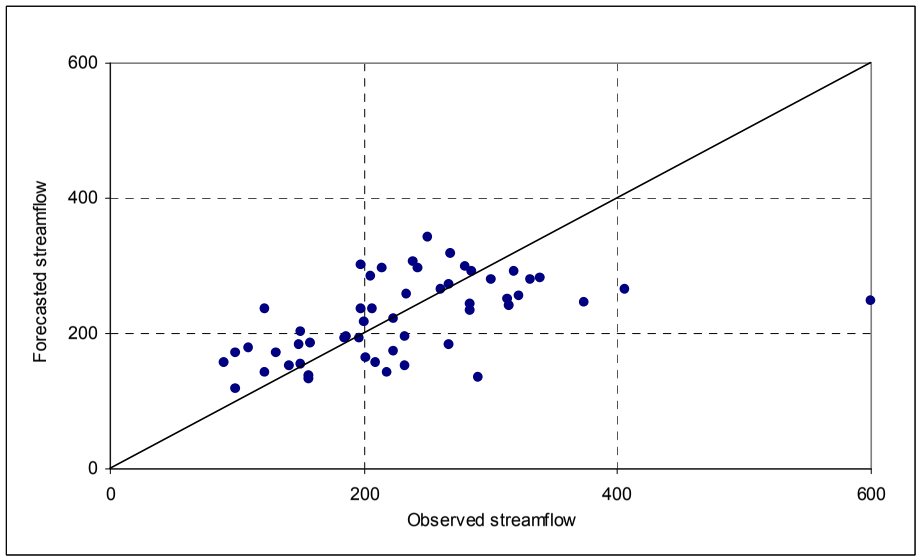

Drop-10%

Fig. D4.1 Comparison of forecast results for Poudre River

Single-site model

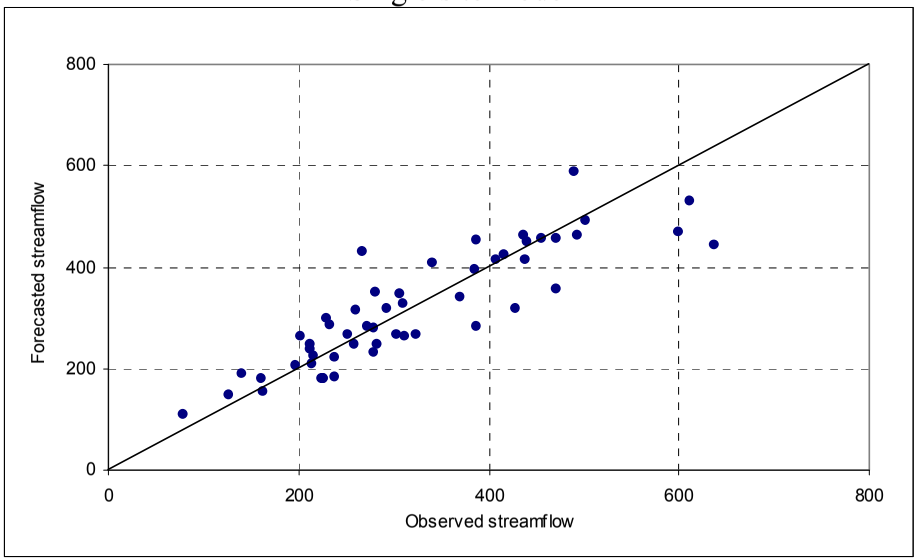

Fitting

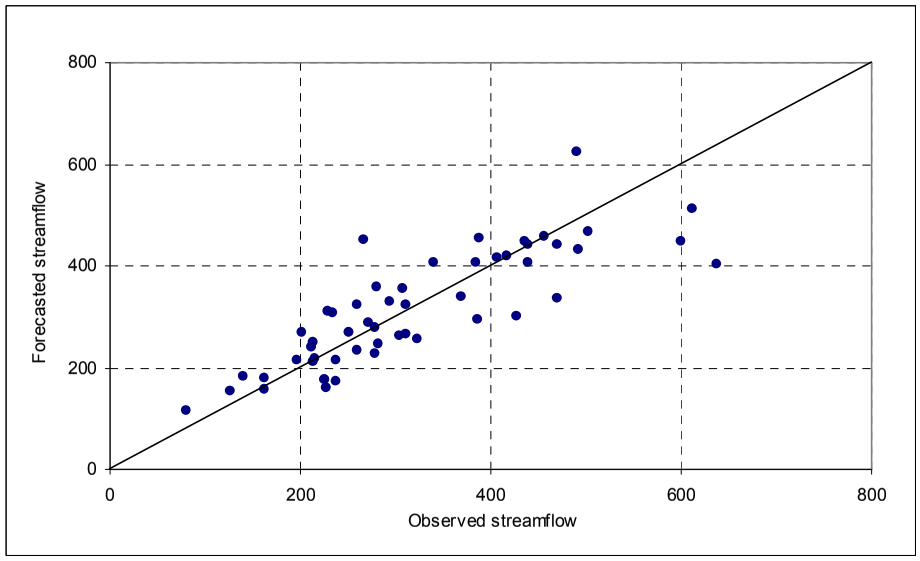

Drop-10%

Multi-site – CCA

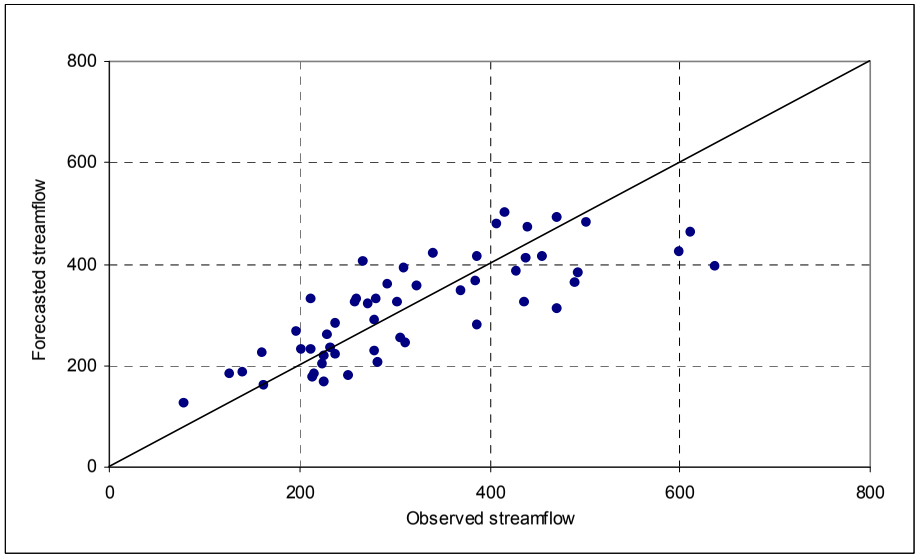

Fitting

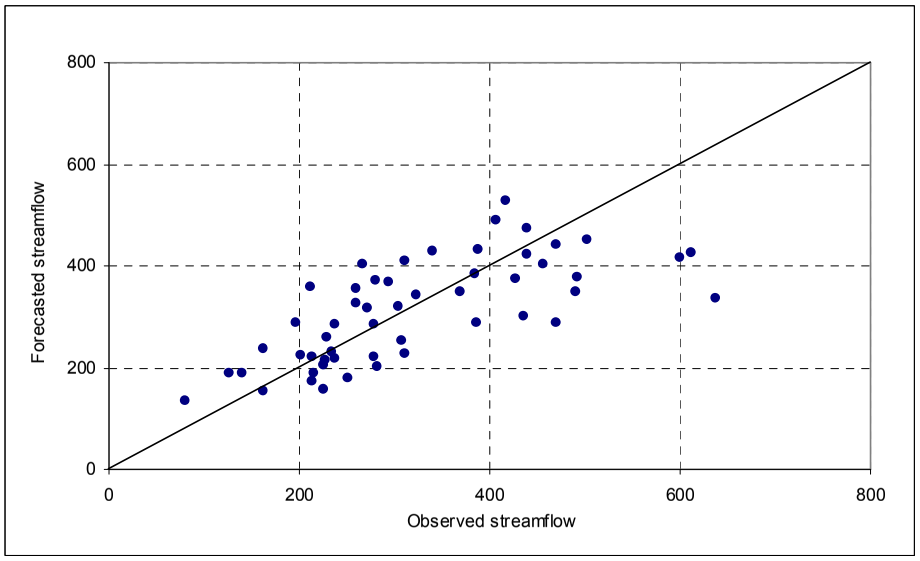

Drop-10%

Fig. D4.2 Comparison of forecast results for Arkansas River

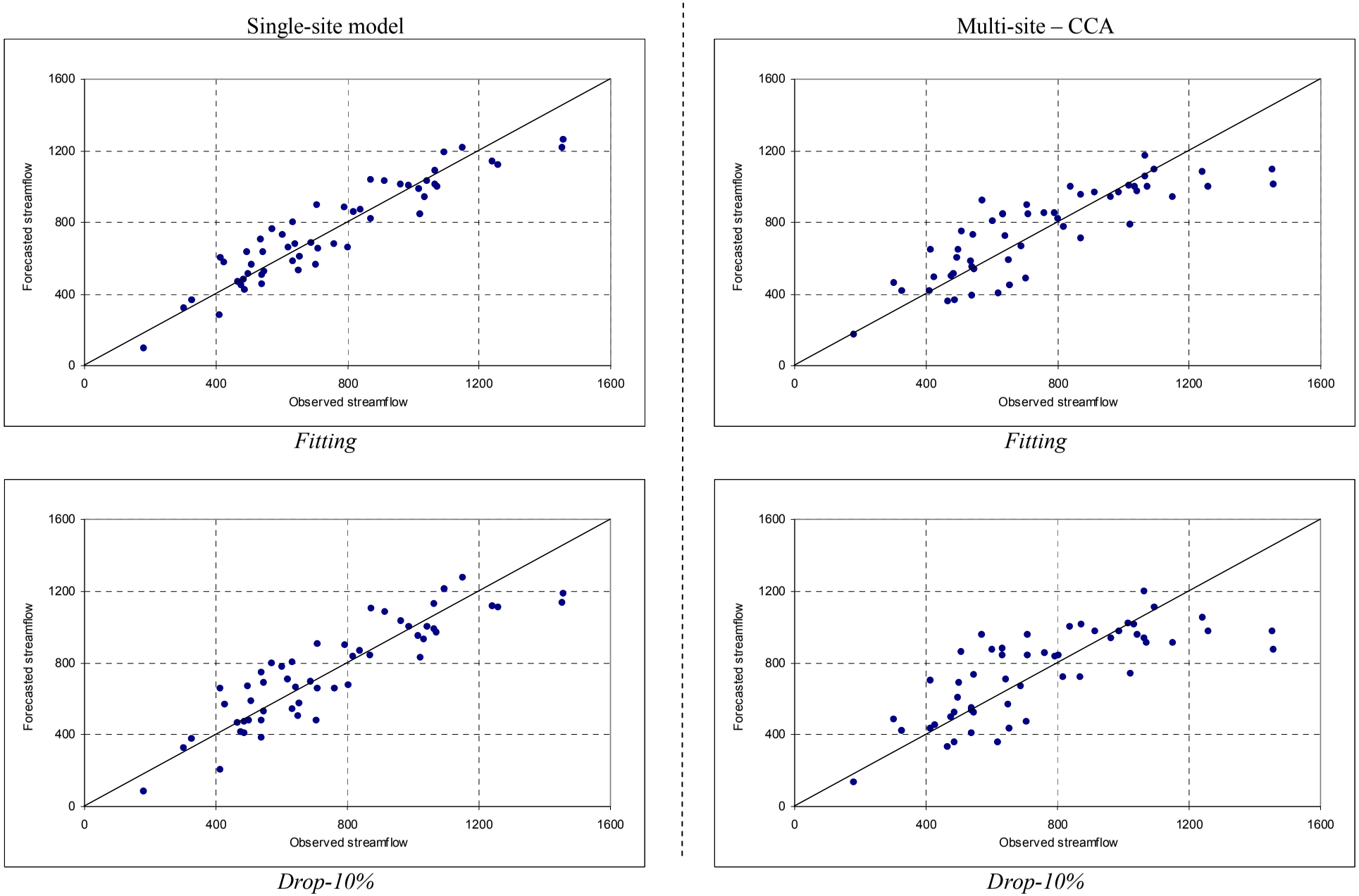

Fig. D4.3 Comparison of forecast results for Gunnison River

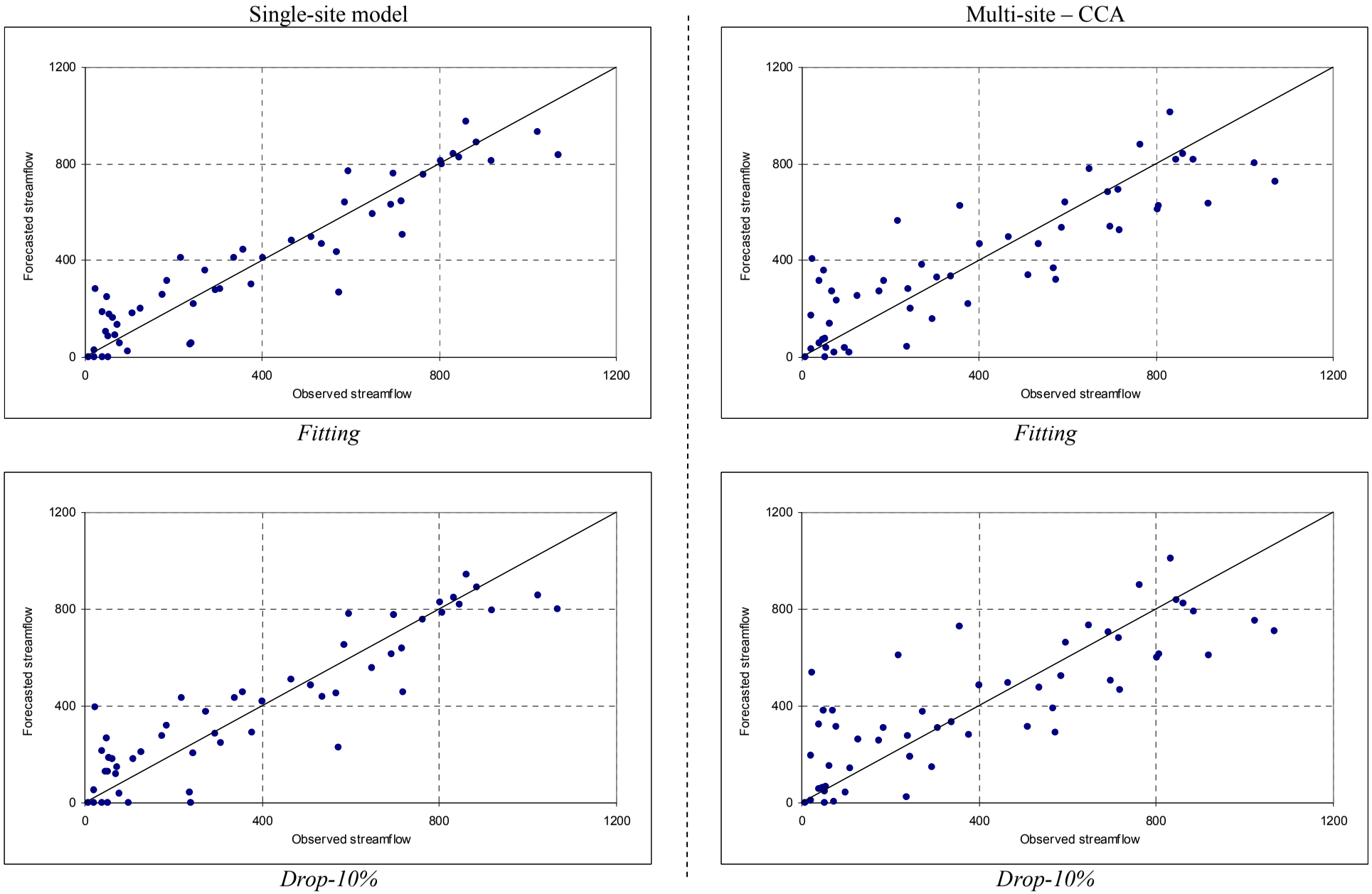

Fig. D4.4 Comparison of forecast results for Rio Grande

Single-site model

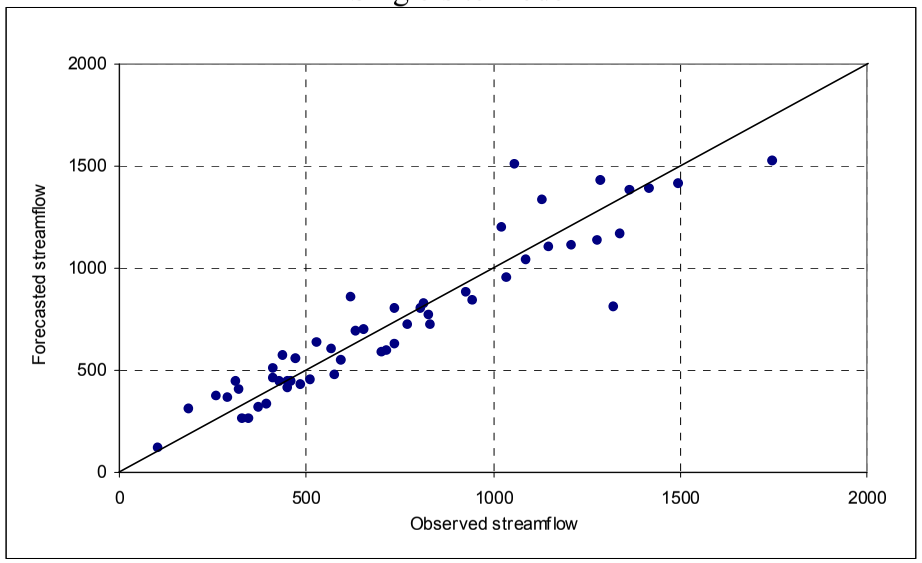

Fitting

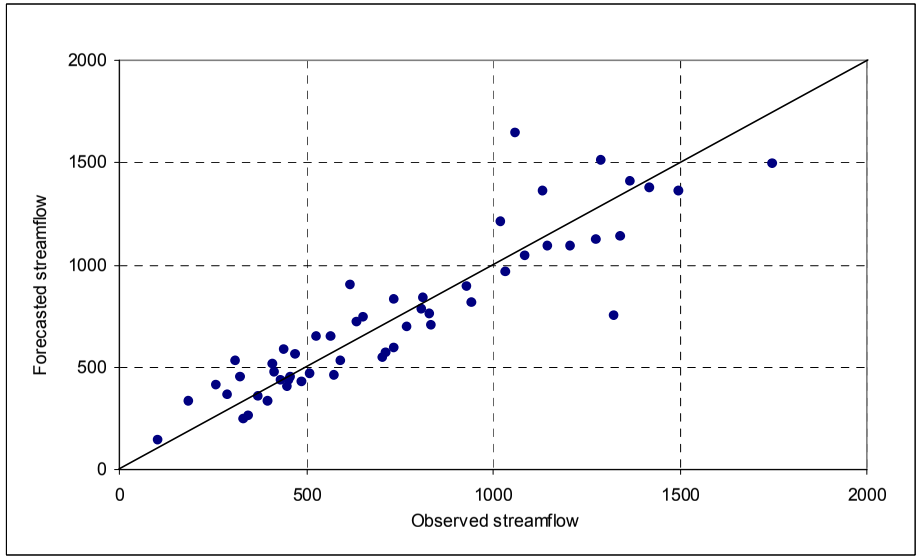

Drop-10%

Multi-site – CCA

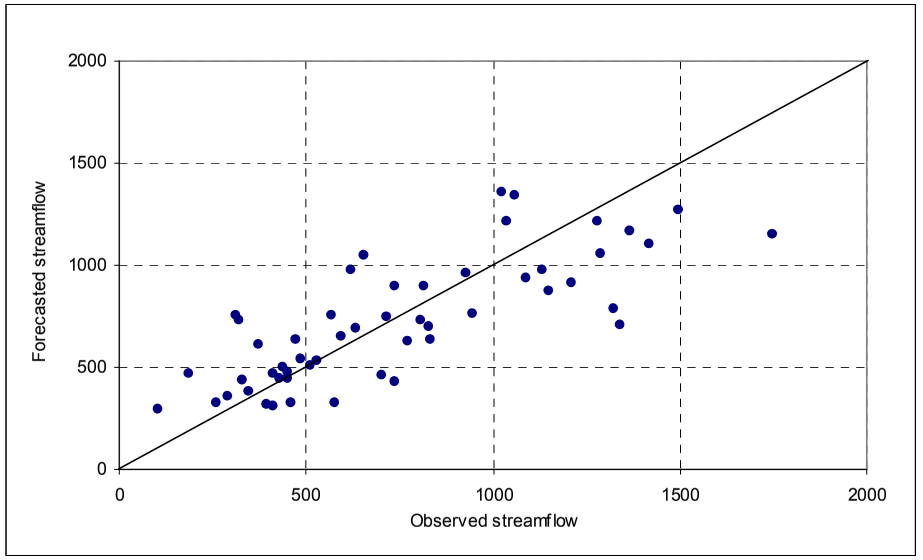

Fitting

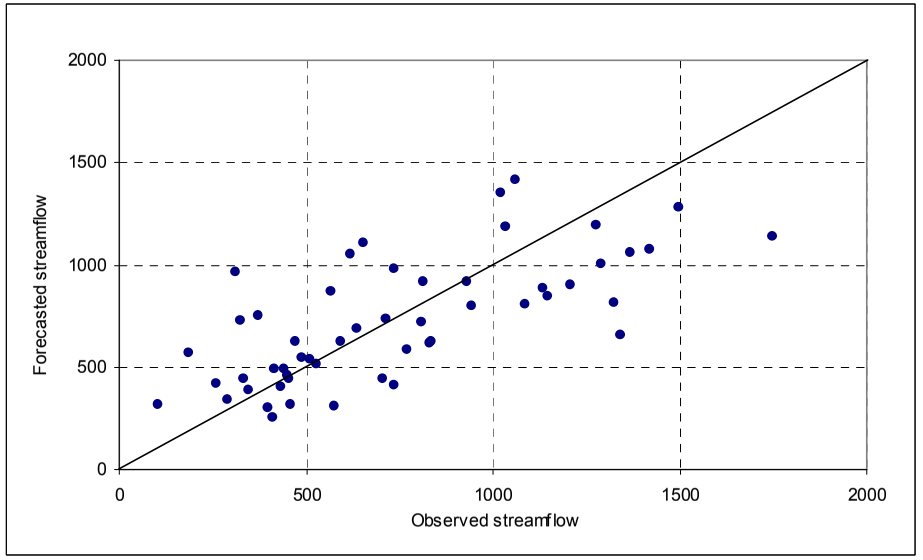

Drop-10%

Fig. D4.5 Comparison of forecast results for San Juan River

Single-site model

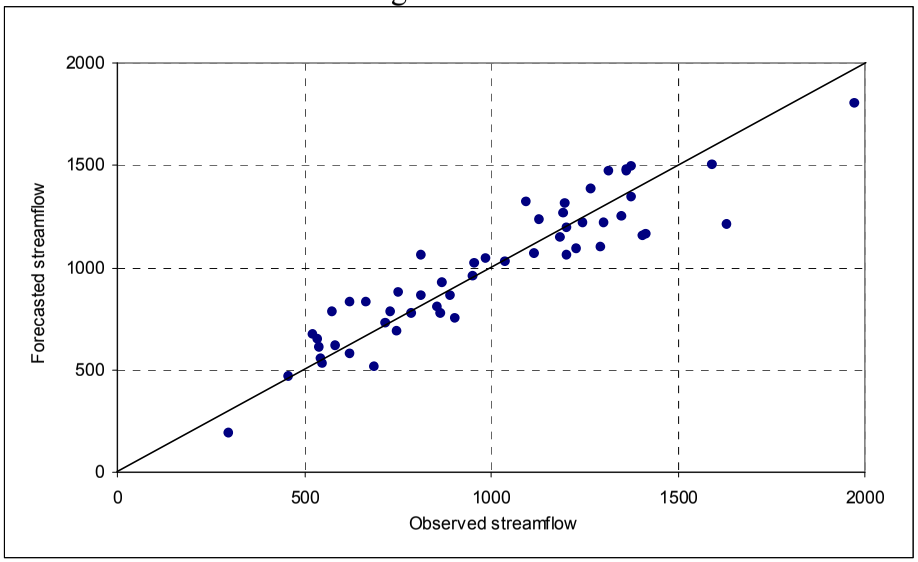

Fitting

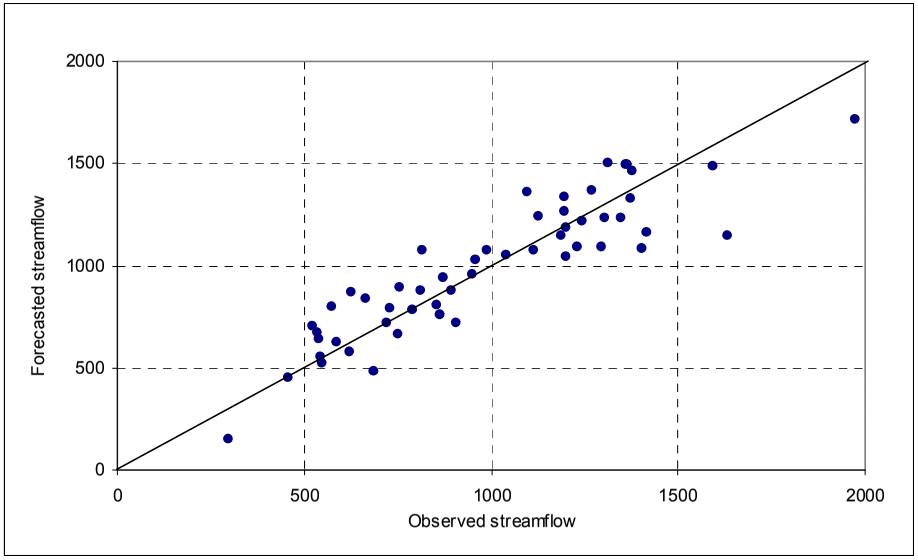

Drop-10%

Multi-site – CCA

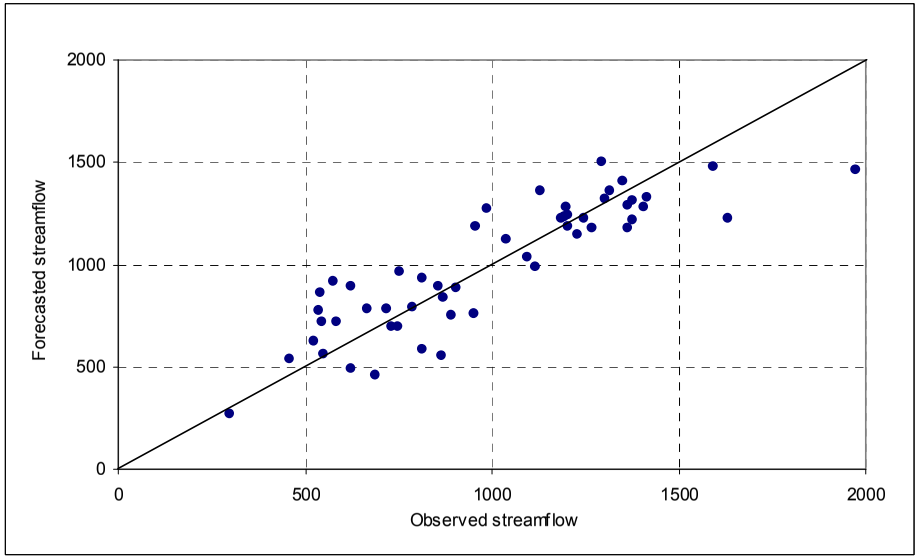

Fitting

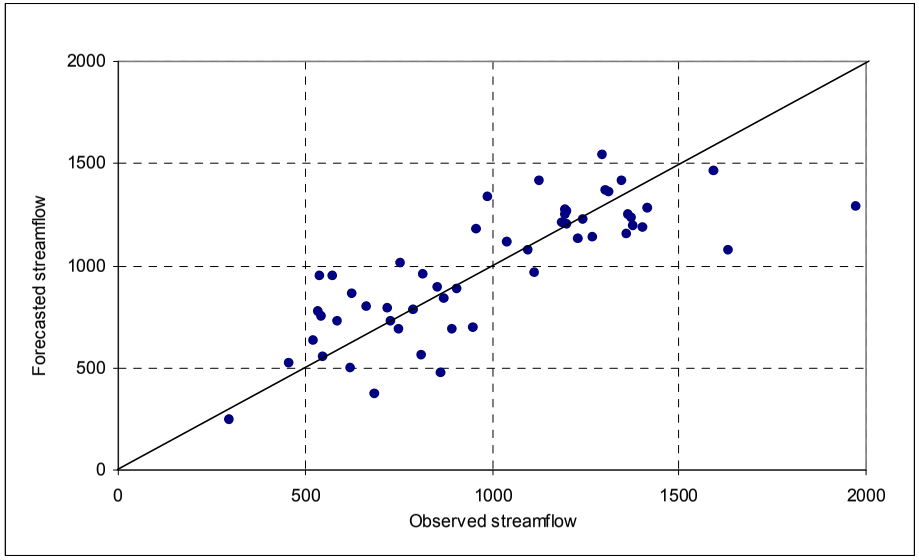

Drop-10%

Fig. D4.6 Comparison of forecast results for Yampa River

D6: Comparison of forecasts for all predictors vs. climatic/oceanic predictors only

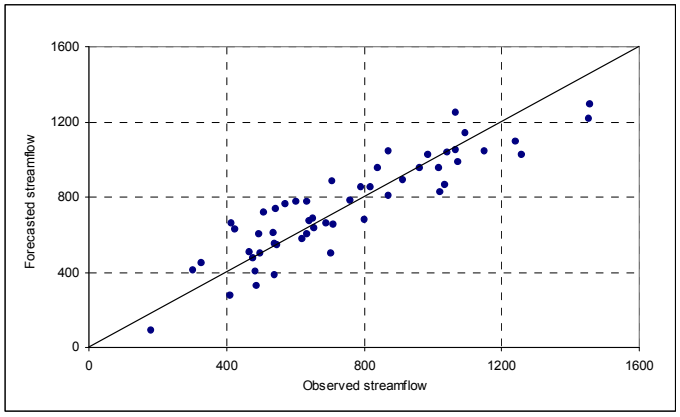

Fitting

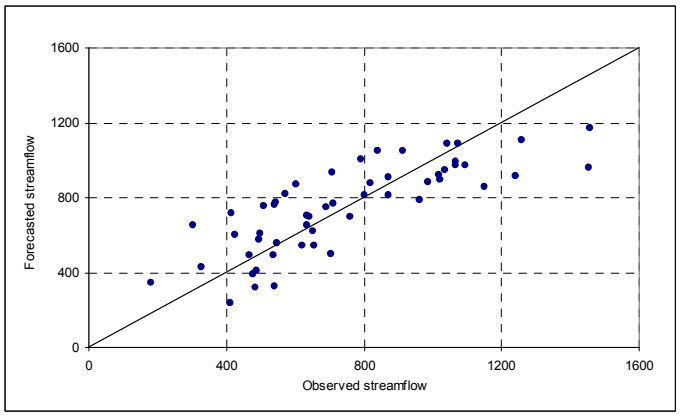

Fitting

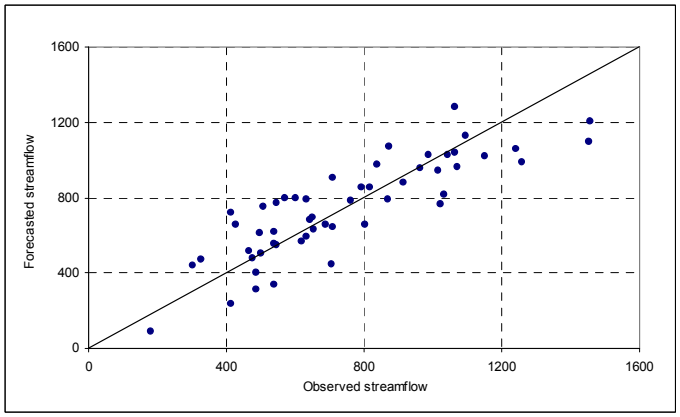

Drop one

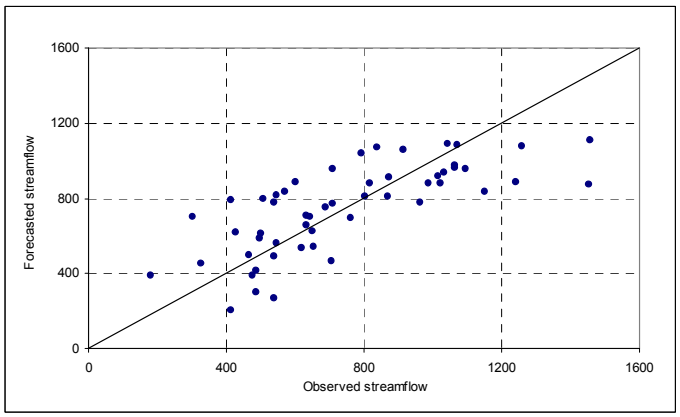

Drop one

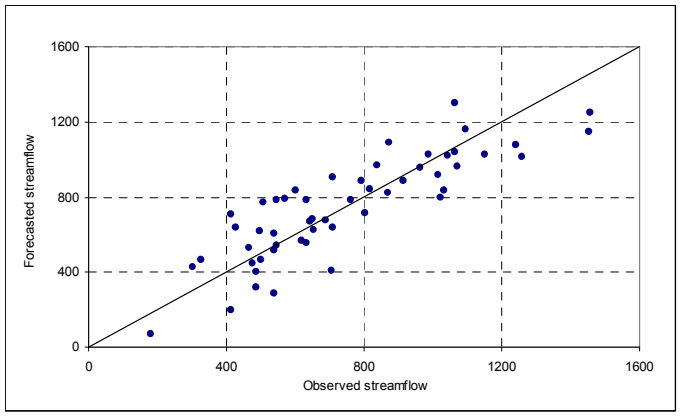

Drop 10%

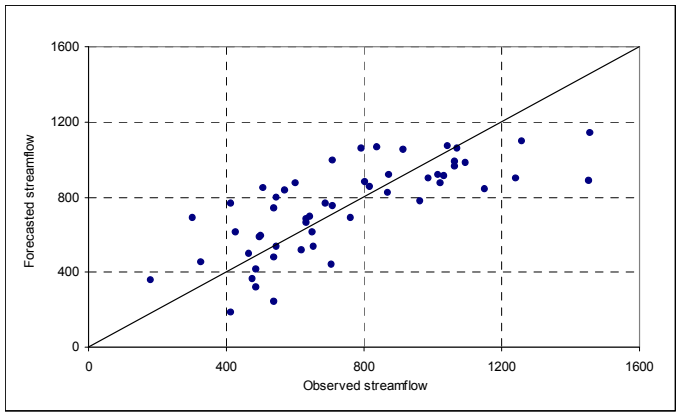

Drop 10%

Figure D6.1 Scatter plots of the forecast results for Gunnison River
(Left panel: all variables; Right: climate/oceanic variables only)

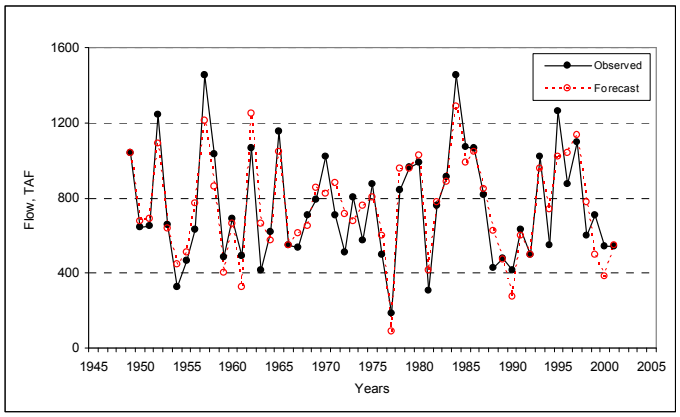

Fitting

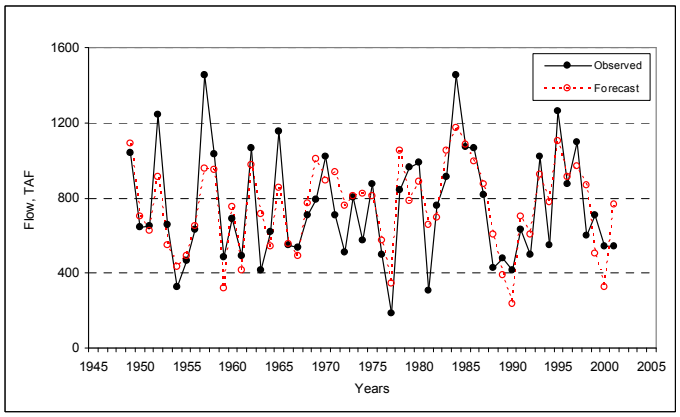

Fitting

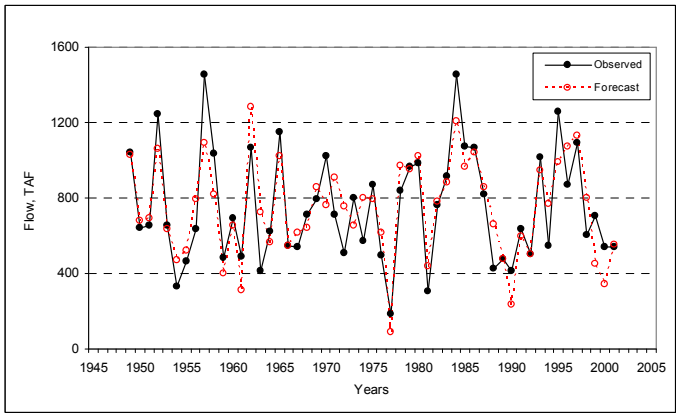

Drop one

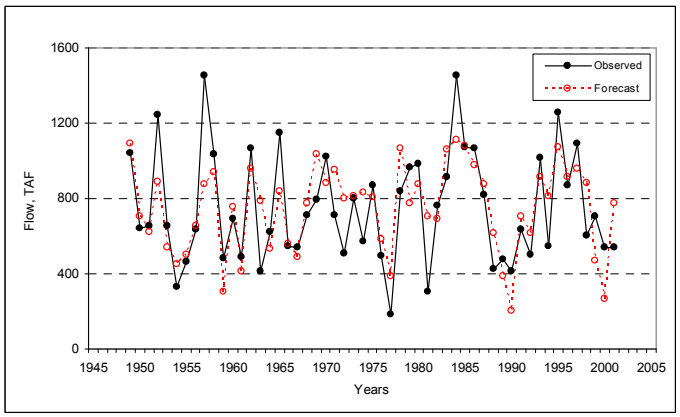

Drop one

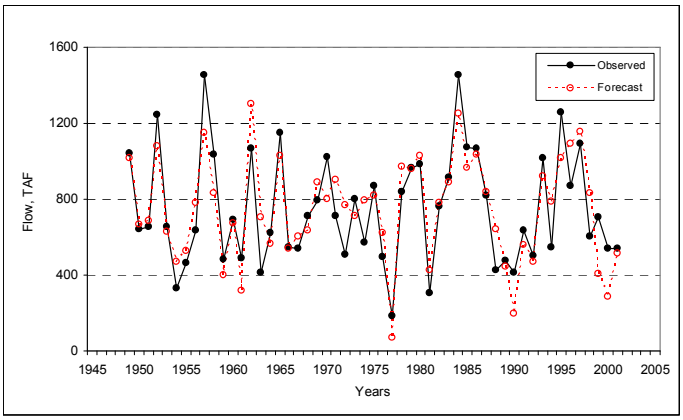

Drop 10%

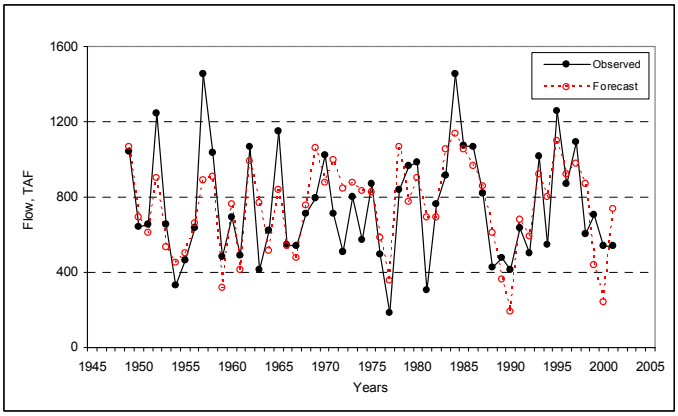

Drop 10%

Figure D6.2 Time series plots of the forecast results for Gunnison River
(Left panel: all variables; Right: climate/oceanic variables only)

Appendix E: Comparisons of R^2s and Forecast Skill Scores

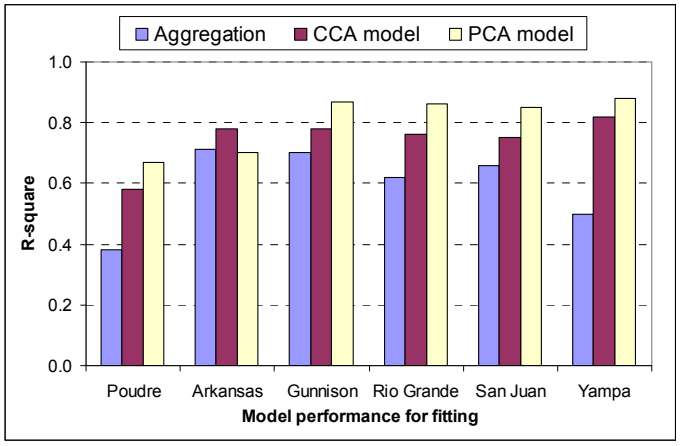

Fitting

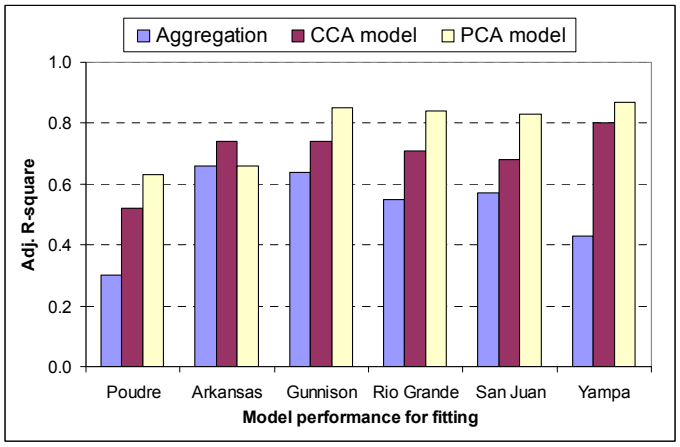

Fitting

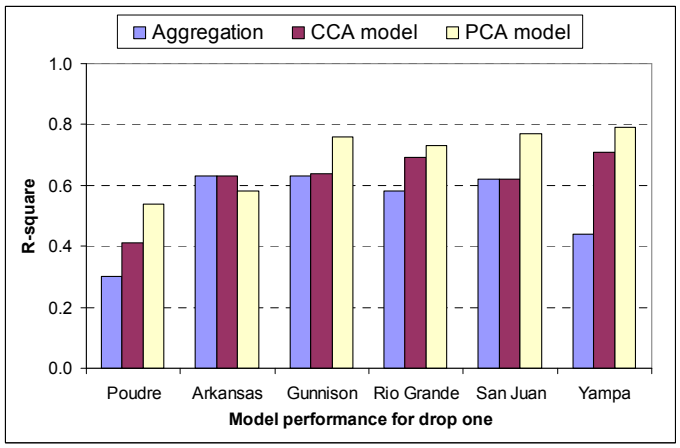

Drop one

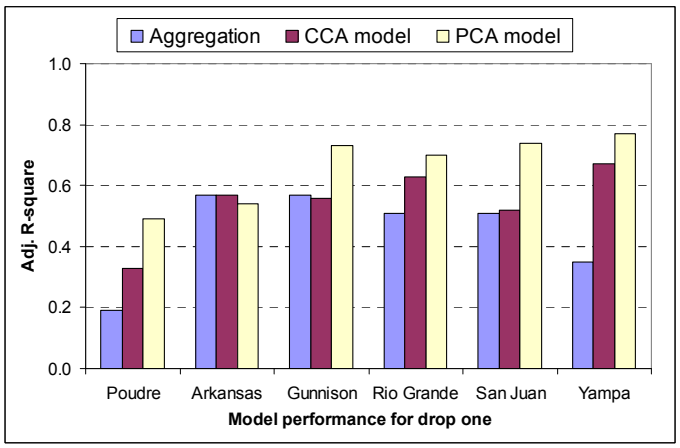

Drop one

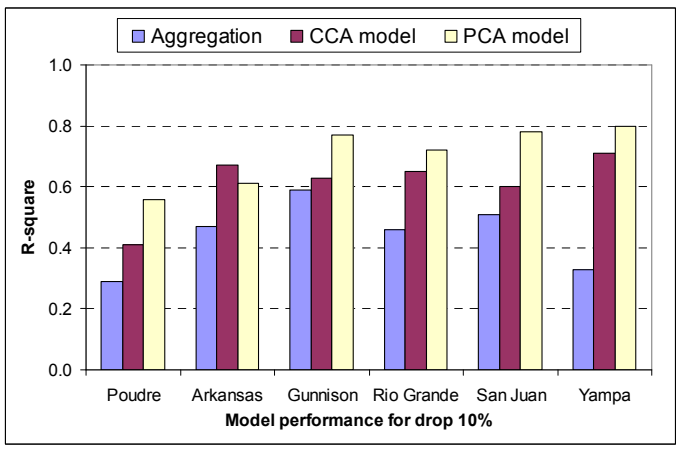

Drop 10%

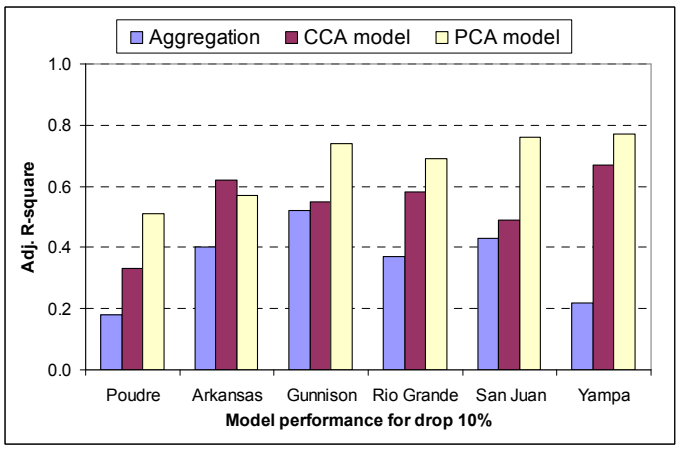

Drop 10%

Figure E.1 Comparisons of R^2 and Adjusted R^2 for the aggregation, CCA model and PCA models (Left panel: R^2; Right: Adjusted R^2)

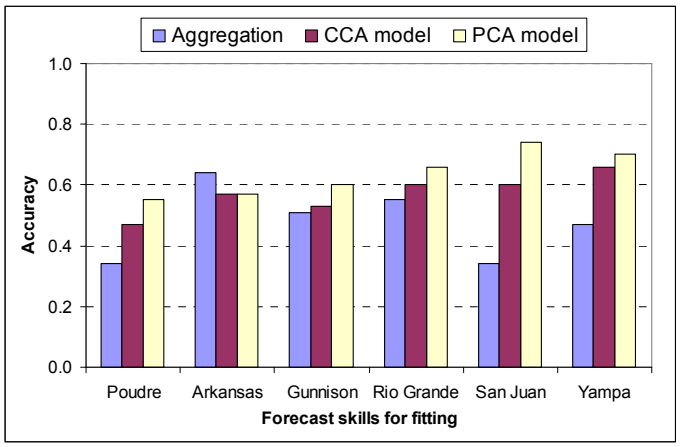

Fitting

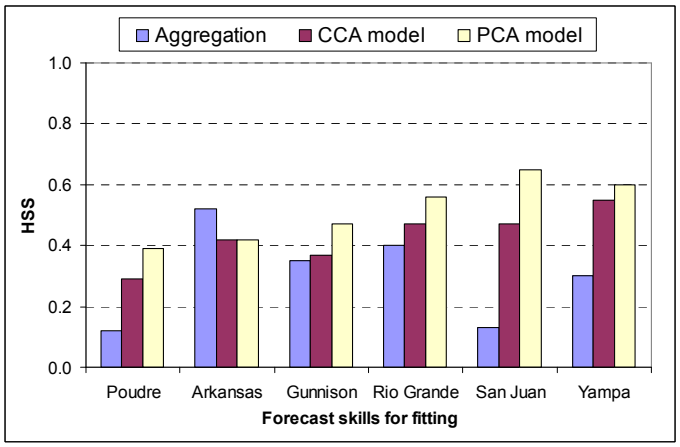

Fitting

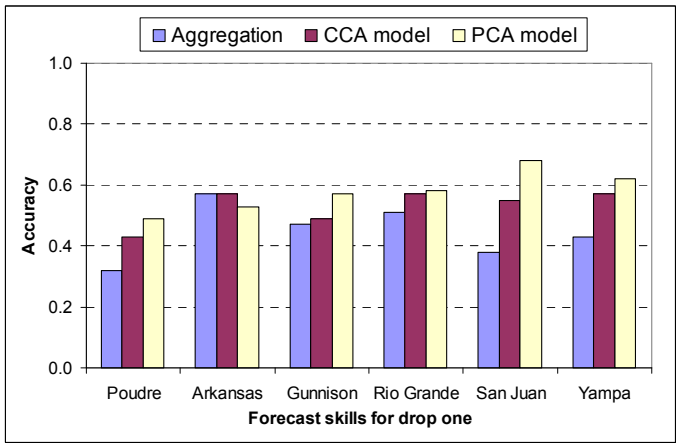

Drop one

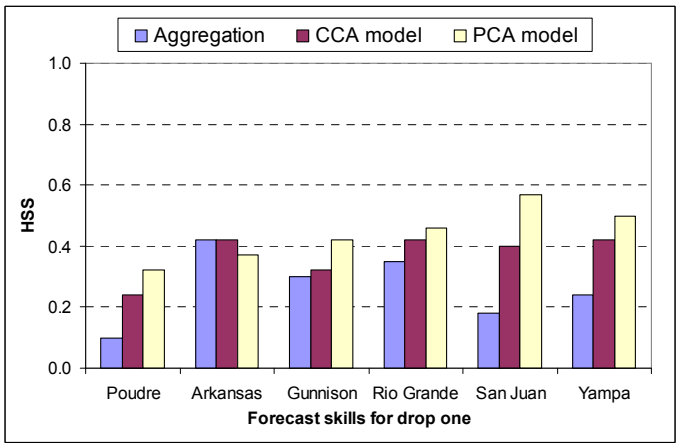

Drop one

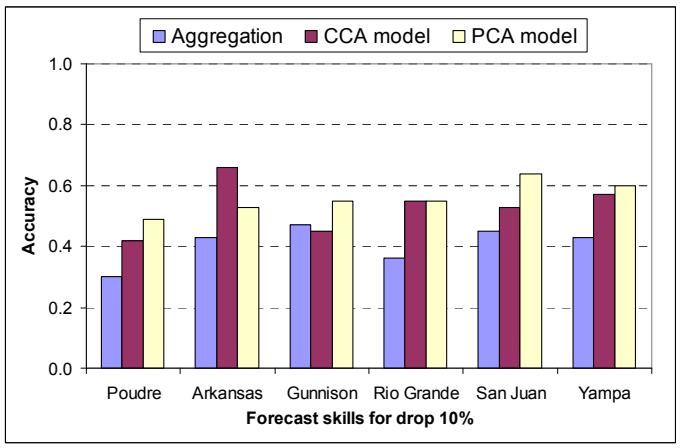

Drop 10%

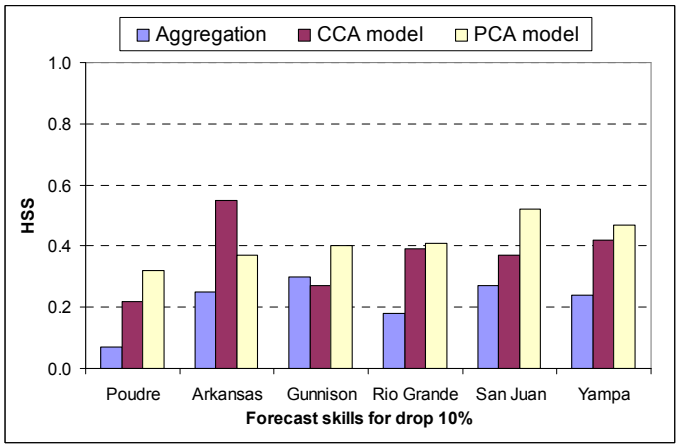

Drop 10%

Figure E.2 Comparisons of forecast skill scores for the aggregation, CCA model and PCA models (Left panel: Accuracy; Right: HSS)

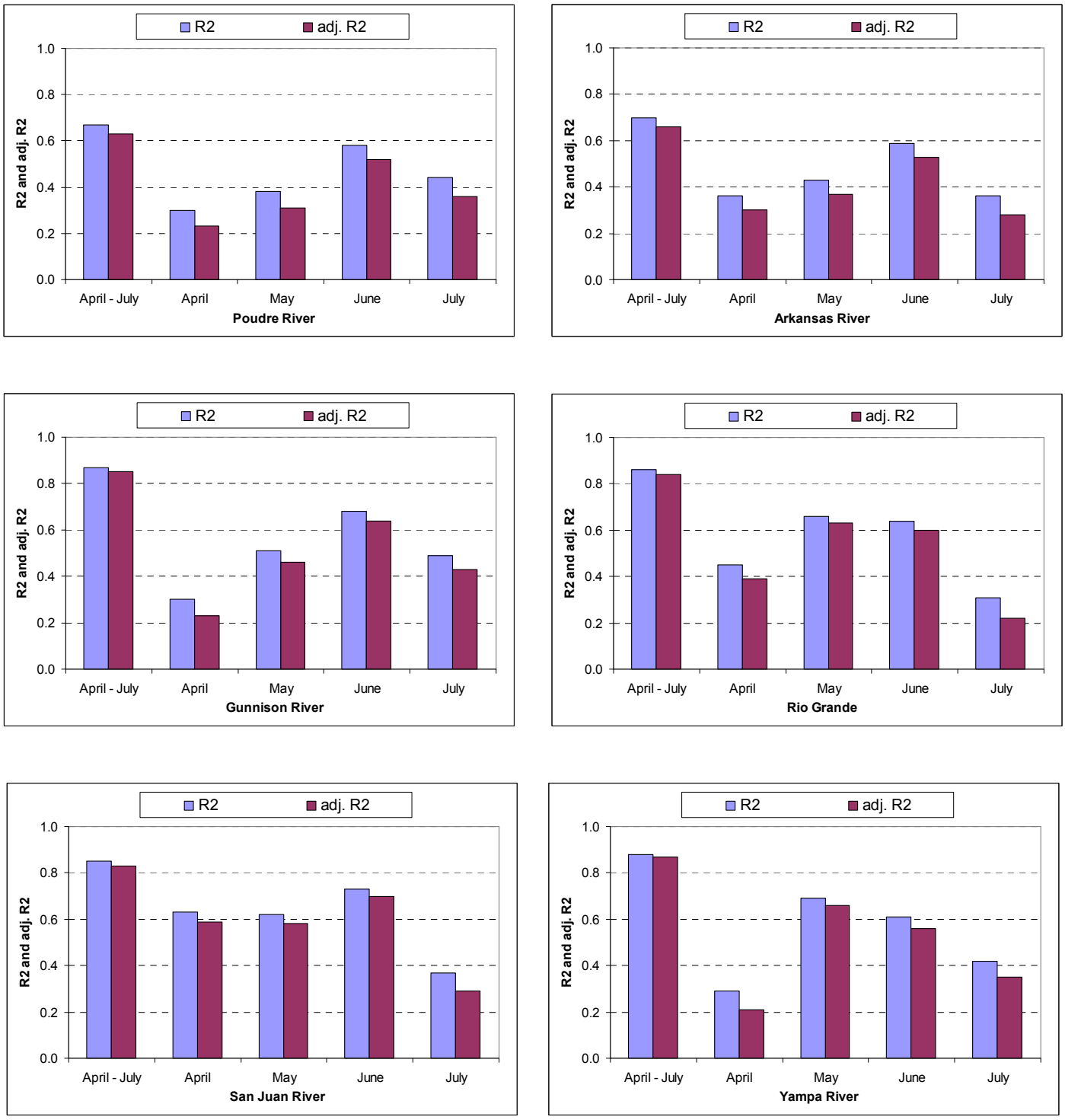

Figure E.3 Comparisons of R^2 and Adjusted R^2 for the PCA model and the temporal disaggregation (fitting)

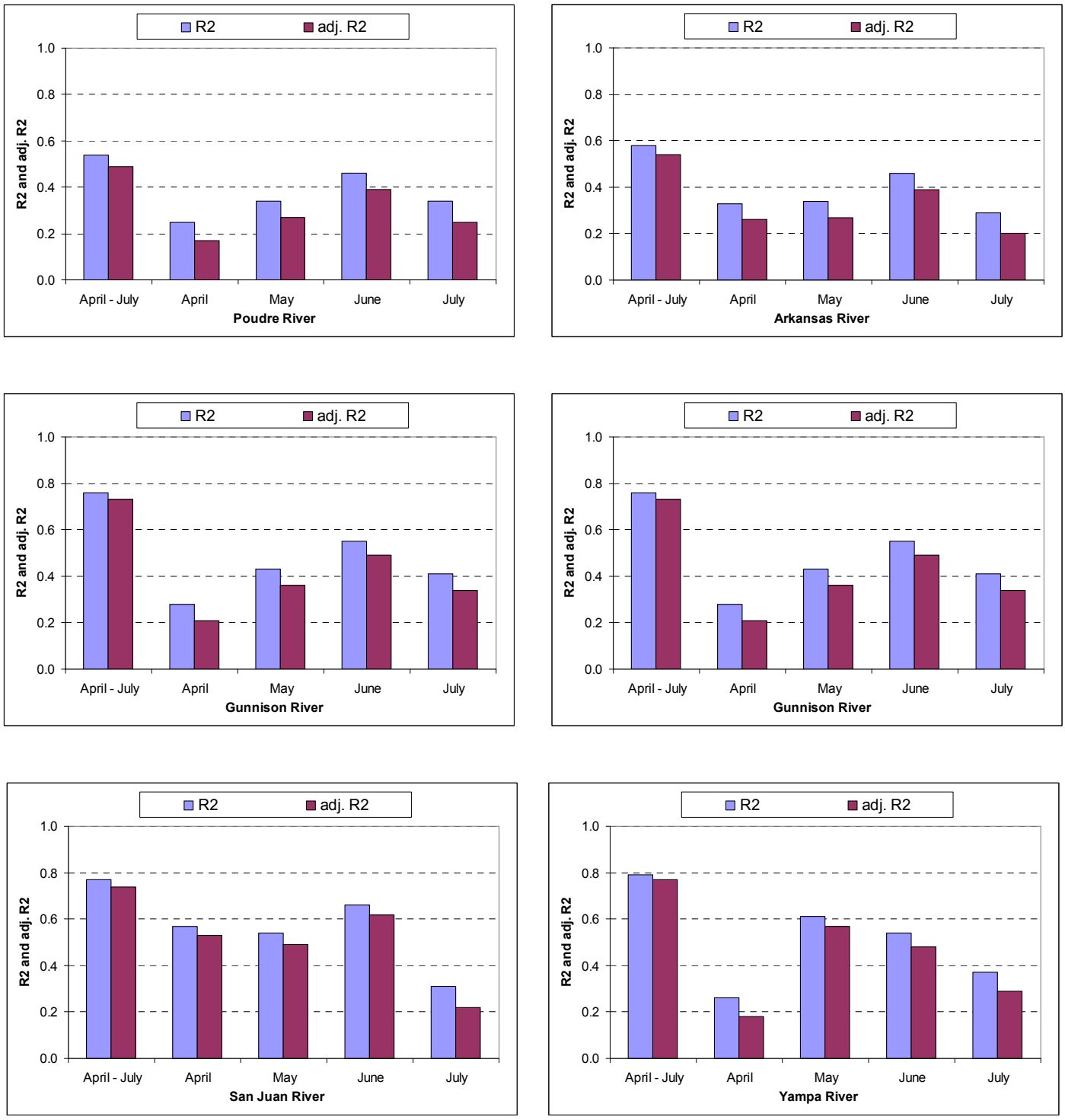

Figure E.4 Comparisons of R^2 and Adjusted R^2 for the PCA model and the temporal disaggregation (drop one)

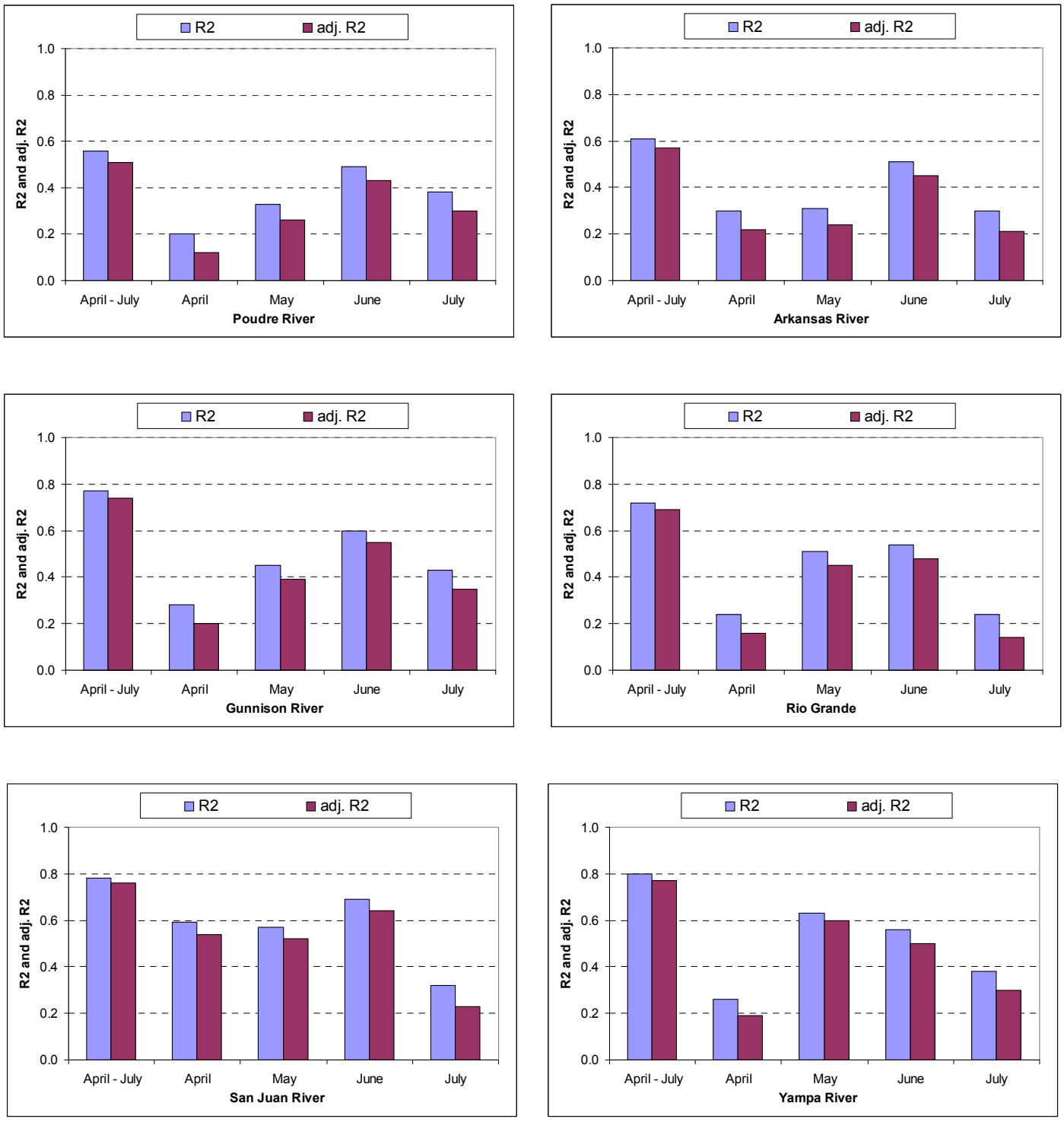

Figure E.5 Comparisons of R^2 and Adjusted R^2 for the PCA model and the temporal disaggregation (drop 10%)

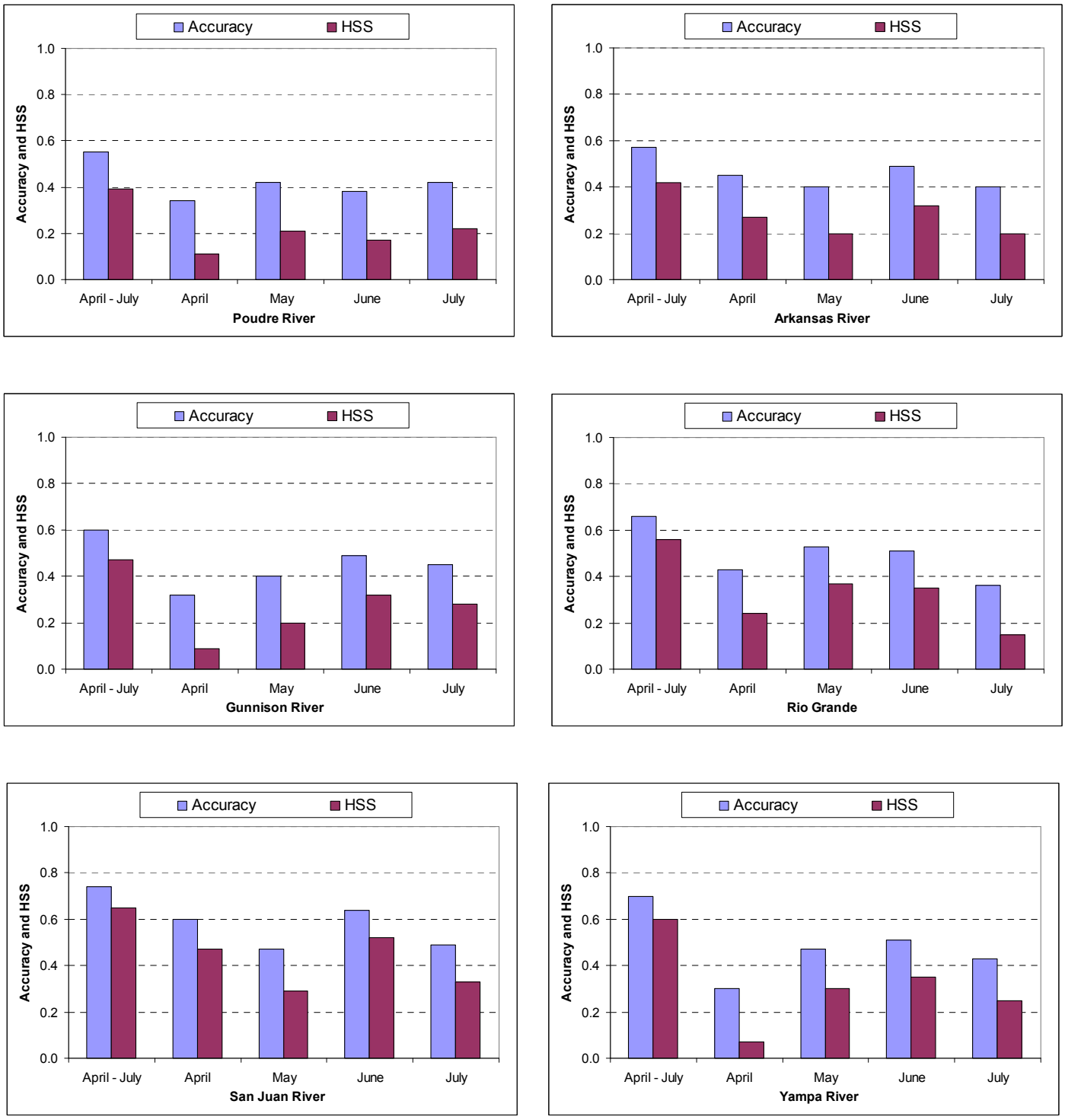

Figure E.6 Comparisons of forecast skills for the PCA model and the temporal disaggregation (fitting)

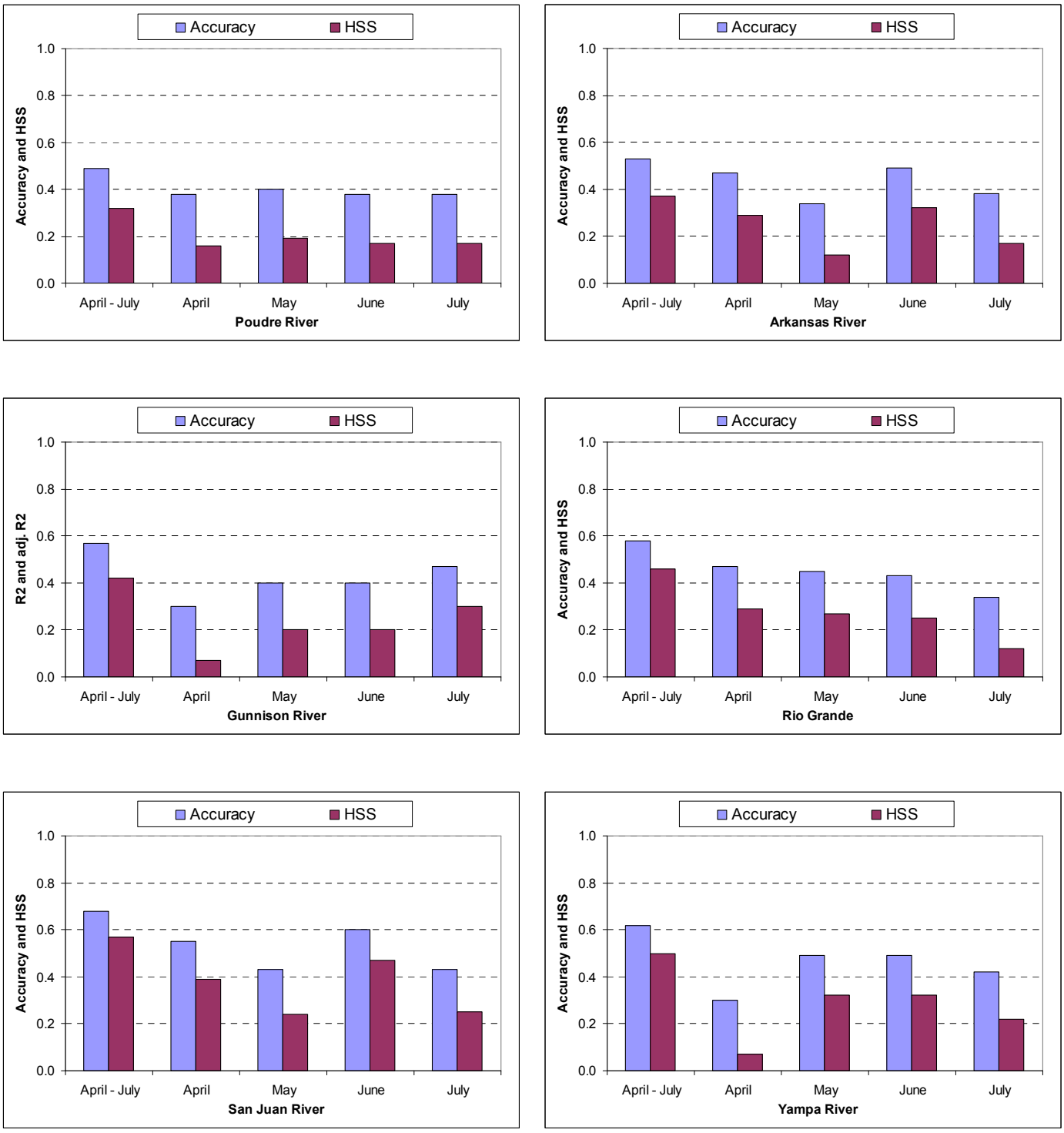

Figure E.7 Comparisons of forecast skills for the PCA model and the temporal disaggregation (drop one)

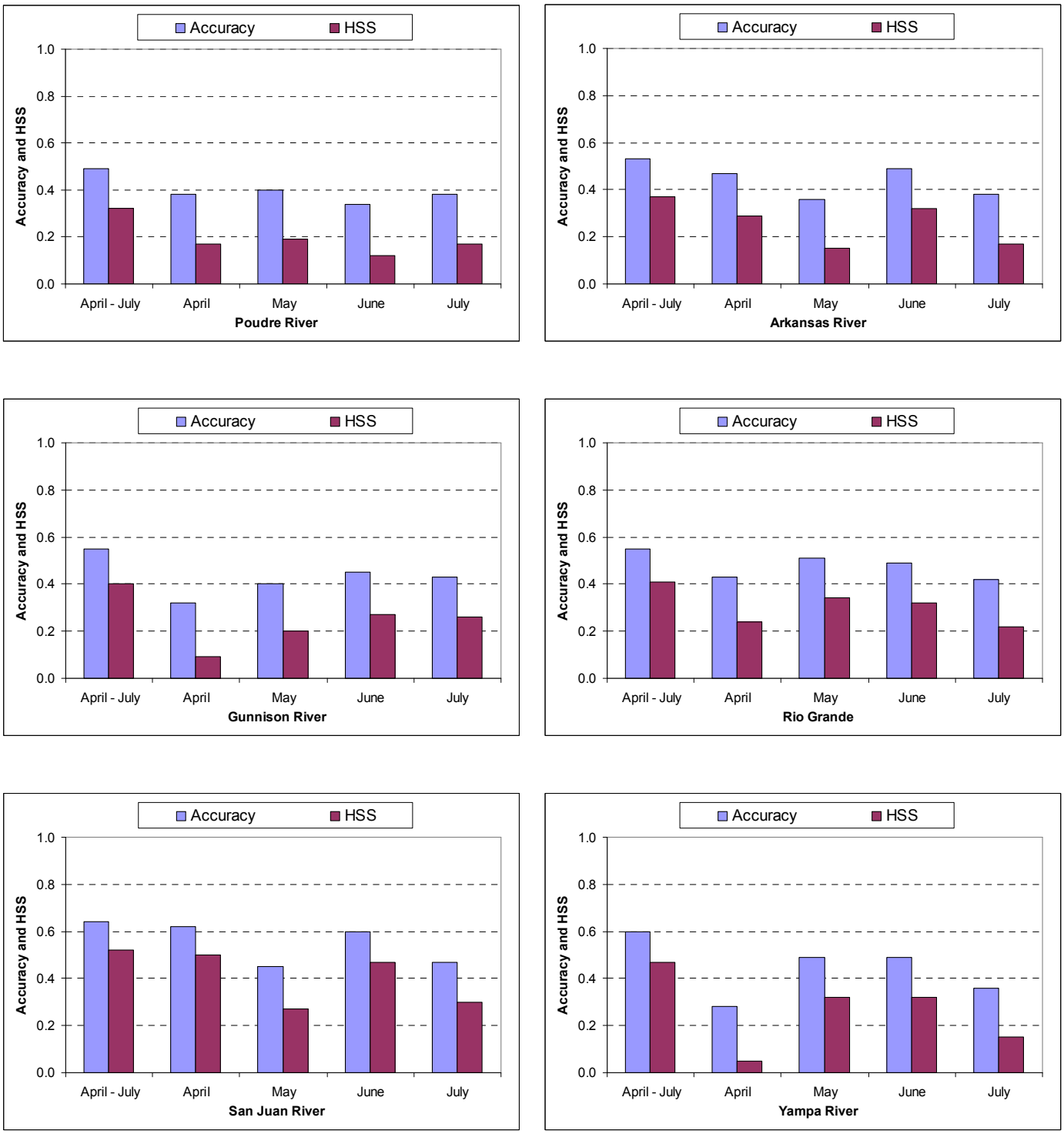

Figure E.8 Comparisons of forecast skills for the PCA model and the temporal disaggregation (drop 10%)